Nitrate sensing and cell wall modification in Staphylococci

Dissertation

der Mathematisch-Naturwissenschaftlichen Fakultät

der Eberhard Karls Universität Tübingen

zur Erlangung des Grades eines

Doktors der Naturwissenschaften

(Dr. rer. nat.)

vorgelegt von

Volker Niemann

aus Hattingen/Ruhr

Tübingen

2015

Gedruckt mit Genehmigung der Mathematisch-Naturwissenschaftlichen Fakultät der Eberhard Karls Universität Tübingen.

Tag der mündlichen Qualifikation:	30.10.2015
Dekan:	Prof. Dr. Wolfgang Rosenstiel
1. Berichterstatter:	Prof. Dr. Thilo Stehle
2. Berichterstatter:	Prof. Dr. Friedrich Götz

Summary

This thesis highlights two topics concerning the regulation of energy metabolism and the cell wall biosynthesis in Staphylococci. Most members of this genus are facultative anaerobic microorganisms able to respire on nitrate as final electron acceptor. The completely apathogenic organism *Staphylococcus carnosus* is used as starter culture in food industry. Dissimilatory nitrate reduction causes desired effects during the ripening process of sausages. First, the nitrate concentration is reduced, and nitrite combines with myoglobin to nitrosomyoglobin to yield the appealing red color of sausages. Secondly, use of starter cultures in food production reduces likewise the risk of food poisoning and food spoilage.

The signal transduction system that regulates the anaerobic respiration has to transduce two signals: The absence of oxygen and the presence of nitrate as the final electron acceptor. The two component system NreBC is composed of an oxygen-sensing histidine kinase with its cognate response regulator, which induces gene expression in the absence of oxygen. In Niemann et al we present two X-ray structures of NreA bound to its physiological ligand nitrate as well as to iodide in the binding pocket. Based on the X-ray structure, point mutations were introduced that diminish nitrate binding. The effects of the mutations were analyzed with isothermal titration calorimetry, CD-spectroscopy and *in vivo* lipase reporter gene assays. Thus, nitrate binding to NreA affecting the expression level of genes necessary for nitrate respiration could be described. The absence of oxygen activates kinase activity, which is further enhanced when nitrate-free NreA is present. In Nilkens et al we could describe how the nitrate status is introduced to the signal transduction pathway. NreA without bound nitrate acts as negative regulator on the NreB kinase activity.

Since the extensive usage of antibiotics, the opportunistic pathogen *S. aureus* has been accumulating antibiotic resistance genes. Thus, the treatment of diseases caused by methicillin- or multi-resistant *Staphylococcus aureus* (MRSA) has become even more challenging. *S. aureus* exhibits a cell wall feature making it resistant to lysozyme. In *S. aureus* the MurT/GatD enzyme complex amidates the isoglutamic acid at the second position of the stem peptide. The presence of isoglutamine at this position contributes to a higher degree of cross linkages in the cell wall and a higher growth rate. MurT/GatD is a cytosolic enzyme complex that amidates the cell wall precursor Lipid II. This reaction affects the viability of *S.aureus* and thus make MurT/GatD or Lipid II promising drug targets. In this thesis, I describe a purification protocol of the intact MurT/GatD complex that yields pure protein, which is suitable for X-ray crystallography.

Zusammenfassung

Diese Doktorarbeit umfasst zwei Themen: die Regulierung des Energiestoffwechsels und die Zellwandbiosynthese bei Staphylokokken. Diese Gattung beherbergt viele fakultativ anaerobe Arten, die mit Nitrat als finalen Elektronenakzeptor atmen können. *Staphylococcus carnosus* ist völlig apathogen und wird als Starterkultur in der Lebensmittelindustrie eingesetzt. Dissimilatorische Nitratreduktion führt zu gewünschten Effekten während der Wurstreifung. Zum einen wird die Nitratkonzentration reduziert und Nitrit verbindet sich mit Myoglobin zu Nitrosomyoglobin, wodurch die gewünschte rote Farbe der Wurst entsteht. Zweitens reduziert die Verwendung von Starterkulturen in der Nahrungsmittelproduktion das Auftreten von Lebensmittelvergiftungen und Lebensmittelverderb.

Anaerobe Atmung wird durch das Signaltransduktionssystem reguliert, welches zwei Reize vereint: Die Abwesenheit von Sauerstoff und die Anwesenheit von Nitrat als finalem Elektronenakzeptor. Das Zweikomponenten System NreBC ist aus einer sauerstoffabhängigen Histidinkinase und seinem dazugehörigen Response Regulator aufgebaut, der in Abwesenheit von Sauerstoff die Genexpression aktiviert. In Niemann *et al.* stellen wir zwei Kristallstrukturen von NreA vor: mit Nitrat als physiologischen Liganden, sowie mit gebundenen Iodid. Auf der Basis der Kristallstrukturen wurden Punktmutationen eingeführt, die die Nitratbindung verringert. Die Wirkungen der Mutationen wurden durch isotherme Titrationskalorimetrie, CD-Spektroskopie und *in vivo* Lipase Reportergen-Assays analysiert. Somit konnte der Einfluss von NreA abhängig von der Ligandenbindung beschrieben werden. Die Abwesenheit von Sauerstoff induziert die Kinaseaktivität, welche weiter verstärkt wird, wenn Nitrat an NreA gebunden hat. In Nilkens *et al*. konnte beschreiben werden, wie der Nitratstatus in den Signaltransduktionsweg integriert wird. NreA ohne gebundenes Nitrat wirkt als negativer Regulator auf die Kinaseaktivität von NreB.

Seit dem umfangreichen Einsatz von Antibiotika weist das opportunistische Pathogen *Staphylococcus aureus* vermehrt Antibiotikaresistenzgene auf. Krankheiten, die durch Methicillin- oder multi-resistenten *S. aureus* (MRSA) verursacht werden, sind so noch schwieriger zu behandeln. *S. aureus* zeigt eine Zellwandbesonderheit auf, die ihn widerstandsfähig gegen Lysozym macht. In *S. aureus* amidiert der MurT/GatD Enzymkomplex die Isoglutaminsäure an der zweiten Position des Stammpeptids. Die Anwesenheit von Isoglutamin an dieser Stelle führt zu einer erhöhten Quervernetzung der Zellwand und zu höheren Wachstumsraten. MurT/GatD ist ein zytosolischer Komplex, der den Zellwandvorläufer Lipid II amidiert und einen starken Einfluss auf die Lebensfähigkeit von *S. aureus* hat. So erscheinen MurT/GatD oder Lipid II als vielversprechende Angriffspunkte für Medikamente. In dieser Arbeit wird ein Reinigungsprotokoll für den intakten Murt/GatD Komplex für die Röntgenkristallographie beschrieben.

Table of Content

Abbreviations

A-H

AIP	Auto inducing peptide
agr	Accessory gene regulator
Amp	Ampicillin
AMP	Adenosine monophosphate
ARNT	Aryl hydrocarbon receptor nuclear translocator
ATP	Adenosine triphosphate
BACTH	Bacterial adenylate cyclase two-hybrid
cAMP	Cyclic adenosine monophosphate
CA-MRSA	Community associated methicillin resistant *Staphylococcus aureus*
CD	Circular dichroism
CHIPS	Chemotaxis inhibitory protein of staphylococci
cGMP	Cyclic guanosine monophosphate
cw	Column volume
DHp	Dimerization histidine phosphotransfer
DNA	Deoxyribonucleic acid
DTT	DL-Dithiothreitol
ECM	Extracellular matrix
Fhl	Formate hydrogen lyase system
FPLC	Fast protein liquid chromatography
GAF	cGMP-binding PDE, Anabaena adenylyl cyclase, FhlA from *E. coli*
GAT	Glutaminase
GATase	Glutamine amidotransferases
GlcNAc	N-acetylglucosamine
HA-MRSA	Hospital associated methicillin resistant *Staphylococcus aureus*
His-P	Phosphorylated histidine
HK	Histidine kinase
HPINE	Histidine protein interaction experiment

I-R

IPTG	Isopropyl-β-D-thiogalactopyroside
ITC	Isothermal titration calorimetry
kb	Kilo base pairs
LS-MRSA	Livestock-associated methicillin resistant *Staphylococcus aureus*
LTA	Lipoteichoic acid
MAP	Mitogen-activated protein
Mb	Mega base pairs
MCSRAMMs	Microbial surface components recognizing adhesive matrix molecules
MHC	Major histocompatibility complex
MGE	Mobile genetic element
MurNAc	N-acetylmuraminic acid
MWCO	Molecular weight cutoff
NAD^+/NADH	Nicotinamide adenine dinucleotide (ox/red)
NLP	NIN-like protein
NTA	Nitrilotriacetic acid
Ntn	N-terminal nucleophile
OD	Optical density
PAS	Per, ARNT, Sim
PBP	Penicillin binding protein
PDE	Phosphodiesterase
PEG	Polyethylene glycol
Per	Period circadian protein
PIA	Polysaccharide adhesion
PG	Peptidoglycan
PMF	Proton motive force
REC	Receiver
RNA	Ribonucleic acid
RR	Response regulator

S-W

SaPI	Staphylococcus aureus pathogenicity Islands
Sar	Staphylococcal accessory regulator
SCC	Staphylococcal cassette chromosome
SEC	Size exclusion chromatography
SDS-PAGE	Sodium dodecyl sulfate polyacrylamide gel electrophoresis
Sim	Single minded protein
TECP	Tris-(2-carboxyethyl)phosphorine
TCS	Two-component system
TCA	Tricarboxylic acid
TSS	Toxic shock syndrome
UDP	Uridine diphosphate
WTA	Wall teichoic acid

1. Introduction

1.1. Discovery of Staphylococci

The genus Staphylococcus was first described as grape-like clusters of cocci in 1881 by Alexander Ogston. Microorganisms were obtained from the pus that flows from an acute abscess, and were characterized by light microscopy. Chain-forming cocci, where division occurred in only one direction, could be distinguished from the grape-like form where fission has to take place in any direction (1). In 1884, Rosenbach was able to obtain pure cultures of Staphylococcus. Based on the golden (lat.: aurum) or white (lat.: albus) colored colonies he termed them *Staphylococcus aureus* and *S. albus,* respectively. Furthermore, osteomyelitis was diagnosed after *S. aureus* was injected in the knee of rabbits and dogs (2). In 1886, Staphylococci were described as Gram-positive cells with a diameter of 0.87 µm, which are often observed as chains of up to four cells, but commonly appear clustered as well (3). In 1940, Chapman et al were able to distinguish between pathogenic and apathogenic Stapylococci based on a coagulase test (4). The taxonomy of cocci was continuously discussed until in 1955 an identification based on oxygen requirements for growth in a standardized complex medium containing glucose was proposed. With this newly developed method, the obligate aerobe genus Micrococcus could be discriminated from the facultative anaerobe Staphylococcus (5). Furthermore, analysis of genome nucleotide composition revealed a significantly higher guanine-cytosine content in micrococcus cells than in staphylococci (69-75% and 31-37%, respectively) (6). In the 1970s the knowledge about the genus Staphylococcus increased rapidly with categorization by chemotaxonomic and genomic methods (domain: Bacteria; phylum: Firmicutes; class: Bacilli; order: Bacillales; family: Staphylococcaceae). In the genus Staphylococcus, more than 36 species are described as nonmotile, nonsporeforming and usually unencapsulated bacteria (7). The genome sizes of Staphylococci is in the range of 2200 – 3100 kb (8). Furthermore, among different *S. aureus* isolates the genome appears to be polymorphic and can be differentiated in a core genome encoding for the housekeeping genes and a variable or accessory genome. The accessory genome contains genes involved in a diverse array of nonessential functions, ranging from substrate utilization and miscellaneous metabolism to virulence factors and drug resistance. Additionally, this genomic region is mainly composed of mobile genetic elements (MGEs) that can be transferred horizontally between bacteria, including bacteriophages, *S. aureus* pathogenicity islands (SaPI), staphylococcal cassette chromosomes (SCC), plasmids, and transposons *(9, 10).* The ability to adopt various virulence genes and antibiotic resistance genes provide the possibility that essentially any *S. aureus* genotype can transform into a life-threatening human pathogen.

1.1. Know thy enemy: *Staphylococcus aureus*

In the late 19th century *S. aureus* was already described as a pathogen causing sepsis, osteomyelitis and wound infections (3). With increasing knowledge and improved methods to isolate specific microorganisms, *S. aureus* could also be found on healthy persons that do not show any symptoms (11). The commensal bacterium could be isolated from different areas of the human skin, for example in the axilla, on the hand, the back of the neck, or the chest. It was shown that *S. aureus* tolerates high salt concentrations, which underlines its capabilities to adapt to environmental changes such as the osmotic pressure (12). However, next to the skin the nose is most commonly either transiently or persistently colonized. It has been reported that the nose is often the endogenous origin of strains that can also causes an infection (13). In case of healthy persons, the innate immune response seems to prevent *S. aureus* from invading the nasal mucosa, which could cause more extensive forms of colonization or even infection (14). Thirty to fifty percent of the healthy population are asymptomatically colonized and approximately twenty percent are transiently colonized (15). Already in 1963, Williams noted that there are higher carrier rates recorded for hospital patients and hospital personnel (11). Over the last 50 years, overall carriage rates declined, a fact that was attributed to improved personal hygiene, changed life standards, and smaller families (16). However, the rates Staphylococci resistant to antibiotics increases in hospitals as well as in the general population (17, 18). Furthermore, other mammals and birds also carry *S. aureus,* but there seems to be a host specificity, based on the presence of certain virulence factors. Sometimes strains can escape their host-specific constraints. A pig-associated and methicillin-resistant strain of *S. aureus* caused serious infections among pig farmers (19). Methicillin- or multi-resistant strains of *S. aureus* are categorized by their occurrence as either community associated (CA-MRSA), hospital associated (HA-MRSA) or livestock associated (LA-MRSA) (20). *S. aureus* is well adapted to humans and under certain circumstances can transform from a commensal to a pathogen. It is equipped with structural components, functioning in concert with secreted products to target tissues at various body sites and evade host defense mechanisms (21). The organism causes skin and soft tissue infections such as furuncles or abscesses. Is the organism introduced into deeper tissue, for example in association with implanted artificial devices or catheters, it can cause serious infections including endocarditis, sepsis, or severe life-threatening toxic shock syndrome (TSS) (Table 1) (22).

Table 1 Diseases caused by S. aureus

Skin and soft tissue infections
Furuncles, carbuncles, paronychia (nail infection)
Wound infection (traumatic, surgical)
Cellulitis
Impetigo (also caused by streptococci)
Bacteremia (frequently with metastatic abscesses)
Endocarditis
Central nervous system infection
Brain abscess
Meningitis (rare)
Epidural abscess
Pulmonary infections
Osteomyelitis
Arthritis
Genitourinary tract infections
Renal abscess
Lower urinary tract infection
Toxin-related diseases
Toxic shock syndrome
Necrotizing pneumonia
Scalded skin syndrome
Extreme pyrexia syndrome
Food poisoning (gastroenteritis)

Table is adapted from Engleberg NC, DiRita V, & Dermody TS (2013)

In many cases, host tissue colonization is a prerequisite for the development of an infection. *Staphylococcus aureus* express cell surface adhesins that mediate the interaction with the extracellular matrix of the host tissue. Microbal surface component recognizing adhesive matrix molecules (MCSRAMMs) are characterized as components that are localized on the microbal surface and bind a macromolecular ligand with high specificity and affinity. The ligands collagen and laminin are exclusively found in the extracellular matrix (ECM), whereas fibronectin and fibrinogen also appear as soluble forms in body fluids. Adhesins of the lectin type that recognize carbohydrates should not be classified as MSCRAMMs even though they may bind to ECM components (23). However, *S. aureus* is equipped with a diverse arsenal of secreted and cell surface-associated virulence factors, including surface proteins that promote adhesion to damaged tissue as well as to artificial or natural surfaces in the host (24, 25). Secreted virulence factors that bind to blood-localized host proteins furthermore facilitate immune evasion. When the outer physical barriers have been broken through, *S. aureus* is confronted with the host's immune system, comprising both innate and acquired responses. A strong inflammatory response is typically stimulated, involving the migration of neutrophils and macrophages to the site of infection. These cells will attempt to engulf and dispose of the

invading organisms with the help of available antibodies (26). Peptide fragments are released by the complement system, as well as formylated peptides secreted from growing bacterial cells. Those are recognized by specific receptors on the neutrophil surface resulting in their migration from the blood to the site of inflammation (26, 27). About sixty percent of *S. aureus* strains secrete chemotaxis inhibitory protein of staphylococci (CHIPS), which interferes with receptor mediated migration of the neutrophils (28). Furthermore, *S. aureus* can secrete extracellular enzymes such as proteases, hyaluronidases, lipases and nucleases that facilitate tissue destruction, allowing *S. aureus* to spread. Alpha-toxin, as an example of membrane-damaging toxins, is released as hydrophilic monomers which bind firmly to host membranes. There they assemble into hexameric ring structures introducing a hole in the cell membrane, thus causing cytolytic effects on host cells and tissue damage (29).

Furthermore, secreted superantigens bind to the exterior surface of the major histocompatibility complex (MHC) class II protein on the surface of antigen-presenting cells and link it to T-cell receptors of T-lymphocytes (30, 31). This binding to MHC class II molecules occurs without the requirement of a presented antigenic peptide and as a result up to thirty percent of T cells become activated and start to proliferate. Furthermore, the induced high level of cytokine expression causes TSS and prevents the development of a normal immune response (30, 32). The expression of virulence factors is controlled by a variety of global regulators, including two-component systems, DNA-binding proteins, and quorum-sensing systems. Unfortunately, transcript analysis revealed differences between broth cultures and *in vivo* animal models (33). In *in vitro* cultures, the expression of cell wall anchored Protein A is induced during early growth and reduced at later time. Secreted proteins, including toxins, hemolysins, and tissue degrading enzymes, are produced at the end of exponential growth (Figure 1) (34).

The expression of virulence factors is controlled primarily by a global regulatory locus *agr* (35). Two distinct transcript units derive from the *agr* locus. RNAII encodes AgrABCD, including the two component system with the transmembrane histidine kinase AgrC and its cognate Response Regulator AgrA that is required for the transcription of RNAII and RNAIII. AgrD is an autoinducing peptide (AIP), which is post translationally processed and exported via transmembrane AgrB (36). With increasing cell density, AgrD accumulates in the surroundings, and if a certain threshold concentration is reached, the histidine kinase AgrC is activated. The positive feedback loop also induces the transcription of RNAIII, which acts as small regulatory RNA up-regulating secreted virulence factors and down regulating surface proteins. This quorum sensing system (Agr) is additionally controlled by staphylococcus accessory regulator (Sar) and alternative sigma factor (SigB). This network of regulatory systems ensures that *S. aureus* is able to adapt to a changing environment, for example by forming biofilms, a

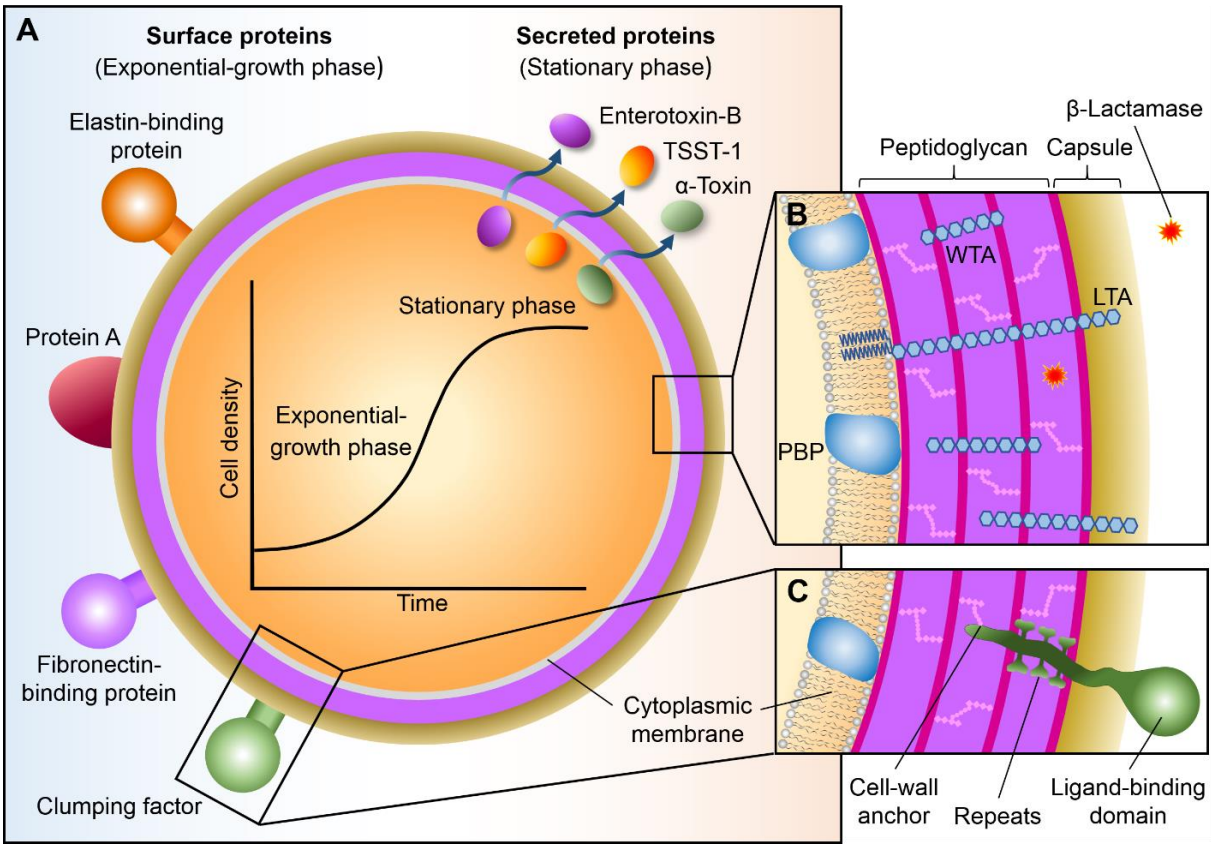

Figure 1 **Structure of *Staphylococcus aureus*. A:** The synthesis of surface and secreted proteins are dependent on the growth phase. Quorum sensing regulation systems control the expression of virulence factors. A selection of prominent surface proteins expressed in the exponential growth phase is depicted on the left side. On the right, examples of proteins secreted in the stationary phase are shown. **B:** A cross section of the cell envelope with penicillin binding proteins (PBP) present in the membrane. Lipoteichoic acids (LTA) anchored in the cell membrane and wall teichoic acids (WTA) covalently linked to peptidoglycan are shown. Some strains are also encapsulated. **C:** Clumping factor is enlarged as an example for surface proteins anchored to the cell wall by a C-terminal LPXTG-motive. Repeat structures are spanning the cell wall, and a binding domain is exposed to the surrounding.

Figure is adapted from Lowey, 1998

multilayered cell cluster embedded in a viscous matrix composed of polysaccharide intercellular adhesion (PIA). The first step of biofilm formation is the attachment of cells to polystyrene surfaces, which is also regulated by the Agr quorum sensing system. Secondly, the proliferation of cells and embedding in the slimy matrix composed of β-1,6-linked N-acetylglucosamine with partly deacetylated sugar residues enables the pathogen to survive better in an hostile environment (37-39). Biofilm formation is not only dependent on cell density, it is also induced by oxygen- and iron-limitation as also when sublethal concentrations of certain antibiotics are present (7). Most likely, the two component system SrrA-SrrB integrates the low oxygen-status into the Agr-controlled survival strategy (40).

The regulatory networks are encoded by the core genome which appears to be highly clonal in different strains. In this case evolution and selection depend mainly on point mutations (41).

The ability of *S. aureus* to adapt to changing environmental conditions provides a remarkable advantage in colonizing the host and withstanding counter attacks. Staphylococcus is also able to adapt by homologous recombination, which provides the influx and loss of virulence determinants carried on mobile elements. Horizontal transfer of DNA occurs in all bacteria by transformation, conjugation and transduction. In *S. aureus* there is little to no evidence that transformation occurs. In contrast, conjugation is a common and efficient mechanism for gene transfer from other species to *S. aureus* (42). Besides the shuttling of virulence factors, specifically the ability to transfer antibiotic resistances is the reason why Staphylococcus infections are becoming a more serious threat.

1.2. Antibiotics and resistance

The discovery and usage of antibiotics in human healthcare introduced a new era with decreased morbidity and mortality for most human beings. Alexander Fleming published in 1929 that “while working with staphylococcus variants a number of culture-plates were set aside on the laboratory bench and examined from time to time. […] It was noticed that around a large colony of a contaminating mould the staphylococcus colonies became transparent and were obviously undergoing lysis”. Filtrated mold broth lead to a sterile solution with remaining antibacterial activity (43). This knowledge was used as an efficient method for penicillin mass-production using fermentation on the basis of a cornstarch medium. During World War II, penicillin prevented thousands of deaths from gas gangrene and other infections. Dorothy Crowfoot Hodgkin used X-ray crystallography to determine the structure of penicillin (44). Based on its atomic structure, production of a fully synthetic penicillin was possible (45). Penicillin is a beta-lactam antibiotic that is structurally similar to the D-alanyl-D-alanine moiety of the pentapeptide bridge of peptidoglycan. Even before the extensive usage of penicillin in human healthcare, staphylococci resistant to penicillin were described (46). The golden era of antibiotics brought out several new antibiotics. With the usage of penicillin, or any other antibiotic, a new environmental pressure exists for the microsome using humans as a host, leading to resistance. Microorganisms are able to take up new genes by horizontal gene transfer, thus making the endogenous human fauna, which had been exposed to various antibiotic treatments before, a perfect antibiotic resistance gene-exchange hotspot.

1.3. *Staphylococcus carnosus* – the harmless brother

Staphylococcus carnosus has never been isolated from human skin or mucosa. However, it might be possible that the skin of certain animals serves as habitat for this organism, which would explain its natural occurrence in meat products (47). In addition, *S. carnosus* exhibits a comparably high content of osmoprotective factors, which is indeed consistent with its usage in starter cultures during the ripening of raw sausage under high salt conditions, but does not provide ultimate evidence for an animal as natural habitat of *S. carnosus* (48).

The genome of *S. carnosus* comprises 2.57 Mb and thus is one of the smallest of the sequenced staphylococcal genomes. The number of predicted open reading frames (ORF) of 2462 coding sequences is also smaller than in *S. aureus* N315, which comprises 2594 ORFs. A gene content analysis shows that 46 to 50% of these genes are conserved in all sequenced staphylococcal species. The conserved genes are predominantly located within a region designated as ‘‘conserved core region’’ (49). Besides a small proportion of these conserved proteins, which cannot be functionally classified yet, the majority of the gene products are involved in basic metabolic pathways, i.e. transport and metabolism of substrates, coenzymes, energy production, transcription and translation or replication. One quarter of *S. aureus* COL gene products involved in pathogenesis, toxin production, and resistance were found to be conserved. Most of these virulence factors contribute to the global regulation of protein expression or to drug resistance. Since these proteins are also found in the non-pathogenic *S. carnosus* they may have a bivalent function: in addition to their role in the development of virulence they could also be engaged in basic metabolic pathways and in enhancement of bacterial fitness (50). Only a prophage, FT M300, and a genomic island, nSCA1, were detected. Due to the mosaic structure of these elements they may have become irreversibly integrated into the genome of *S. carnosus* TM300 and are no longer active (47).

There is evidence that repetitive DNA sequences facilitate the plasticity of genomes by allowing enhanced genomic diversification due to recombination events (51). Repetitive sequences are rare in *S. carnosus*, indicating comparably low genome plasticity and an almost complete absence of recombinatorial exchange of genetic material. These genomic features suggest that *S. carnosus* has adapted to the constant environmental conditions it is exposed to as a meat starter culture bacterium. The lack of changes in selective pressure in this habitat has probably eliminated the need for versatile adaptive mechanisms and thus led to a comparably small genome size. A similar reductive evolution has been described for *Lactobacillus delbrueckii ssp. bulgaricus*, which is applied in dairy industry for the production of yoghurt. The genomic data of this organism provides also evidence for a reduction of genome size (52).

The absence of exotoxin and hemolysis activities in *S. carnosus* despite the presence of the corresponding genes is probably caused by pleiotropic effects exerted by truncations found in

genes of the global regulatory systems Agr and Sae. The same reasons might apply for the lack of exoenzyme activities of *S. carnosus* despite the presence of various intact genes coding for lipases, proteases and nucleases (50).

During the ripening process of dry sausage, *S. carnosus* exerts several desired functions (53). First, *S. carnosus* gradually reduces nitrate to nitrite (54). Due to this reaction, the nitrate concentration is decreased and the generated nitrite can combine with myoglobin to form nitrosomyoglobin, which results in the typical red color of sausage. In the second step, nitrite is further reduced to ammonia, thus diminishing the concentration of unbound nitrite (55).

One of the main advantages of starter cultures in fermented food processing is that the fermentation and ripening processes can be carried out under controlled conditions. In this way, food poisoning and food spoilage microorganisms can be suppressed, and the course of the fermentation process and its termination can be monitored more reliably (47).

2. NreABC

2.1. Flexible respiration in bacteria

Life depends on ordered structures harboring machineries for replication, metabolism and homeostasis that need to be constantly maintained. According to thermodynamics, energy is required to build up and maintain an ordered structure such as a cell. Oxidation of reduced compounds releases free energy, which can be used by a living cells. The highest yield of free energy is released by oxidative phosphorylation, also known as respiration. The free energy released during this electron transfer process from low-redox-potential electron donor to a high redox-potential electron acceptor is coupled to the translocation of protons across a membrane. The generated trans-membrane electrochemical proton gradient or proton motive force (PMF) ($\Delta\Psi$) can drive the synthesis of ATP (56, 57). Three and a half billion years ago, first respiratory processes have evolved in the hyperthermal reducing environment utilizing either Fe(III) or S(0) as electron acceptors (58). With progressing evolution and the abundance of photosynthetic organisms, the end product of photosynthesis, oxygen, accumulated in the atmosphere. This provided efficient respiration with oxygen as electron acceptor, which is crucial for life of higher animals and plants. NADH, generated by glycolysis and the tricarboxylic acid (TCA) cycle, is reoxidized to NAD^+. In most pro- and eukaryotes, NADH oxidation is accomplished by respiratory complex I, the electrogenic NADH:quinone oxidoreductase, a highly conserved multisubunit enzyme that is composed of 13 subunits in *Escherichia coli* and even 45 subunits in eukaryotic mitochondria (59-61). The enzyme couples the oxidation of NADH and the reduction of quinone to the translocation of cations (H^+ or Na^+) across a membrane, thereby generating $\Delta\Psi$ (62-65). This is followed by electron transfer through a range of redox cofactors, bound to integral membrane or membrane-associated protein complexes. The process terminates in the reduction of oxygen, a high-redox-potential electron acceptor (Figure 2). Mitchell proposed that the chemi-osmotic phenomena in bacteria are involved in the energization of various membrane-bound processes, such as active transport of neutral and ionic solutes and ATP synthesis via the membrane-bound proton-translocating ATPase (66-70).

There is some respiratory flexibility in the mitochondria of yeast, filamentous fungi and ancient protozoa, but bacteria and archaea exhibit the most extreme respiratory flexibility. In these organisms, a diverse range of electron acceptors can be utilized including elemental sulfur and sulfur oxyanions, organic sulfoxides and sulfonates, nitrogen oxyanions and nitrogen oxides, organic N-oxides, as well as transition metals such as Fe(III) and Mn(IV) (71-75). This respiratory diversity can be found amongst psychrophiles, mesophiles and hyperthermophiles and contributes to the ability of prokaryotes to colonize many of Earth's most hostile microoxic

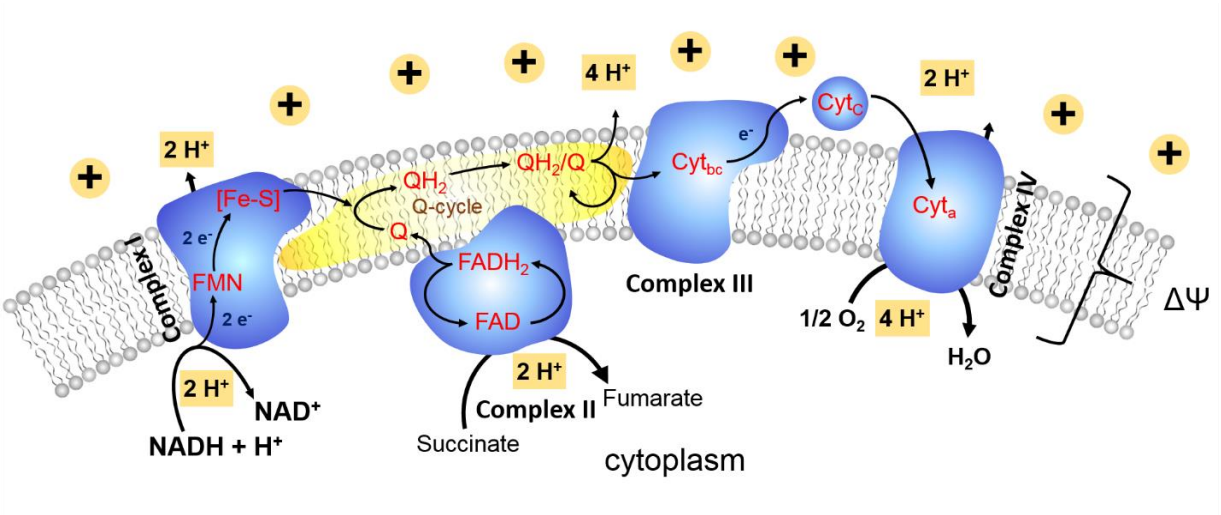

Figure 2 **Schematic representation of respiration chain with oxygen as final electron acceptor.** The NADH:quinone oxidoreductase (Complex I) appears often as an entry point of respiratory chains. The following electron transfer is coupled with proton translocation over the membrane. In addition to O_2 alternative final electron acceptors with a high redox potential such as NO_3, S(0) or Fe(III) are common among bacteria. The generated trans-membrane proton electrochemical gradient or proton motive force (ΔΨ) provides energy for membrane coupled processes like anti- and symport or ATP synthesis.

and anoxic environments (57). The ability to respire nitrate is widely spread among bacteria that can dissimilate the produced nitrite to gaseous compounds (denitrification) or to ammonia (dissimilatory nitrate reduction to ammonia). Denitrification is the major biotic process leading to the loss of fixed nitrogen from the environment as well as removal of excess nitrate from surface and wastewaters, accumulated mainly as a result of agricultural N-fertilizer application. When reduced to ammonia, the nitrogen is not removed from the environment, but transformed into a less mobile form due to absorption by mainly negatively charged soil surfaces, such as silicate clay for instance. In either case, the reduction of nitrate therefore plays a central role in preventing leaching and pollution of the ground water (76).

Staphylococci are facultative anaerobic organisms able to use nitrate as final electron acceptor in anaerobic respiration. Nitrate respiration results in the generation of a membrane potential and a pH-gradient of the same order of magnitude as that generated by electron flow in the respiratory chain. This electrochemical proton gradient is involved in driving active transport in a similar way as under aerobic conditions (70). The major membrane-bound nitrate reductase, termed NarGHIJ, is widely spread among bacteria. This enzyme couples the reduction of nitrate to the formation of a transmembrane proton gradient and is composed of three subunits, α, β, and γ, as well as several cofactors. NarGHIJ is arranged in two domains with the α- and β-subunits constituting the cytoplasmic domain and the γ-subunit constituting the membrane domain required for attachment of the α- and β-subunits to the cytoplasmic side of the inner membrane (76-78). The nitrate-reducing system in Staphylococci displays similarities to the nitrate reductases of *E. coli*. Nitrate is reduced to ammonia in two steps. First nitrate is taken

up, then reduced to nitrite which is subsequently exported (54, 79, 80). After the depletion of nitrate, nitrite is imported and reduced by the cytosolic NADH-dependent nitrite reductase NirBD. The nir operon encodes for *nirR*, *sirA*, *nirB*, *nirD*, and *sirB*. Next to the two essential structural genes *nirA* and *sirB*, the gene products SirA and SirB appear to be necessary for biosynthesis of the siroheme prosthetic group. The protein NirR shows no convincing similarity to proteins with known functions but it is thought to be involved in the reduction process or in regulation (55). Ammonia, the end product, is exported by an unknown mechanism but is also available for assimilatory metabolism.

The genes encoding for nitrate reductase (*narGHIJ*) and nitrite reductase (*nirBDR* and *sirAB*) are arranged in a gene cluster containing further genes associated with nitrate respiration (Figure 3). NarT shares 75% identity with the *S. aureus* nitrite-nitrate antiporter NarK and is likely to be involved in nitrate and nitrite transport (81, 82). Furthermore NreABC (for nitrogen regulation) as an oxygen and nitrate sensing system, has been identified and characterized in *S. carnosus* (79, 83-85). Upon oxygen depletion, autophosphorylation activity of the cytoplasmic histidine kinase NreB increases, which depends on the formation of an oxygen-labile iron-sulfur cluster (86). The subsequently phosphorylated response regulator NreC binds to the promoters of the nitrate reductase, and nitrite reductase operons and of the narT gene to enhance transcription (Figure 3) (79). NreA could be characterized as nitrate sensor that introduce the nitrate status into the NreBC signal transduction (see paragraph 2.3.1; 2.3.2 and Appendix) (84, 85).

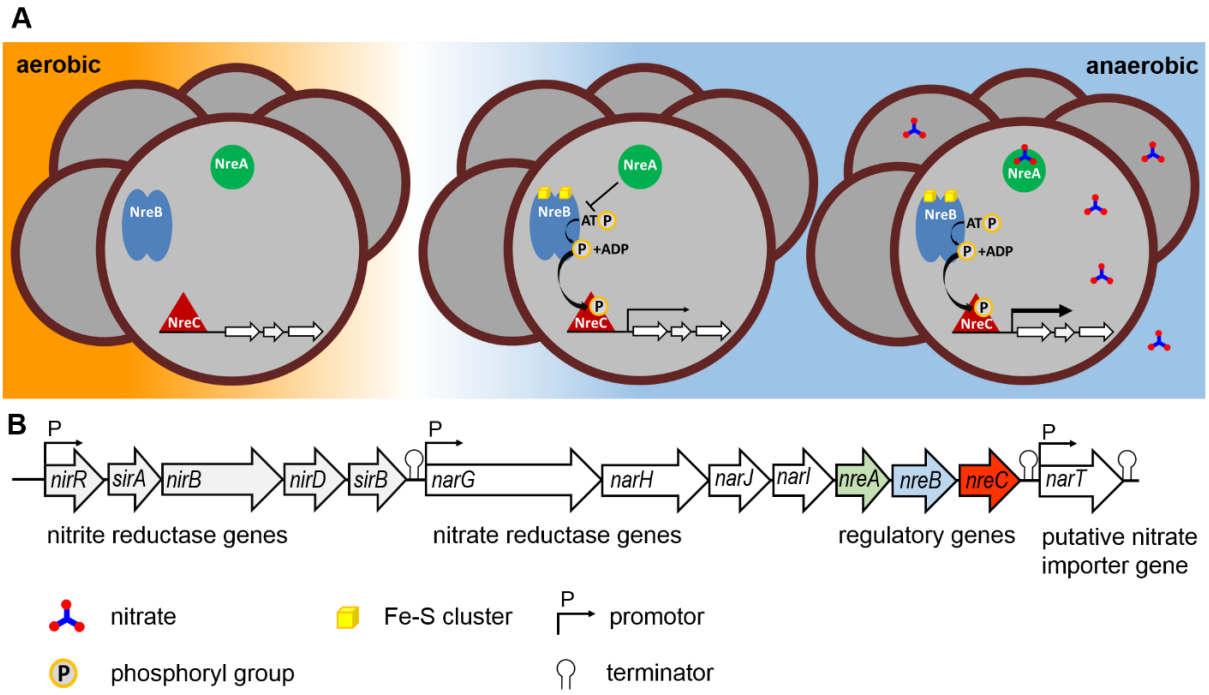

Figure 3 **Schematic representation of the NreABC signal transduction. A:** NreABC are shown under aerobic conditions (left), anaerobic without (middle) and in the presence of nitrate (right). The histidine kinase NreB is active under anaerobic conditions where the oxygen labile iron-sulfur cluster is formed. Phosphorylated response regulator NreC binds to the promoter regions of the gene cluster encoding for nitrate transport, nitrate reduction and nitrite reduction (shown in B). NreA without bound ligand inhibits the kinase activity, which is abolished when nitrate is bound. Under anaerobic conditions and in presence of nitrate gene expression is induced to maximum level. **B:** Gene cluster encoding for the structural genes of NADH dependent nitrite reductase (*nirBDR*). Its cofactor siroheme is synthesized by the gene product of two genes (*sirAB*). The gene cluster encodes also for the membrane bound, proton motive force generating nitrate reuctase (*narGHIJ*). The NreABC regulon controls also its own expression (*nreABC*). The narT-gene encodes for a putative nitrate antiporter.

2.2. Two component signal transduction

Seven pillars, short PICERAS (Program, Improvisation, Compartmentalization, Energy, Regeneration, Adaptability, Seclusion), have been proposed to define the fundamental principles on which a living system is based. Signal perception and signal transduction are inextricably linked to adaptability (87). Bacteria as all other living organisms have to sense and respond adequately in order to survive changing environmental conditions. Environmental changes are sensed by sensory domains of receptors, affecting domains of these receptors that subsequently trigger appropriate cellular responses including increased gene expression, changes in motility (chemotaxis), as well as changes in secretion and many other processes (88). Two-component systems (TCS) were believed to be specifically bacterial signal transduction system, whereas serine-, threonine and tyrosine-dependent kinases were seen exclusively in eukaryotes. Increasing numbers of sequenced genomes of bacteria, plants and lower eukaryotes revealed the presence of TCS (88, 89).

TCS are the major signal transduction systems in bacteria. They are composed of a histidine kinase (HK) and a response regulator (RR). A prototypical TCS consists of a membrane-integrated HK, which perceives a stimulus, and a cytoplasmic RR, which mediates the output, generally by an alteration in gene expression. HK and RR exchange information via phosphotransfer from a conserved histidine to an aspartic acid (90). Similar to most signaling proteins, the HK superfamily has a modular architecture with diverse input domains linked to a conserved catalytic core. Such a design allows the coupling of a wide variety of input signals to appropriate output responses. In prototypical HKs, the cytoplasmic kinase core consists of two distinct domains: a C-terminal catalytic and ATP binding HATPase c domain and a dimerization histidine phosphotransfer (DHp) domain. Two HK monomers dimerize via a four-helix bundle and the catalytically active HATPase c domain cross-phosphorylate each other on the conserved histidine in the DHp domains (91-94). Dimerization appears obligatory for HK functions but signaling does not occur through signal mediated dimerization of kinase domains unlike the regulatory mechanisms of many eukaryotic receptor families. It is believed that perception of stimuli causes alteration of protein-protein interactions within the HK dimer surface and that these perturbations are relayed to the kinase core domains (95). The formation of phosphoramidates instead of phosphoesters seen in Ser/Thr/Tyr protein kinases are the main unique feature of HKs. The high-energy bonds formed by the phosphoryl group and the imidazole ring of His are relatively unstable, making His-P residues more suitable as phosphotransfer intermediates than stoichiometrically phosphorylated sites for protein recognition. The chemical instability of His-P hinders the detection of HK phosphorylation by conventional analysis. Therefore histidine kinase activity is commonly assayed *in vitro* by incubating with [γ-^{32}P] ATP (93).

RR of a prototypical TCS typically consist of an N-terminal phosphoacceptor receiver (REC) domain and a C-terminal DNA-binding output domain that activates or represses transcription of specific target genes (88, 89, 96). The REC domain functions as a phosphorylation-activated switch. Phosphorylation occurs at a conserved Asp residue, generating a high-energy acyl phosphate that provides energy coupling to drive a conformational change in the REC domain (93). There is diversity of attached or independent effector domains providing an almost limitless variety of output responses that can be controlled by RRs (97). In prokaryotes, RRs are usually the last components of signaling pathways, directly effecting the responses. Most of the RRs contain output domains that can be categorized into nucleic acid binding, enzymatic, and protein/ligand binding domains (93). Eukaryotic RRs are often intermediates linking TCSs to common eukaryotic mitogen-activated protein (MAP) kinase cascades or cyclic nucleotide second messengers (98). HKs are coupled to a diverse array of sensory domains, enabling to sense a wide variety of stimuli, including small molecules, light, turgor pressure, cell envelope stress, redox potential, and electrochemical gradients. The sensory domains are usually located N-terminal to the kinase core and share little primary sequence similarity. Stimuli are sensed by these domains either directly or indirectly through protein-protein interactions with auxiliary proteins. Nearly 33% of HKs contain at least one PAS domain, which can bind small ligands and sense changes in light, oxygen, redox potential, and the overall energy level of a cell. PAS is an acronym based on the names of three proteins, some also acronyms, in which it was first discovered: (I) period circadian protein (Per), (II) aryl hydrocarbon receptor nuclear translocator (ARNT) protein and (III) single-minded protein (Sim) (99, 100). Another family of small-molecule binding domains, the GAF domain (101), is present in ~9% of all HKs. Again, the GAF acronym is derived from the names of the first three classes of proteins recognized to contain this domain: mammalian cGMP-binding phosphodiesterase (PDE), Anabaena adenylyl cyclase, and formate hydrogen lyase system activator (FhlA) from *E. coli* (101). Both PAS and GAF domains have rather high sequence variability and structural plasticity, making them versatile signaling domains not only for stimuli recognition but also for signal transduction, due to their propensity for protein-protein interactions (93). The PAS and GAF domains reveal similar structures, characterized by a central anti-parallel beta-sheet that forms the scaffold of a ligand-binding pocket, which can accommodate a variety of small-molecule ligands such as haeme, flavin, cAMP and cGMP (99, 101-105).

The description of the first TCSs included the discovery of crosstalk between nitrogen assimilation and chemotaxis suggesting complex interactions between different regulatory systems and signal integration (106, 107). It is proposed that there is not a fixed number of components in a signal transduction chain but that it can comprise one to three or more components (88). Additionally, it is discussed that TCSs contain additional regulation or signal entry points. A number of auxiliary regulators have been shown to influence the activities of

simple two component signal transduction systems. Among these, many have been demonstrated to influence RR activity by altering phosphorylation status, DNA binding ability, recruitment of RNA polymerase, or simply through protein-protein interactions (94).

2.3.1 Summary of Nilkens et al

Mol Microbiol. 2014 Jan;91(2):381-93. doi: 10.1111/mmi.12464. Epub 2013 Dec 6.

Nitrate/oxygen co-sensing by an NreA/NreB sensor complex of Staphylococcus carnosus.

Nilkens S[1], Koch-Singenstreu M[1], **Niemann V**[2], Götz F[3], Stehle T[2,4], Unden G.[1]

Author information

[1]Institute for Microbiology and Wine Research, Johannes Gutenberg University of Mainz, Germany Electronic address: unden@uni-mainz.de.

[2]Interfaculty Institute of Biochemistry, Universität Tübingen, Hoppe-Seyler-Strasse 4, D-72076 Tübingen, Germany.

[3]Interfaculty Institute of Microbiology and Infection Medicine, Universität Tübingen, Auf der Morgenstelle 28, D-72076 Tübingen, Germany.

[4]Department of Pediatrics, Vanderbilt University School of Medicine, Nashville, TN 37232, USA

Staphylococci are facultative anaerobic organisms, able to respire in the absence of oxygen by using nitrate as final electron acceptor. Genes encoding for nitrate reductase (*narGHIJ*) are under control of the NreABC regulatory system. NreBC appears as a TCS, in which NreB serves as oxygen sensor HK and NreC as cognate RR. Phosphorylated NreC-P binds to the *narGHIJ* promoter and induces expression. Results of bacterial adenylate cyclase two-hybrid (BACTH) system and histidine protein interaction experiment (HPINE) reveal *in vivo* interactions between NreB and NreA, between NreB and NreC, but not between NreA and NreC. Gel shift assays with NreA and the *narG*-promoter sequence do not indicate an interaction, neither in the presence nor in absence of nitrate. Additionally, the effect of NreA on NreB phosphorylation depending on nitrate was monitored with radiolabeled [^{33}P] under anaerobic conditions. The nitrate sensor NreA modulates kinase activity of the oxygen sensor NreB. In the absence of nitrate, NreA inhibits NreB phosphorylation, whereby in the presence of nitrate NreA does no longer inhibit phosphorylation of NreB. In accordance with these data, the nitrate binding deficient NreA variant Y95A permanently inhibits phosphorylation of NreB. However, dephosphorylation rates of NreB-P are not affected by wild type NreA or NreA Y95A, independent of nitrate availability. Therefore, NreA has no phosphatase activity and does not stimulate such an activity.

A Reporter gene system with a lipase gene under control of the *narG* promoter provides quantitative expression data in dependence of the presence of oxygen and nitrate. In a wild-typic genetic background for NreABC, the absence of oxygen increases reporter gene-expression slightly and the presence of nitrate increases expression further to maximum level. In an *nreABC* knock out strain, the reporter gene activity remains very low under all conditions. The slight *narG* induction upon anaerobiosis in an *nreA* knock out strain is comparable to the

wild type but here the presence of nitrate does not further increase expression. The overexpression of NreA results in a stronger inhibition of *narG*-reporter gene expression under aerobic conditions and in the absence of nitrate. The Y95A mutant of NreA is deficient to bind nitrate and thus inhibits even in the presence of nitrate.

In conclusion, *in vivo* and *in vitro* experiments show that NreA interacts physically and functionally with NreB in a nitrate dependent manner. NreA acts as negative regulator inhibiting kinase activity of NreB in the absence of nitrate. However, when nitrate is supplied, its presence is integrated by NreA into the two component oxygen response system NreBC. Therefore, NreAB represents a regulatory system in which two biochemically different stimuli are integrated in the regulation of gene expression required for anaerobic respiration.

Contribution to this work:

I was involved in writing and prove reading of the manuscript Nilkens et al.

2.3.2 Summary of Niemann et al

J Mol Biol. 2014 Apr 3;426(7):1539-53. doi: 10.1016/j.jmb.2013.12.026. Epub 2013 Dec 31.
The NreA protein functions as a nitrate receptor in the staphylococcal nitrate regulation system.
Niemann V[1], Koch-Singenstreu M[2], Neu A[3], Nilkens S[2], Götz F[4], Unden G[5], Stehle T[1,6].

Author information
[1]Interfaculty Institute of Biochemistry, Universität Tübingen, Hoppe-Seyler-Strasse 4, D-72076 Tübingen, Germany.
[2]Institute for Microbiology and Wine Research, Universität Mainz, Johann-Joachim-Becherweg 15, D-55128 Mainz, Germany.
[3]Max Planck Institute for Developmental Biology, Spemannstrasse 35, D-72076 Tübingen, Germany.
[4]Interfaculty Institute of Microbiology and Infection Medicine, Universität Tübingen, Auf der Morgenstelle 28, D-72076 Tübingen, Germany.
[5]Institute for Microbiology and Wine Research, Universität Mainz, Johann-Joachim-Becherweg 15, D-55128 Mainz, Germany. Electronic address: unden@uni-mainz.de.
[6]Department of Pediatrics, Vanderbilt University School of Medicine, Nashville, TN 37232, USA. Electronic address: thilo.stehle@uni-tuebingen.de

In the absence of oxygen, Staphylococci are able to use nitrate as final electron acceptor in an alternative respiration chain. The nitrogen response elements are composed of a two component system NreBC, acting in concert with the nitrate sensor NreA to modulate the expression of nitrate reductase (*narGHIJ*). In the absence of oxygen, the HK NreB is phosphorylated and the phosphoryl group is subsequently transferred to NreC, in that way enhancing its binding to the *narGHIJ*-promoter. Maximum *narG*-expression is only achieved under anaerobic conditions combined with nitrate supply. In the absence of nitrate NreA inhibits phosphorylation of NreB, thus rendering NreA as a negative regulator. To obtain structural insights into the nitrate sensing mechanism of NreA, crystal structures of NreA with bound iodide or nitrate were solved at 2.2 Å and 2.35 Å resolution, respectively. NreA exhibits a GAF domain fold that is a common structure in biological systems as they provide a robust scaffold for small ligand binding. Both ligands, iodide and nitrate, are bound in the same mainly hydrophobic binding pocket and are completely shielded from the solvent. Negative charge of the ligand is partly compensated by a helix dipole moment. Mutagenesis of residues contributing to ligand binding were used to further elucidate the role of NreA as a negative regulator. Based on the structural knowledge, conservative mutations such as Y95L or W45F were introduced, in which the biochemical and structural character of the amino acids are kept and functionality should be maintained. In contrast, drastic changes such as Y95A and W45A should diminish hydrophobic interactions and ligand binding. With isothermal titration calorimetry (ITC), the affinity of NreA wild type and mutants to nitrate were determined. Wild

type NreA binds nitrate with a dissociation constant (K_D) in the low micromolar range. Mutations decreased the affinity depending on how drastic the introduced changes were. Almost identical circular dichroism (CD) spectra of NreA-mutants compared to the wild type reveal that the mutations do not disturb the overall fold. Protein stability of mutants in comparison to wild-typic NreA were determined by recording melting curves at a prominent minimum in the corresponding CD-spectrum. Only minimal changes in the melting temperatures of the NreA variants allow to correlate the mutations in the binding pocket with ligand binding and eventually with *in vivo* data. A Lipase reporter gene assay was used to describe the influence of NreA-mutants on *narG*-expression *in vivo*. Minor changes in the binding pocket of NreA, which only slightly reduce the affinity to nitrate, exhibit wild-typic expression levels of *narG*. However, drastic changes in the binding pocket leading to a stronger decrease in nitrate affinity, are exhibiting a nitrate independent expression of narG *in vivo*. In combination, the *in vitro* and the structural data of NreA provide important insights into the effect of nitrate binding in the NreABC regulation system.

My contribution this work:

Experiments including mutagenesis, purification, CD-spectroscopy, crystallization, data collection, phase determination, model building and refinement as well as structural analysis and interpretation were performed by myself. Text, tables and figures describing structural data and *in vitro* experiments were written or prepared by myself.

2.4. Outlook

The regulation of anaerobic respiration is well described. The exact mechanism by which the only GAF domain protein NreA inhibits NreB phosphorylation in the absence of nitrate remains unclear. Indeed, a direct interaction between NreA and NreB is known to take place *in vivo*. Interaction studies *in vitro* or even solving NreAB complex structures would be interesting but challenging projects. The purification of NreB with an oxygen labile iron sulfur cluster in the input domain would require special equipment for this approach. Interaction studies between NreA and only the kinase domain of NreB could provide first insights into where and how regulation occurs. The only drawback of this experiment would be the absence of a control enabling the interpretation of a negative result. Still, the question remains if NreA interacts with the input domain of NreB by forming a PAS-GAF-domain complex, or if NreA binds to the kinase domain, interfering with kinase activity or phosphoryl group transfer.

Nitrate as nitrogen source is a limiting factor for plant growth. The nodulation-specific NIN proteins are involved in nodule organogenesis and rhizobial infection under nitrogen starvation conditions. Arabidopsis NLP7 (NIN-like protein 7) in particular is a major player in the primary nitrate response (108). Based on sequence analysis, it is proposed that a GAF domain acts as the nitrate binding site in NLP7. In the group of Anne Krapp (Paris, France) chimera will be cloned where the only GAF-domain protein NreA replaces the predicted GAF domain in NLP7. Furthermore, based on sequence comparisons between different NLPs and NreA, amino acids were predicted to be involved in nitrate binding in NLP7. Mutations abolishing binding, comparable to Niemann et al, may support the investigation of NLPs.

3. MurT/GatD

3.4. Staphylococcus cell wall

Peptidoglycan (PG) or murein is an essential and specific component of the bacterial cell wall found on the outside of the cytoplasmic membrane of almost all bacteria. The main structural features of PG are linear glycan strands cross-linked by short peptides (Figure 4) (109-111). The general architecture and morphology of the bacterial cell envelope provides the basis to distinguish two mayor groups of microorganisms. In 1884 Hans Christian Gram developed the Gram staining method, which allows to distinguish between Gram-positive and Gram-negative bacteria. On the basis of differential staining with a crystal violet-iodine complex and a safranin counterstain, the cell walls of Gram-positive organisms retain this complex after treatment with alcohol and appear purple, whereas Gram-negative organisms decolorize following such treatment and appear pink (112). In Gram-positive bacteria a PG sacculus composed of up to forty layers of glycan strands form the outermost part of the cell. In Gram-negative bacteria this mostly single layered macro-molecule is located within the periplasm between the cytoplasmic membrane and the outer membrane. In Gram-positive bacteria the stain is retained in a 40 – 80 nm thick multilayer sacculus since it is approx. ten times thicker compared to the Gram negative cell wall (7, 113, 114).

However, PG is a continuous covalent macromolecular structure found exclusively in eubacteria (113). Its main function is to preserve cell integrity by withstanding the internal osmotic pressure. It is also responsible for the maintenance of a defined cell shape and is intimately involved in the cell division process (110). Sacculi can be isolated in their intact structure but never in their native three-dimensional shape, which inevitably is lost when the cellular pressure is released. Nevertheless, isolated sacculi reflect the specific shape of the cell from which they have been prepared. This illustrates that the murein sacculus maintains the morphology of the bacterium. Unfortunately, until now it has

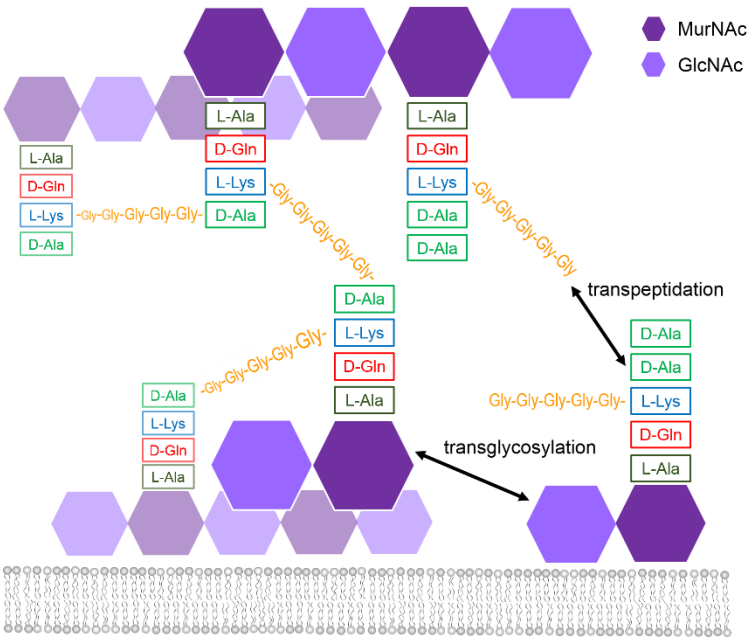

Figure 4 **Schematic representation of the cell wall cross-linking in staphylococci.** The glycan strands of GlcNAc and MurNAc are linked by β1,4 glycosidic bonds. This strands are cross linked by a pentaglycine inter peptide bridges connecting the stem peptides of different glycan strands.

not been possible to obtain a detailed image of the structure. Thus, it is still not known how the threads in the net are arranged with respect to the overall shape of the sacculus. Moreover, it is still uncertain whether some kind of order exists at all. On the other hand, the chemical composition of the cell wall is well known. The glycan strands are made up of alternating N-acetyglucosamine (GlcNAc) and N-acetylmuraminic acid (MurNAc)
residues linked by β1,4 glycosidic bonds. A flexible stem peptide composed of five amino acids crosslinks the glycan strands. The pentapeptide is attached to the D-lactoyl group of each MurNAc residue. A certain degree of variation exists either in the peptide stem or in the position or composition of the interpeptide bridge (Table 2) (113).

Cross-linking of the glycan strands generally occurs between the carboxyl group of D-Ala at position four and the amino group of the diamino acid at position three, either directly or through a short peptide bridge (109). In *S. aureus* the primary peptide chain has the sequence L-Ala-D-Glu-L-Lys-D-Ala-D-Ala with a glycine interpeptide bridge attached to the ε-amino group of L-lysine. Cross-links are formed by a transpeptidase reaction in which a terminal D-alanine is lost from one primary chain and the sub-terminal D-alanine becomes linked to the free amino group of a pentaglycine bridge (Figure 4) (115). In exponentially grown cells in rich medium, more than 80% of the subunits are crosslinked in *S. aureus*. The extremely high degree of crosslinking is only possible because their long and flexible pentaglycine interpeptide bridges are able to span distances between peptides otherwise much too far apart to be crosslinked (7). Although variations in the PG structure mainly affect the peptide fraction, modifications of the glycan strand, such as acetylation of the MurNAc C6 hydroxyl group, have also been reported (116). To date, this modification has been found in *S. aureus* and only few other human pathogens (117). The additional acetyl group renders these bacteria resistant against lysozyme cleavage. This modification is important since it does not only prevent cell lysis, but also results in a reduced host response due to a decreased release of immune-stimulatory PG fragments (117). The PG of staphylococci is also exceptional as apart from small proportion of residual uncross-linked primary pentapeptide side chains, it has almost no free carboxyl groups since the D-glutamic acid α-carboxyl group is amidated (7, 116).

S. aureus also provide an example of the second type of PG modifications, the presence of O-acetyl substituents on N-acetymuramic acid residues. In this organism 50% of the muramic acid residues are present as the 4-N, 6-O-diacetylderivative (116).

Table 2 Amino acid variation in the stem peptide

Position	Residue encountered	Examples
1	L-Ala	*Most bacteria*
	Gly	*Mycobacterium leprae, Brevibacterium imperiale*
	L-Ser	*Butyribacterium rettgeri*
2	D-Isoglutamine	*Most Gram-positive species, Mycobacteria*
	Threo-3-Hydroxyglutamate	*Microbacterium lacticum*
3	Meso-A2pm	*Most Gram-negative species, Bacilli, Mycobacteria*
	L-Lys	*Most Gram-positive species*
	L-Lys/L-Orn	*Bifidobacterium globosum*
	LL-A2pm	*Streptomyces albus, Propionibacterium petersonii*
	L-2,4-Diaminobutyrate	*Corynebacterium aquaticum*
	L-Homoserine	*Corynebacterium poinsettiae*
	L-Ala	*Erysipelothrix rhusiopathiae*
	L-Glu	*Arthrobacter J. 39*
	Amidated meso-A2pm	*Bacillus subtilis*
	L-5-Hydroxylysine	*Streptococcus pyogenes*
	Nγ-Acetyl-L-2,4-diaminobutyrate	*Corynebacterium insidiosum*
4	D-Ala	*All bacteria*
5	D-Ala	*Most bacteria*
	D-Ser	*Enterococcus gallinarum*
	D-Lac	*Lactobacillus casei, Enterococci with acquired resistance to Vancomycin*

Table is adapted from Vollmer *et al.* 2008

3.5. Biosynthesis of peptidogyclan

The PG biosynthesis in Staphylococcus, as in other bacteria, takes place in the cytoplasm at the membrane and ends with the assembly of the PG precursor in the nascent cell wall envelope (Figure 5) (110). The enzymes MurA and MurB convert uridine diphosphate-N-acetyglucosamine (UDP-GlcNAc) to uridine diphosphate-N-acteylmuramic acid (UDP-MurNAc). Compared to Gram negative microorganisms, Gram-positive bacteria have two distinct *murA*-genes encoding for UDP-N-acetylglucosamine enolpyruvyl transferases. X-ray structures of MurA are known with bound natural substrate and the drug Fosfomycin, a phosphoenolpyruvate analog covalently linked to the cysteine residue in the active site. MurA-stuctures reveal a two-domain protein with an unusual fold composed of an inside out alpha/beta barrel, which is built up from the sixfold repetition of one folding unit**.** MurA catalyzes

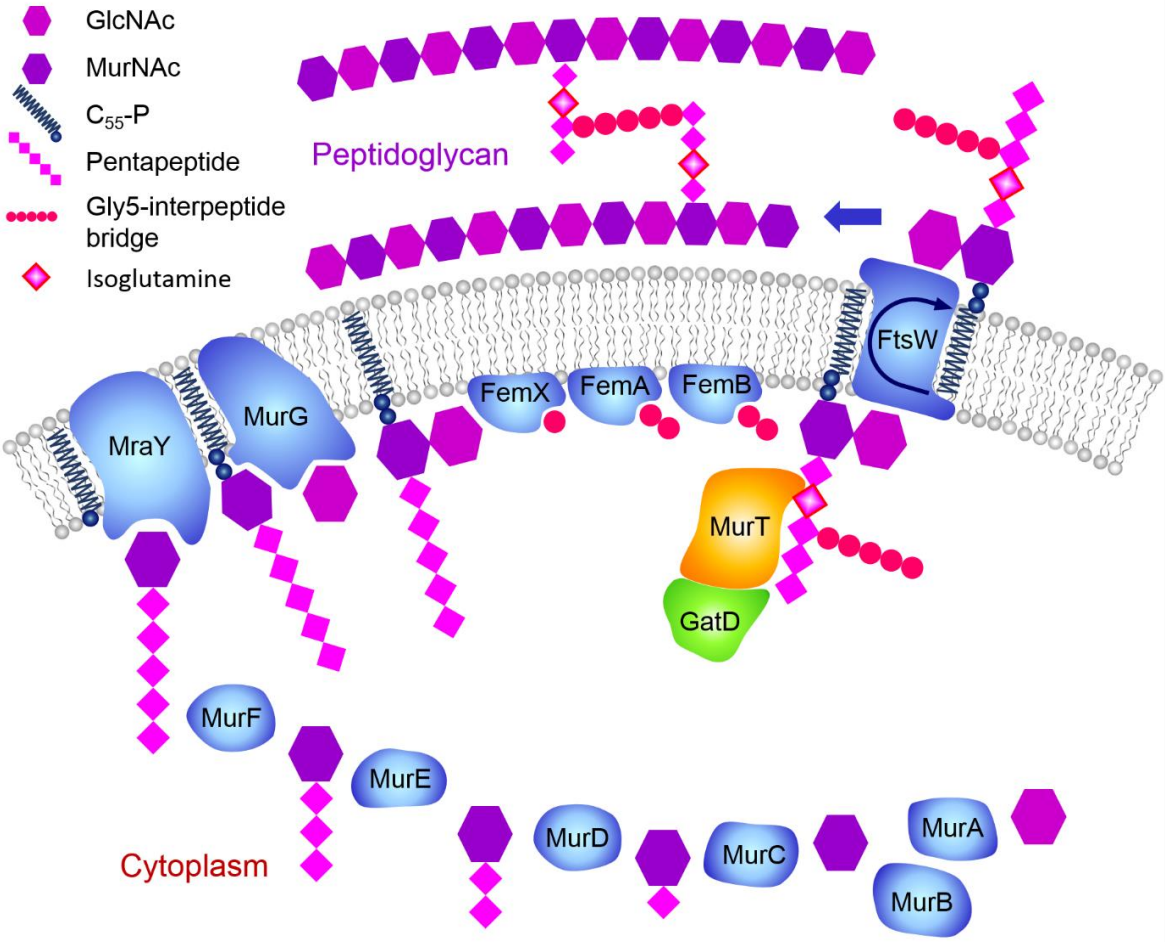

Figure 5 **Model of peptide glycan biosynthesis**. MurAB and the ligases MurC-F accomplish the synthesis of the soluble peptidoglycan precursor UDP-MurNAc-pentapeptide in the cytosol. The membrane anchored bactoprenol accepts the soluble precursor and MurG adds GlcNAc, resulting in Lipid II. FemXAB catalysis the addition of the Gly_5-interpeptide bridge. MurT/GatD enzyme complex amidates the iso-glutamate at the second position of the pentapeptide. The Peptidoglycan precursor is flipped over the membrane where it is inserted in the nascent peptidoglycan.

Figure is adapted from Münch *et al.* 2012.

the transfer of phosphoenolpyrovate (PEP) to the hydoxyl at carbon 3 of UDP-GlcNAc, resulting in enolpyruvyl UDP-GlcNAc. (118-122). Subsequently, the pyruvyl moiety is reduced to a lactyl group with NADPH to UDP-MurNAc by the flavoprotein UDP-N-acetylpyruvylglucosamine reductase MurB. Structure comparisons suggests that MurB exist in at least two distinct classes, type I MurB of *E. coli* and type II MurB of *S. aureus*, with differences in the construction of the substrate binding domain as well as substrate binding itself (122-125). MurCDEF are four ATP-dependent amino acid ligases that catalyze the stepwise addition of L-alanine, D-glutamate, L-lysine and finally the dipeptide D-alanyl-D-alanine onto UDP-MurNAc (Figure 6) (126-128). The first step, the addition of L-alanine to the lactyl group of UDP-MurNAc is carried out by MurC. With each step the polypeptide tail is growing longer and so the active sites of the Mur-ligases have to be specific ensuring that the terminal carboxylate group is positioned close to the ATP for activation (122). Nonetheless, all four Mur-ligases reveal a similar composition of three domains. The N-terminal domain is primarily responsible for UDP-MurNAc substrate binding and resembles a Rossmann fold. A central domain consisting of an ATP binding domain exhibit similarities to ATPases and GTPases. The C-terminal domains are most probably associated with binding of the incoming amino acid (Figure 6) (129).

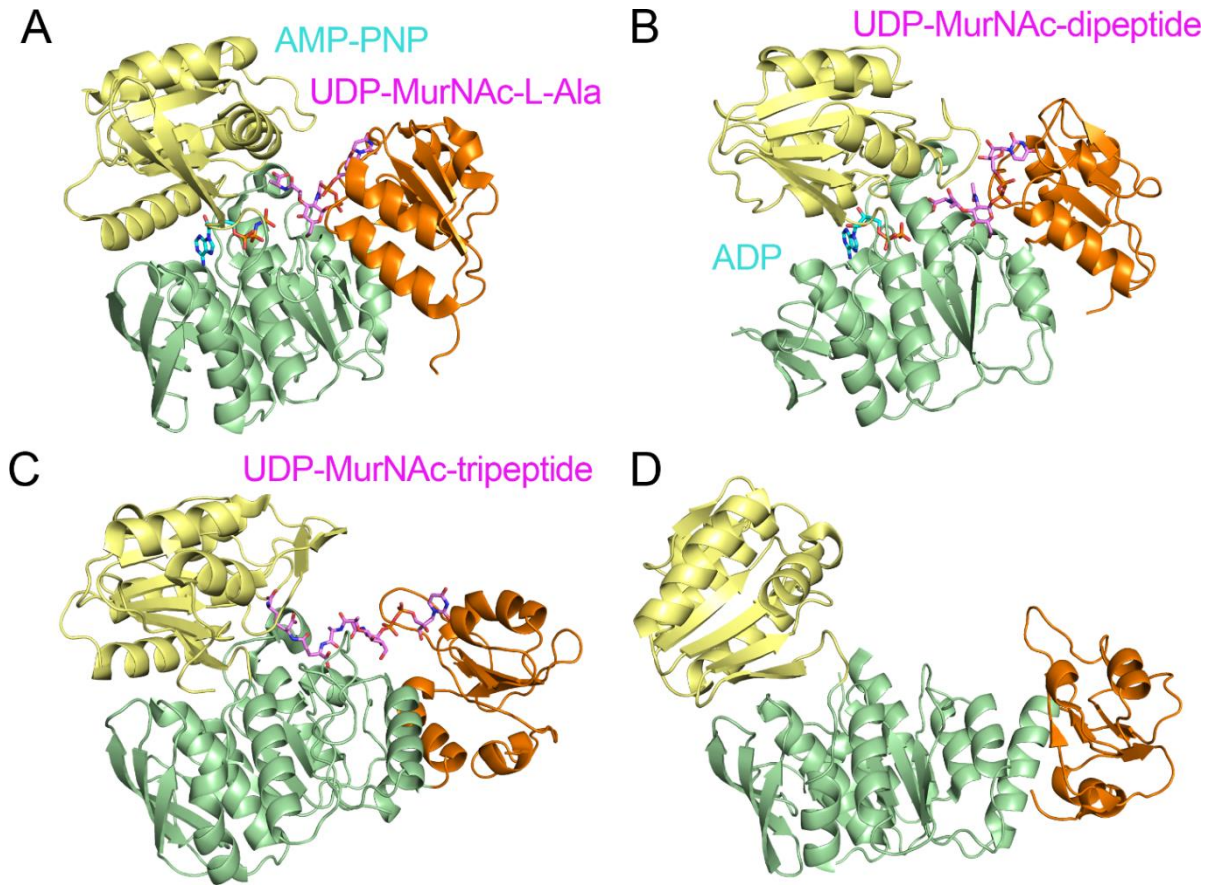

Figure 6 **X-ray structures of the Mur-ligases MurC, MurD, MurE and MurF**. The N-terminal domains of all the Mur ligases are represented in yellow, central domains in green and C-terminal domains in orange. **A:** MurC-structure resolved to 1.7 Å along with its UDP-MurNAc-L-Ala product (pink) and the non-hydrolysable ATP analogue AMP-PNP (cyan) (Mol *et al*., 2003). **B:** MurD-structure resolved to 1.7 Å with its UDP-MurNAc-L-Ala-D-Glu product (pink) and AMP (cyan) (Bertrand *et al*., 1999). **C:** MurE-structure resolved to 2 Å with its UDP-MurNAc-L-Ala-D-Glu-mA2pm product (cyan) (Gordon *et al*., 2001). **D:** MurF-structure resolved to 2.3 Å in its 'open' substrate-free conformation (Yan *et al*., 2000). Crystal structure co-ordinates were retrieved from the Protein Data Bank (http://www.rcsb.org/pdb/): MurC, 1P3D; MurD, 2UAG; MurE, 1E8C; MurF, 1GG4

The following steps of the PG synthesis are catalyzed by integral membrane proteins (Figure 7). The cytosolic UDP-MurNAc-pentapeptide is transferred by the prenyl sugar transferase MraY onto an undecaprenol phosphate carrier also known as bactoprenol (C_{55}-P) whereby UMP is released. The product of the MraY-reaction is commonly named Lipid I and is anchored in the membrane on the cytoplasmic site (126, 130, 131). It has been estimated that there is a low abundance of Lipid I in the cell (700 molecules/cell). Therefore a reaction coupling between MraY and MurG has been proposed (132). The glycosyltransferase MurG transfers GlcNAc from UDP-GlcNAc to the hydroxyl at carbon 4 of the lipid-linked MurNAc-pentapeptide (Lipid I), resulting in Lipid II. The formation of the β-1,4 glycosidic bond follows an ordered Bi-Bi mechanism in which the donor

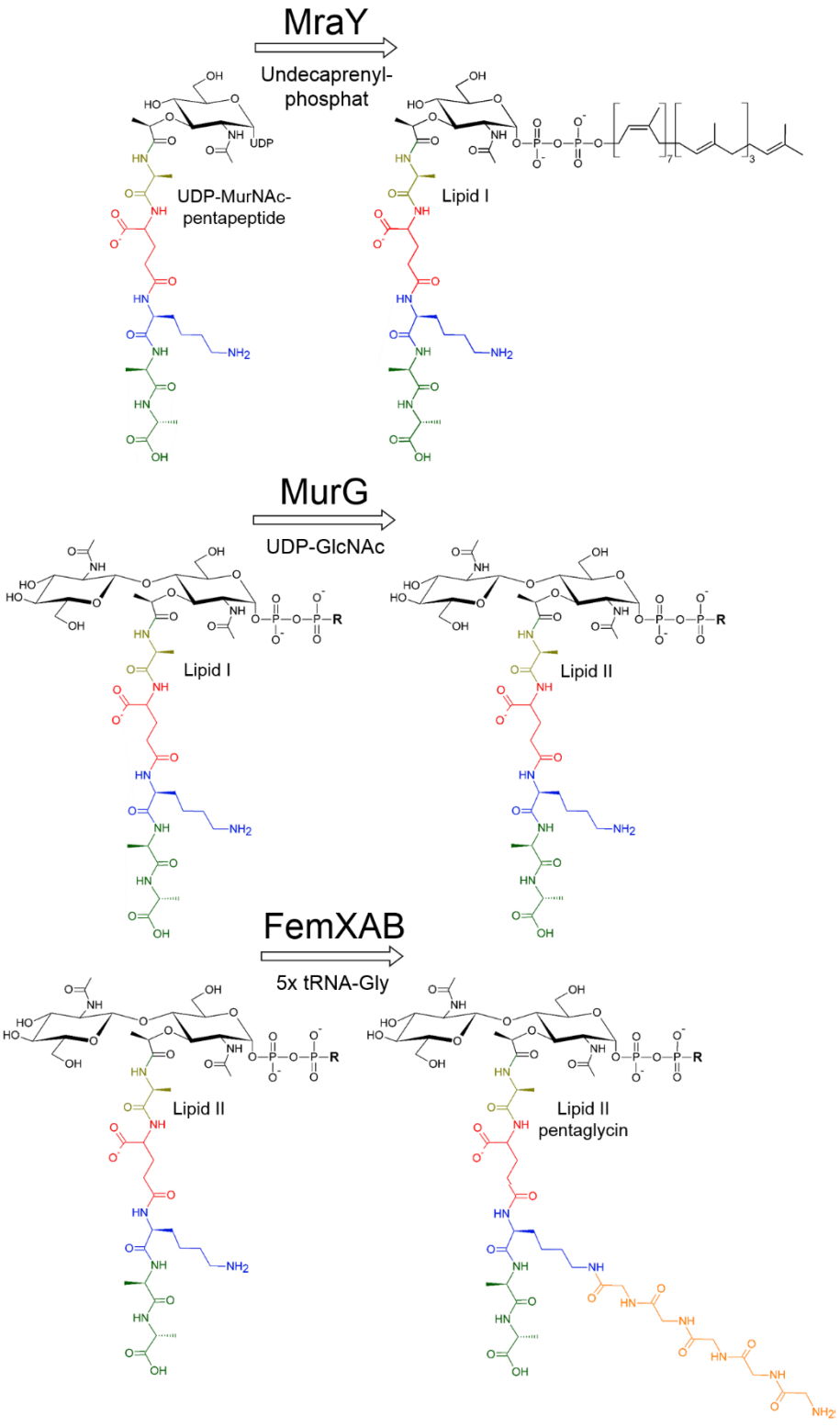

Figure 7 **Chemical structures of membrane bound cell wall precursor**. MraY couples UDP-MurNAc-pentapeptide to Undecaprenol-phosphat resulting in Lipid I. Subsequently MurG transfers UDP-GlcNAc to sugar moiety of Lipid I. The product, Lipid II is substrate for FemXAB which adds the pentaglycin crossbridge on the epsilon amino group of the pentapeptide lysine side chain. **R:** Undecaprenyl-moiety

UDP-GlcNAc binds first, followed by the acceptor Lipid I (126, 133, 134). The presence of a pentaglycine crossbridge connection of stem peptides in the PG network is common in Gram-positive bacteria. The catalytic mechanism of how the pentaglycine crossbridge is added to Lipid II remains unclear despite several X-ray structures of the transmembrane enzymes FemABX are available (126, 135, 136). The final cytoplasmic reaction in the PG synthesis is the amidation of the carboxyl group of isoglutamate in the stem peptide. It is proposed that the membrane bound FtsW acts as flippase and shuttles the PG precursor to the outer side of the membrane. After release form bactoprenol, a family of D,D-transpeptidases and D,D-carboxypeptidases, the so-called penicillin-binding proteins (PBPs), introduce the GlcNAc-MurNAc-pentapeptide into the growing cell wall (111).

3.6. Amidation of Lipid II

To successfully infect an organism, a pathogen has to breach several defense mechanisms of the host. The first line the pathogen has to conquer is the host's surface. Here, it must overcome the constitutive or innate defense system and the host's phagocytic response. Body fluids and tissues of animals naturally contain bactericides, a variety of anti-microbial substances that kill microbes or that inhibit their growth. Lysozyme is one of the most important and widespread compounds of the constitutive defense. This enzyme cleaves the β-1,4 glycosidic bond between N-acetylmuramic acid (MurNAc) and N-acetylglucosamine (GlcNAc) of bacterial cell walls. Lysozyme is produced by various tissues such as mucous membranes, the lower respiratory tract, or intestinal tract. During infection the concentration of lysozyme is increased in body fluids, such as serum, saliva, sweat, and tears (137). To hinder lysozyme action, the basic structure of *S. aureus* PG is known to undergo at least two major secondary modifications: O-acetylation of the free OH-groups in the glycan strand, and amidation of the carboxyl group of D-isoglutamate, the second residue of the stem peptide, (Figure 8). These modifications result in the formation of D-isoglutamine. O-acetylation of the *S. aureus* PG confers lysozyme resistance to the bacteria (137, 138). Amidation of the stem peptide is frequent among Gram-positive bacteria. However, the physiological roles of this chemical modification have remained a matter of speculation (109). Characteristically, the PG of *S. aureus* is extensively crosslinked, with up to 80% of the stem peptides interconnected (139, 140). A mutant that is unable to amidate PG shows a severely reduced growth rate, but also decreased resistance to beta-lactam antibiotics and to lysozyme hydrolysis. The reduced growth rate suggests that an amidated PG may provide better substrates for proteins that catalyze PG biosynthesis and cell division. Lack of the amide group may create an imbalance between the synthetic and hydrolytic machineries of the cell since for crosslinking of stem peptides at least one of the substrates has to be amidated (138, 141).

In *S. aureus* COL a small operon composed of two genes, *murT* and *gatD,* was identified to be responsible for the conversion of isoglutamic acid to isoglutamine in the stem peptide of PG precursor Lipid II. The amino acid sequences of the gene products MurT and GatD show similarity to Mur-ligases and to CobB/CobQ-like glutamine amidotransferases (GATases) respectivly (138). GATases are responsible for the incorporation of nitrogen into amino acids, amino sugars, purine and pyrimidine nucleotides, coenzymes, and antibiotics (142). Amidotransferases or transamidases can be distinguished from the aminotransferases or transaminases, which catalyze the pyridoxal- 5'-phosphate-dependent transfer of the α-amino nitrogen from amino acids to α-keto acids (143). GATases catalyze the reaction without the utilization of cofactors or hydrolysis of ATP. However, for some GATases a preliminary

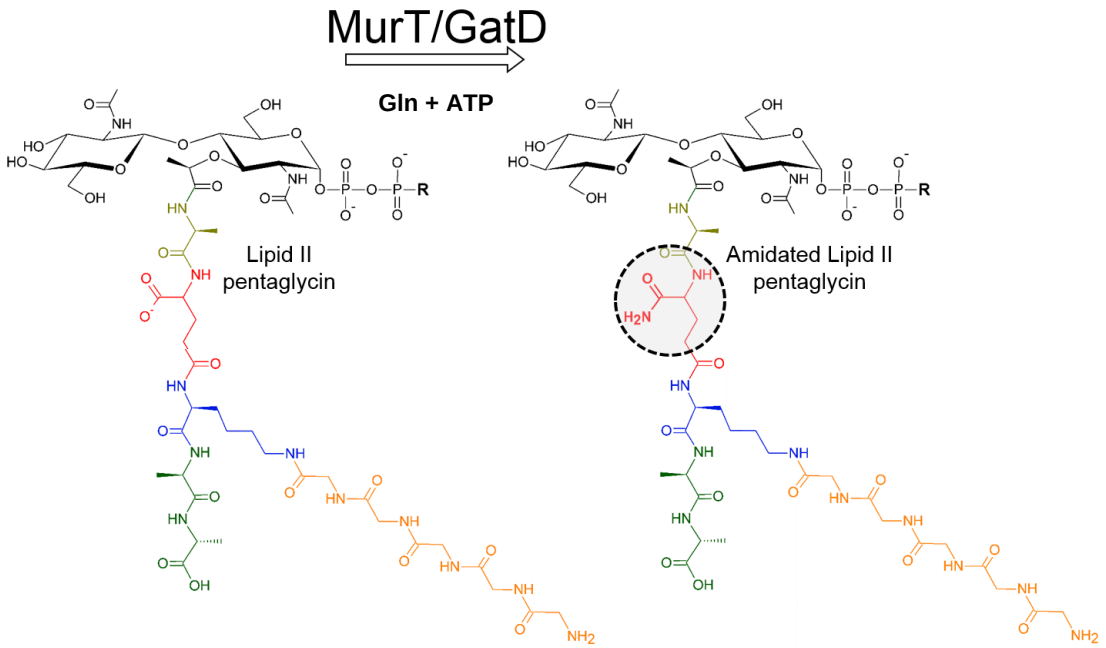

Figure 8 **Chemical structures of the substrate and product of MurT/GatD enzyme complex.** The cytosolic glutamine amidotransferase is composed by the Class-I type glutaminase GatD and the Mur-ligase MurT. Glutamine acts as amino donor. In an ATP dependent reaction the carboxyl group at the second position of the stempeptide of Lipid-II is amidated (dashed circle). **R**: Undecaprenyl-moiety

activated acceptor substrate with the expense of one molecule of ATP is required (144). GATases consist of at least two globular domains or subunits, a glutaminase (GAT) and a synthase domain. Hydrolysis of glutamine in the GAT domain yields ammonia, which is transferred to a synthase (or ATP-dependent synthetase) domain specific acceptor substrate through a channel, which is usually 10–40 Å long. Since this channel is solvent-inaccessible NH_3 release and the formation of non-reactive ammonium ions are prevented, which would have toxic side effects within the cell. These ammonia channels are predominantly formed by the synthase domain and their formation has been shown to also require the presence of the acceptor substrate in most GATases (142).

The amidotransferase reaction is initialized by the thiol-group of a conserved cysteine residue of GAT, which conducts a nucleophillic attack on the δ-carbonyl group of the glutamine substrate to form ammonia. After being transferred through the channel ammonia acts as a nucleophile on an NH_3 acceptor substrate, which is bound to the synth(et)ase domain (142, 145). GATs and synth(et)ase domains can be distinguished in the primary sequence of every GATase, but their relative structural arrangement is highly variable (143, 144). Depending on the active site residues, GATases are categorized into different classes: Class I or triad GATs use histidine and glutamate residues for the activation of the cysteine thiol-group. In contrast, the main characteristic of Class II GATs is the specific location of the catalytic cysteine at the amino terminus of the peptide chain, which determines the name N-terminal nucleophile (Ntn)

GATs. In addition, several other GATs exist, which could not be aligned with either groups. Most triad GAT domains share a common open α/β structure fold, whereas Ntn GAT domains are mainly composed of antiparallel β-sheets and assemble into homooligomers (142, 144). Comparisons of the primary sequences of GAT domains revealed that typical Class I GAT domains are about 200 residues long and include three conserved regions that contain an invariant glycine residue in each (143, 144). The 243 amino acid GatD protein involved in stem peptide amidation in *S. aureus* can be categorized as a Class I-type GAT domain. Furthermore, GatD carries a conserved cysteine and histidine residues of the Class I-type GAT domain. However, a conserved glutamate is missing to complete the catalytic triad, while a glycine residue of unknown function appears highly conserved (140, 146). Together MurT and GatD provide all domain functions required to catalyze the amidation reaction of the PG precursor. It was shown that MurT could substitute the ATP-dependend formation of UDP-MurNAc-tripeptide catalyzed by the Mur-ligase MurE. MurT exhibits a typical Mur-ligase central domain including the ATP binding motif and may be responsible for the recognition of the acceptor substrates (140).

Four distinct steps for the Class I-type GAT reaction mechanism have been proposed in case all substrates are bound by the GATase (Figure 9). First, a nucleophillic attack of the catalytic cysteine residue (GAT) on δ-carbonyl carbon of glutamine leads to formation of a tetrahedral intermediate, whose negative charge is stabilized by an oxyanion hole. The acceptor substrate might be activated by utilizing ATP. Secondly, the collapse of the tetrahedral intermediate leads to the formation of native ammonia after abstraction of a proton by the histidine residue (GAT). A covalent γ-glutamyl enzyme thioester adduct is formed. In the third step, a water molecule attacks the thioester adduct, leading to the formation of a second tetrahedral intermediate. In the meantime, native ammonia is transferred to the acceptor site and attacks the electrophilic group of the acceptor substrate. In case of MurT/GatD this would be the carboxyl group of isoglutamate of Lipid II. The final step at the GAT-site regenerates the catalytic cysteine residue by the collapse of the second tetrahedral intermediate and release of glutamate. The aminated product occurs at the acceptor site (144).

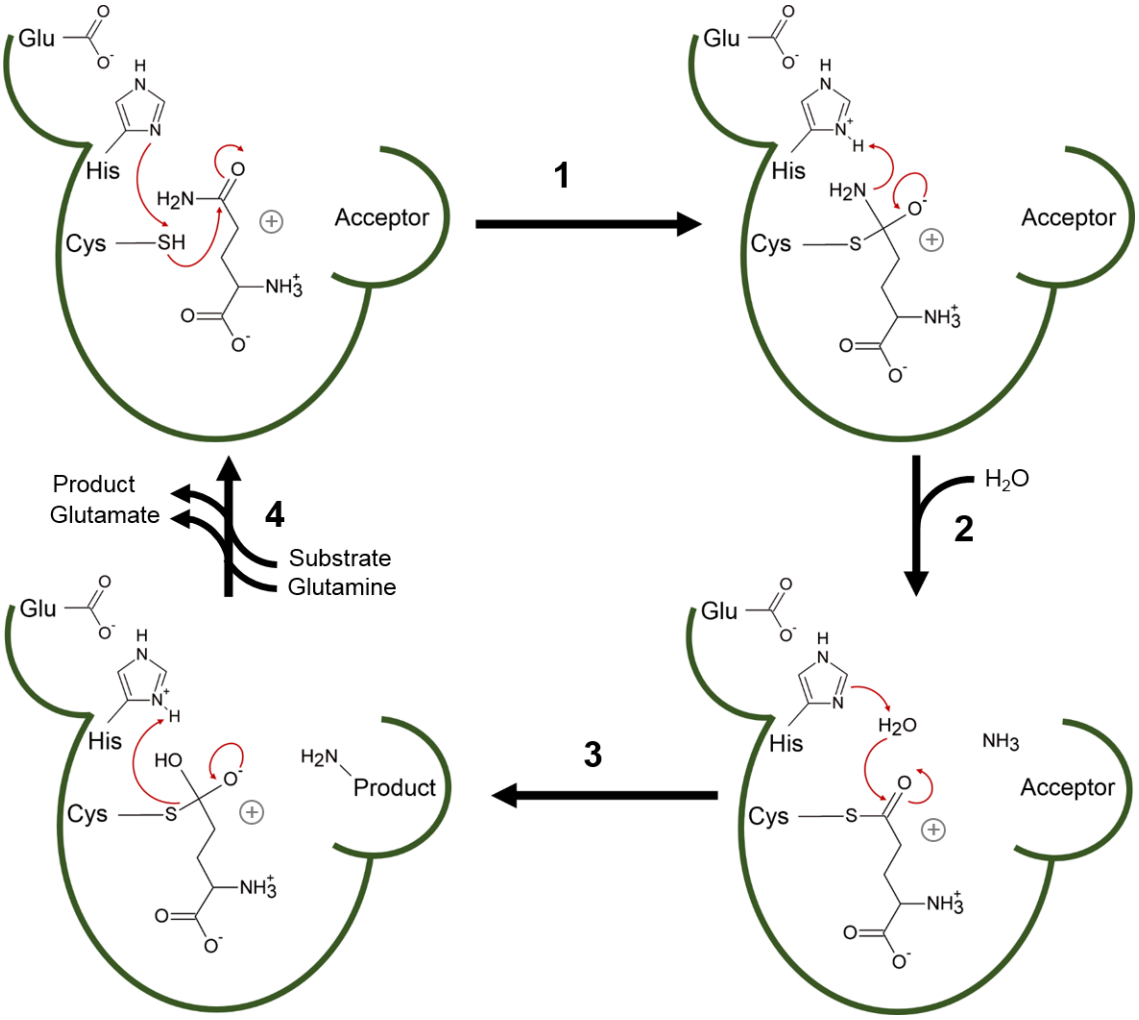

Figure 9 **Proposed catalytic mechanism for glutamine-dependent amidotransferases**. After the amino acceptor substrate and glutamine as amino donor have bound four distinct reaction steps lead to an amidated product. The basic character of histidine enhances the nucleophilic character of the catalytic cysteine that attacks at the δ carbonyl carbon of glutamine leading to a tetrahedral intermediate. An oxyanion hole (+) stabilizes the negative charge of the intermediate. Secondly, the collapse of the tetrahedral intermediate releases ammonia. In step three, a water molecule attacks the thioester intermediate forming a second tetrahedral intermediate. Additionally, the ammonia is transferred to the acceptor site. In the fourth step, the catalytic cysteine is regenerated and glutamate and the amidated product are released.

To regulate the amidation reaction, hydrolysis of glutamine occurs significantly only when the acceptor is bound to the synthase domain, initiating an interdomain signal transduction that activates the glutaminase function. Thus, the active conformation of the glutaminase site is achieved only after acceptor binding. In GATases, flexible loops of the synthase and GAT domains seem to function as gates to give access to the active site by adopting open and closed conformations (142).

3.7. Materials

Equipment

ÄKTA Ettan LC FPLC	GE Healthcare
BioLogic Duo Flow FPLC	BioRad
Centrifuge 5415D	Eppendorf
Centrifuge Haereus multifuge 1 L-R	Thermo scientific
Digital Sonifier	Brandson
Sorvall™ RC 6 Plus super speed centrifuge	Thermo scientific
SLC4000 rotor (Sorvall™ RC 6 Plus)	Thermo scientific
SS34 rotor (Sorvall™ RC 6 Plus)	Thermo scientific
Superdex SD 200 HR 10/300	GE Healthcare
Superdex SD 200 PC 3.2/30	GE Healthcare
UNITRON plus incubation shaker	Infors HT

Consumables

50 000 MWCO Concentrator Vivaspin Turbo 4	Sartorius
50 000 MWCO Concentrator Vivacell 100	Satorius
Filter paper 0.22 mm	Millipore
Ni^{2+}- NTA agarose beads	Qiagen
Spin X Cenrifuge Tube Filter 0.22 µm	Costar
Econo-Pac® Chromatography Column	Biorad
PD Desalting column	GE Healthcare

Chemicals

DL-Dithiothreitol (DTT)	Sigma
Glycerol	Roth
Imidazole	Sigma
Isopropanol	Sigma
Isopropyl-β-D-thiogalactopyroside (IPTG)	PEQlab
Magnesium chloride	Sigma
Monosodium phosphate	Sigma
Polyethyleneglycol (PEG) 8000	Sigma
Potassium chloride	Merck
Sodium chloride	Roth
Tris-(2-carboxyethyl)phosphorine (TCEP)	Sigma
Trizma acid (Tris(hydroxymethyl)aminomethane)	Sigma

Antibiotics and Enzymes

Ampicillin	Sigma
DNase I	Fermentas
Lysozyme	Sigma
Protease complete inhibitor	Roche
RNaseB	Sigma

Media

Luria Both (LB) medium 25 g/L in ddH_2O (autoclaved) Sigma

Solutions

1000 x Ampicillin stock 100 mg/mL in ddH_2O
IPTG stock 1 M in Isopropanol
TCEP stock 0.5 M in Trizma/HCl pH 8.0
DTT stock 1 M in ddH_2O

Buffers

The pH-value of buffers containing Tris were adjusted at 4°C.

SSP-buffer	
10 mM	NaH_2PO_4 pH 7.5
150 mM	NaCl

Lysis-buffer	
50 mM	Trizma/HCl pH 8.5
300 mM	NaCl
10 mM	imidazole

Wash-buffer	
50 mM	Trizma/HCl pH 8.5
300 mM	NaCl
50 mM	imidazole

Elution-buffer “150”	
50 mM	Trizma/HCl pH 8.5
300 mM	NaCl
150 mM	imidazole

Elution-buffer “200”	
50 mM	Trizma/HCl pH 8.5
300 mM	NaCl
200 mM	imidazole

SEC-buffer	
50 mM	Trizma/HCl pH 8.5
500 mM	NaCl
50 mM	$MgCl_2$
5 mM	KCl

3.5 Methods

Construct design

To ensure heterologous expression of an active MurT/GatD enzyme complex in *E. coli* the corresponding operon from *Staphylococcus aureus* N315 was cloned in pET21b vector by Daniela Münch (140). This maintains a polycistronic mRNA with translation of *murT* and *gatD* in an equal stoichiometry for formation of a physiologic heterodimer. For affinity purification, a His_6-tag was added to the C-terminus of the *gatD* gene. For heterologous expression, the plasmid was transformed into *E. coli* BL21. To simplify the expression procedure, a glycerol stock was prepared and stored at -80°C.

Expression

With a pipet tip the frozen bacteria were scratched from the surface of the glycerol stock and were used to inoculate a pre-culture. In order to select for the desired strain, 100 µg/ml Ampicillin (Amp) was added to all LB-cultures described in the following. Furthermore, to avoid contamination the inoculated pre-culture was limited to only 0.5 - 1 ml LB-Amp in an incubation tube. After eight hours cultivation at 35°C at 120 rpm shaking, the culture exhibited visible turbidity. The second pre-culture of 200 ml LB-Amp in a 1 l baffled Erlenmeyer flask was inoculated with the first one and the incubation was continued overnight for approximately 12 hours. The pre-culture was grown into the stationary phase overnight and 40 ml was used to inoculate the main cultures of 1.5 l LB-Amp in a 5 l baffled Erlenmeyer flask. Cultures were grown to an OD_{600} of 0.5 at 35 °C with 80 rpm. For gene expression, IPTG was added to a final concentration of 0.25 mM and the temperature was reduced to 33 °C. After 3 - 4 hours, the cells were harvested by centrifugation (SLC4000 rotor, 7 000 rpm, 20 min, 4°C). After the supernatant had been discarded, the cell pellet was carefully taken out of the centrifuge beakers with a spatula. The pellet was transferred into a 50 ml reaction tube. The remaining cells were resuspended in SSP buffer and were transferred to the 50 ml reaction tube. After centrifugation (Haereus multifuge 1 L-R, 4 000 rpm, 30 min, 4°C) the cleared supernatant was discarded and the pellet was weighed and stored at -20°C until use.

Purification

For each purification, at least 15 g cell pellet were used. 10 ml of lysis-buffer were added to resuspend 1 g cell pellet. A homogeneous suspension was achieved after 30 min of stirring on ice. DNase I (0.1 U/ml final concentration), a small spatula tip of RNase A and 200 µg/ml of lysozyme were added. To protect the target protein from degradation, one complete protease inhibitor tablet (Roche) was added per 50 ml lysate. After 30 min stirring on ice, the cells were disrupted via sonication with 20 kHz and an amplitude of 80 watts. To maintain a low temperature, the cell disruption was performed on ice and in intervals of 360 x (0.5 s on / 2.5 s off). Next, the lysate was centrifuged (SS34 rotor, 10 000 rpm, 10 min, 4°C). For affinity purification, the turbid supernatant was transferred into 50 ml reaction tubes. Before usage, the Ni-NTA agarose beads were washed two times: the slurry was centrifuged (max. 4 000 x g, 2 min), supernatant discarded and the Ni-NTA agarose beads were resuspended in lysis-buffer. Two milliliter of Ni-NTA agarose slurry equals to one milliliter column volume (cv). To avoid a reduced flow through clogging, 1 ml cv was used for 50 ml of lysate. The nickel affinity batch was incubated for 120 min stirring on ice. The Ni-NTA agarose bound target protein complex was pelleted via centrifugation (2 000 x g, 10 min, 4°C). The supernatant was pipetted out carefully without swirling up the pellet containing the target protein complex. The remaining Ni-NTA agarose pellet was resuspended in 30 ml of lysis-buffer with additional 5 mM DTT. Two times 15 ml of Ni-NTA agarose suspension was transferred in a 25 ml gravity flow column. To reduce the losses, low amounts of lysis-buffer were used to take up remaining Ni-NTA agarose from the 50 ml reaction tubes. The Ni-NTA agarose suspension was also transferred to the gravity column. After the Ni-NTA agarose was sedimented, 5 cv lysis-buffer was added as the first on column wash step. To remove non-specifically bound proteins 3 x 5 cv and 3 x 1 cv wash-buffer with 50 mM imidazole were added. To elute the protein complex, 3 x 5 cv and 3 x 1 cv elution-buffer with 150 mM and 200 mM imidazole were added to the column. To ensure that the eluate contains the target protein complex the fractions were analyzed by SDS-PAGE. To remove the imidazole as fast as possible PD 10 desalting columns were used according to the protocol. The MurT/GatD protein complex was transferred to the SEC-buffer containing 5 mM DTT. By this procedure, the volume of the protein solution was increased by 40%. Nevertheless, under these conditions the protein could be stored overnight at 4 °C. The MurT/GatD protein complex was concentrated to maximum 15 mg/ml with 50 ml 50 MWCO concentrators (Sartorius). To avoid aggregation during concentration the force was limited to 500 x g and the centrifugation was interrupted every 10 min to mix the protein sample in the reservoir. Before and after the usage of the concentrators, the membrane was washed with SEC-buffer to remove impurities. The protein solution was filtered with 22 µm pore size before 500 µl per run were subjected to size exclusion chromatography. The superdex 200 10/300 column, installed to a BioRad FPLC system at 4°C, was equilibrated with SEC-buffer

containing 5 mM DTT. The elution fractions were analyzed by SDS-PAGE. Fractions containing the MurT/GatD protein complex with a purity of > 90% were pooled and subjected to size exclusion chromatography. DTT in the SEC-buffer was substituted by TCEP, which is more stable during longtime storage and crystallization.

Crystallization

For crystallization the protein was concentrated to 5.5 mg/ml and applied to a 0.22 µm spin filter. Several commercially available 96 well crystal screens were used to screen for an initial hit. Sitting drop vapor diffusion experiments were performed by a pipetting robot mixing 0.3 µl protein solution with 0.3 µl mother liquor. Crystallization plates were stored at 4° C and 20 °C.

3.6. Results

Based on a protocol established by Daniela Münch at University of Bonn, the expression and purification procedures of MurT/GatD were adapted to the needs of protein crystallization. The *murT/gatD* operon of *S. aureus* was already cloned in pET21b vector and transformed in *E. coli* BL21 (Figure 10). Translation of the polycistronic mRNA resulted in MurT/GatD complex formation *in vivo*. The complex remained stable during cell disruption and Ni-affinity purification (140). The goal was to obtain monodisperse, soluble and >95 % pure protein complex suitable for crystallization.

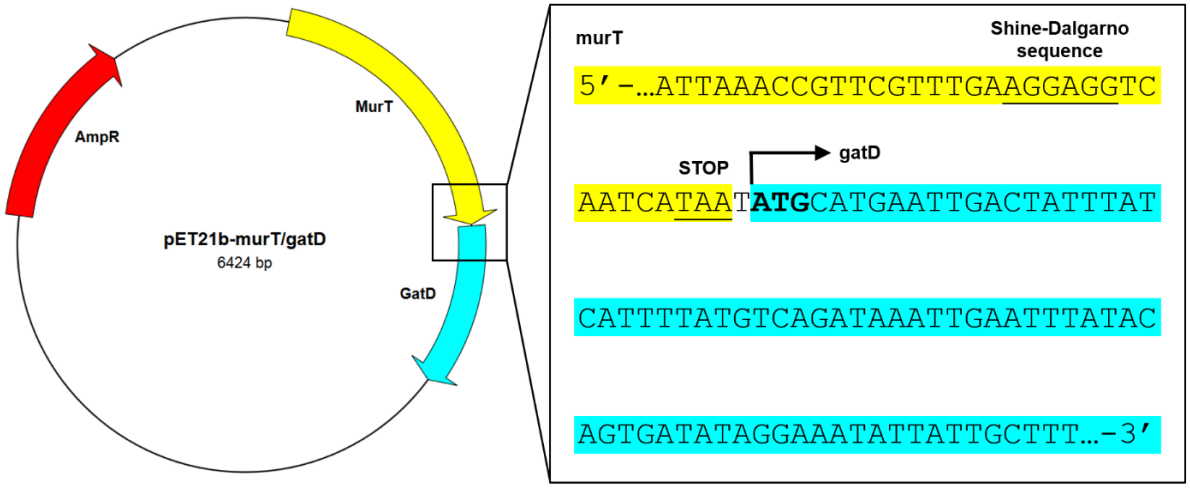

Figure 10 **Schematic representation of pET21b-murT/gatD expression vector.** Genes encoding for murT and gatD-His_6 are depicted as arrows in yellow and cyan, respectively. Ampicillin resistance is depicted as a red arrow. The +DNA strand at the border between the murT- and the gatD-genes is highlighting the polycistronic characteristics of the expression construct. The Shine-Dalgarno sequence present at the 3'-end of the murT-gene enables ribosome binding for translation of gatD-His_6. One base pair is separating murT and gatD.

Expression

LB-Amp medium was used to grow *E. coli* BL21 transformed with pET21b-*murT/gatD*. To ensure aeration during large scale expression, 4 x 5 l baffled Erlenmeyer flasks were filled with maximal 1.5 l medium each. The main cultures were inoculated with 40 ml LB-Amp overnight culture being in stationary growth phase. This led to an optical density (OD_{600}) of approximately 0.08 – 0.1. The cultivation temperature was adjusted to 33°C, and the rotation speed was set to 80 rpm to avoid foam formation and allow sufficient aeration. At an OD_{600} of 0.5, expression was induced with different concentrations of IPTG (0.25, 0.5, 0.75 and 1.0 mM). The accumulation of MurT and GatD during the expression was visualized by SDS-PAGE (Figure 11). Two bands with masses corresponding to the molecular weights of MurT (49.2 kDa) and GatD (28.5 kDa) were present. The MurT band appeared to be a little stronger than the GatD band. However, the total amount of expressed complex did not show significant differences depending on the IPTG-concentration. To obtain a high quality/quantity ratio, the expression was induced with 0.25 mM IPTG. Furthermore, the expression was restricted to 4 h because no further accumulation of the complex has been seen at longer induction times. Between 18 and 20 g cell (4 x 4.5 – 5 g) wet weight were harvested out of 6 l medium.

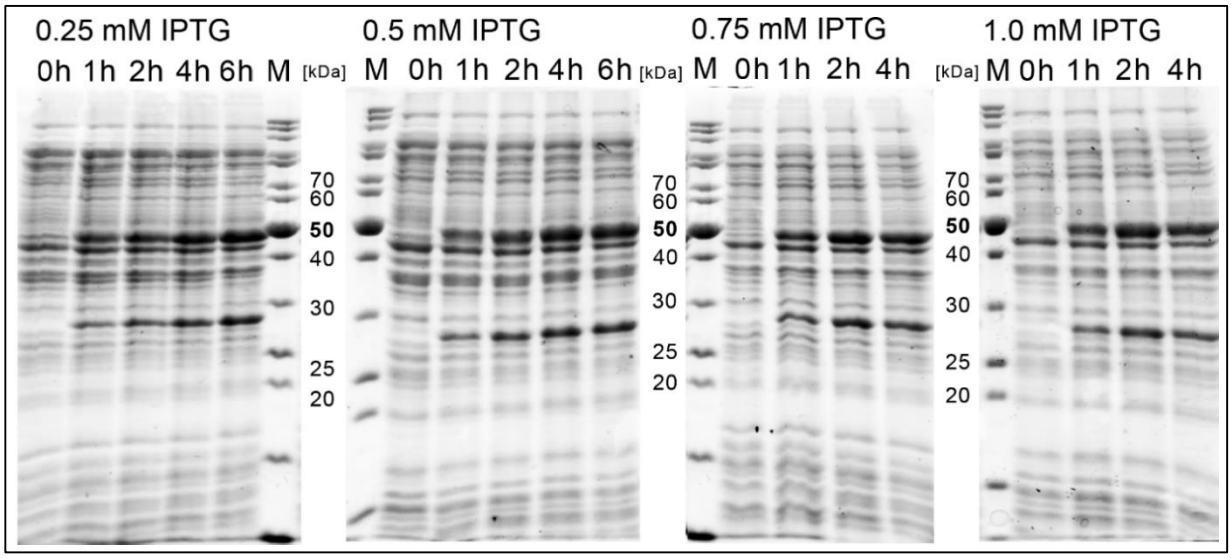

Figure 11 **SDS-PAGE of MurT/GatD complex expression in dependence of IPTG concentration.** The effect of four different IPTG concentrations (0.25, 0.5, 0.75, 1.0 mM) on the expression quantities of MurT (49.2 kDa) and GatD (28.5 kDa) during expression in *E. coli* BL21 at 33°C in LB-Amp. Samples were taken before induction at 0h, and after 1 h, 2 h, 3 h and 4 h for all four expression conditions. For cultures induced with 0.25 and 0.5 mM IPTG an additional sample was taken after 6 h. The increase of optical density during growth was balanced with proportional increased volume of loading dye.

Purification

The frozen cell pellets were thawed and resuspended with cold lysis-buffer containing magnetic beads and stirred at room temperature. A ratio of 1 g cell pellet per 10 ml lysis-buffer resulted in 200 ml (4 x 50 ml) lysate. One “complete inhibitor tablet” per 50 ml lysate was added to avoid proteolysis. After approximately 15 min, the pellets were thoroughly resuspended until no remaining chunks of pellet were visible. Subsequently, lysozyme, RNase, and DNase were added and incubated while stirring on ice. This ensured a homogeneous solution without clots. Sonification was performed in intervals and on ice. The subsequent centrifugation was restricted to 10 000 x g for 10 min, leading to a turbid lysate. Ni-NTA agarose beads were added for batch incubation for 2 hours shaking at 4°C. The turbid Ni-NTA agarose batch contained non-bound impurities and insoluble compartments. These could be removed from Ni-NTA bound target protein after a short centrifugation and subsequent resuspension of the Ni-NTA-pellet with lysis-buffer. This step ensured a quick elution by gravity as follows. The Ni-NTA suspension was transferred to gravity flow columns with maximum 1 ml cv. After the lysate had passed through the column a Ni-NTA agarose gel bed has been formed. To remove remaining impurities, the stepwise addition of wash buffer containing 50 mM imidazole led to 3 x 5 ml and 3 x 1 ml fractions. SDS-PAGE revealed that the fractions of the wash steps contained MurT/GatD-complex but also remaining impurities (Figure 12). The elution with first 150 mM and then 200 mM imidazole containing buffers were collected in 3 x 5 ml and 3 x 5 ml fractions. SDS-PAGE analysis of these fractions reveal > 90% MurT/GatD complex with no significant differences in purity and quantity between the imidazole concentrations (Figure 12). Fractions collected from both 150 mM and 200 mM imidazole buffer elution steps were pooled and used for further purification. A buffer exchange to SEC-buffer was performed with PD-columns. The MurT/GatD complex remained stable in the new buffer, containing DTT as reducing agent, and could be stored until the next day at 4°C for further purification.

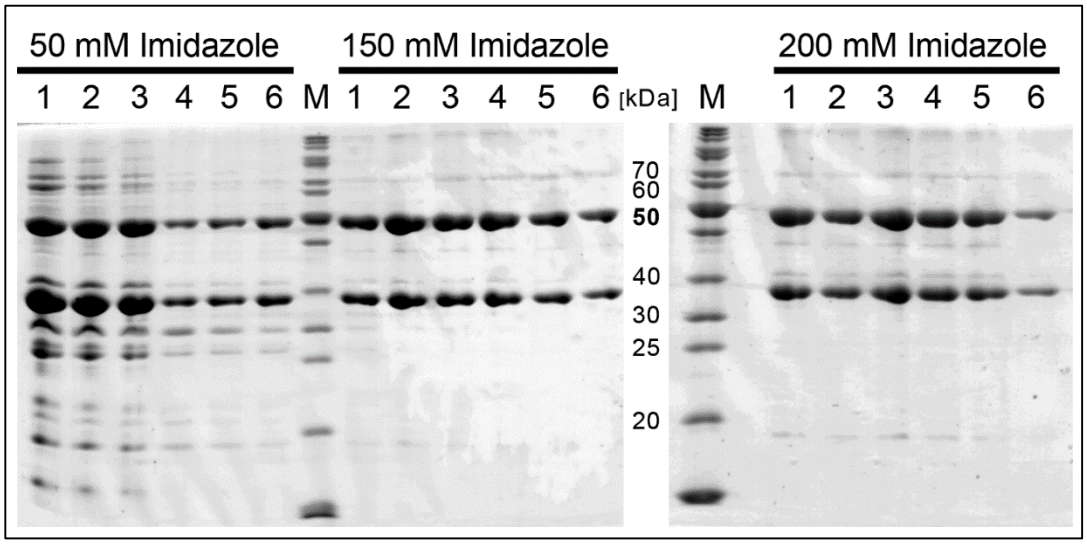

Figure 12 **SDS-PAGE of elution of MurT/GatD complex from Ni-NTA agarose.** In all fractions independent of the imidazole concentration MurT (49.2 kDa) and GatD (28.5 kDa) were present. For each imidazole concentration the volume of the first three fractions (1-3) were 5 ml and for the last three fraction (4-6) 1 ml. In the fraction eluted with 50 mM imidazole impurities are present. The complex eluted with 150 mM and 200 mM imidazole without differences in purity and quantity and both were used for further purification.

The volume of the protein sample had to be reduced for size exclusion chromatography. Sartorius concentrators with a 50.000 MWCO polyethersulfone-membrane were used to concentrate the MurT/GatD complex, which revealed the lowest losses during this process (data not shown). An approximately 500 µl protein sample with a maximal concentration of 15 mg/ml were filtered and subjected to an equilibrated Superdex 200 10/300 installed on a BioRad FPLC. Size exclusion chromatography had to be performed several times to process all material. Two peaks appeared in the chromatograms, one corresponded to the void volume and the second one to the MurT/GatD complex (Figure 14). The first peak exhibits a slight tailing. Fractions of the second peak were analyzed by SDS-PAGE and revealed MurT and GatD present in equal amounts (Figure 13). The fractions corresponding to the tailing exhibit a slight excess of GatD and impurities with a mass lower 30 kDa. Based on SDS-PAGEs, fractions of the chromatograms containing MurT/GatD complex were pooled. The fractions were concentrated with the Sartorius concentrators used previously. An approximately 500 µl protein sample with a maximal concentration of 15 mg/ml were filtered and subjected to an equilibrated Superdex 200 10/300 installed in BioRad FPLC. Only one peak was present in the re-chromatogram with an absence of the aggregation peak and the tailing (Figure 15). The presence of only one peak indicates that the re-subjected fractions contain a stable MurT/GatD heterodimer. SDS-PAGE analysis visualized the content of the peak (Figure 16).

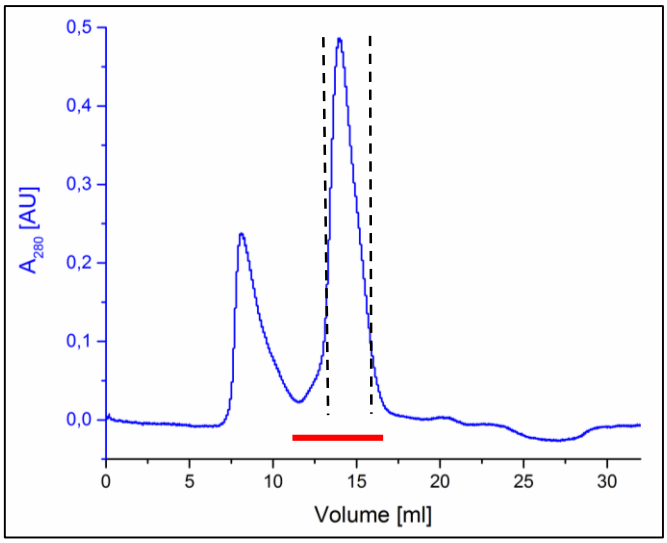

Figure 14 **Exemplary Size Exclusion Chromatogram of MurT/GatD.** 12 mg/ml protein complex was subjected to SD 200 10/300 column. Two peaks are present, one peak at void volume at 7.8 ml and another peak at 14 ml corresponding to the approximate mass of the MurT/GatD complex were present. The horizontal red bar indicates which fractions were analyzed by SDS-PAGE. The vertical dashed lines indicate the region of the second peak used for further purification.

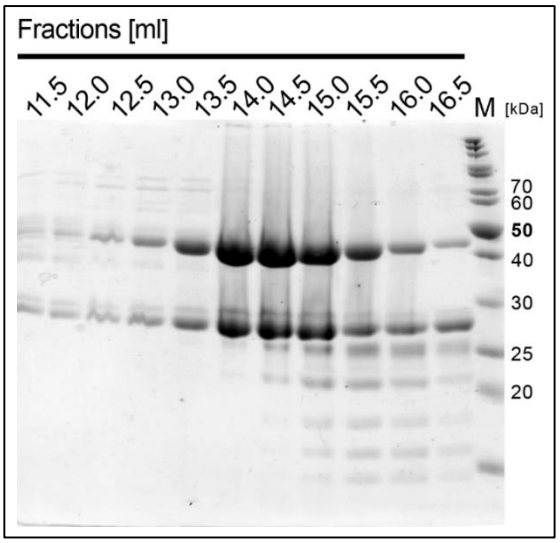

Figure 13 **SDS-PAGE of the second peak of SEC fractions.** In all fractions MurT (49.2 kDa) and GatD (28.5 kDa) are present. In the early fractions (11.5 - 13.5 ml) a small amount impurities with higher molecular mass were visible. Additional bands with lower molecular weight are in the later fractions (14.5 – 16.5 ml). Fractions containing MurT/GatD complex (14.0 ml, 14.5 ml and 15.0 ml) were pooled and used for further purification.

Fractions containing MurT/GatD complex were pooled and concentrated with a Satorius concentrator designated for crystallization experiments. The concentrated sample was analyzed by analytical SEC. Approximately 30 µl of concentrated protein sample (12 mg/ml) was subjected to Superdex 200 3.2/30 PC column installed on an ÄKTA Ettan FPLC. Only one sharp peak at 1.48 ml was present in the chromatogram (Figure 17). The elution volume indicated the presence of a homodimer MurT/GatD. The corresponding SDS-gel showed bands for MurT and GatD in a 1:1 stoichiometry. In the later fractions, minor impurities <30 kDa were present (Figure 18). The overall purity of the sample subjected to the analytical size exclusion column was >95%. Therefore the sample fulfilled the requirements, in purity and homogeneity, for crystallization.

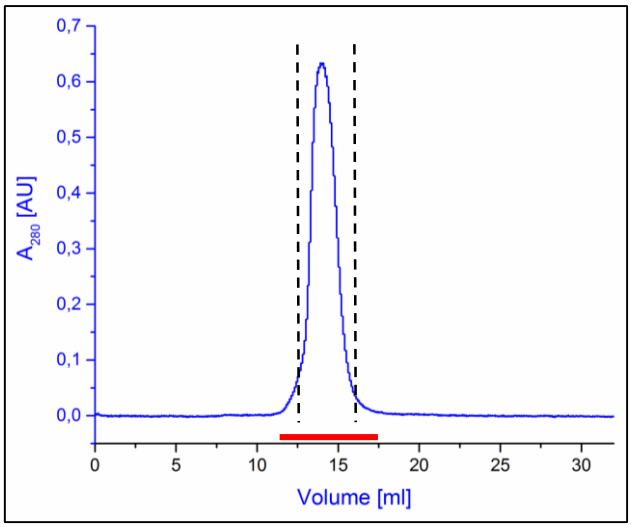

Figure 15 **Size Exclusion Chromatogram (re-chromatography) of MurT/GatD.** 14 mg/ml protein complex was subjected to SD 200 10/300 column. One peak at an elution volume of 14 ml was present. The horizontal red bar indicate which fractions were analyzed by SDS-PAGE. The vertical dashed lines indicate proportion of the second peak which were used for further purification.

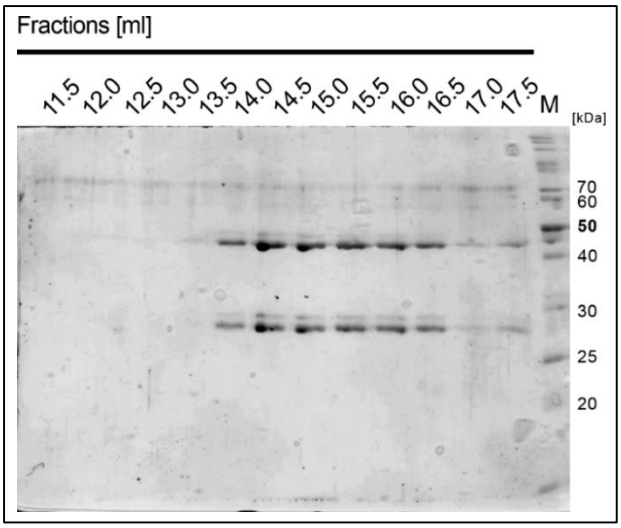

Figure 16 **SDS-PAGE of SEC of Murt/GatD (re-chromatography).** In all fractions MurT (49.2 kDa) and GatD (28.5 kDa) are present. A small band above GatD is present. Fraction 13.5 – 16.5 ml were pooled, concentrated and used for crystallization.

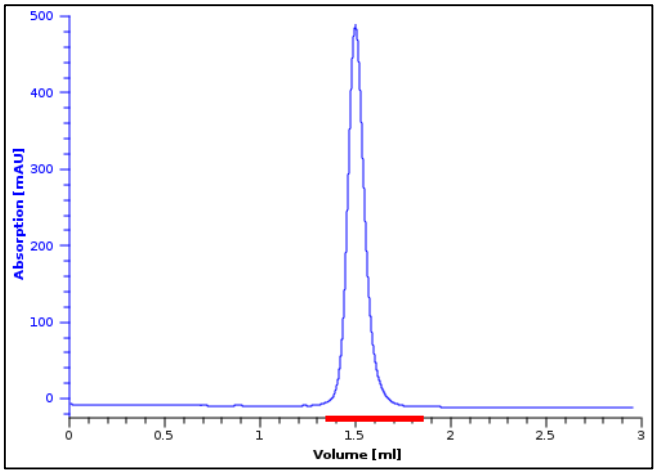

Figure 17 **Analytical Size Exclusion Chromatogram of MurT/GatD.** 12 mg/ml protein sample was subjected to SD 200 3.2/30 PC column. A single peak at 1.48 ml elution volume was present indicating a homodisperse solution.

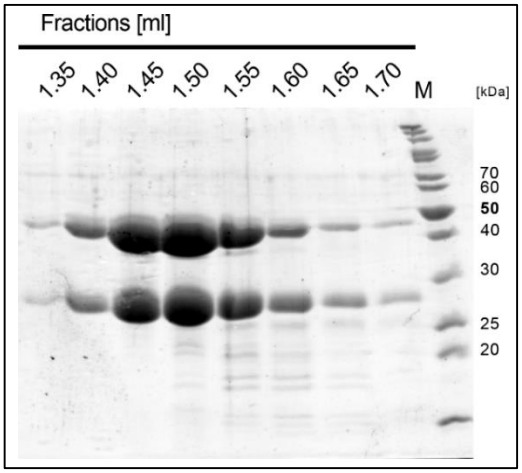

Figure 18 **SDS-PAGE of analytical SEC of MurT/GatD** .In all fractions MurT (49.2 kDa) and GatD (28.5 kDa) are present. In the later fraction impurities of different size (<30 kDa) are present. Estimated by eye, the load exhibited a purity of >95%.

3.7. X-ray crystallography in brief

Once pure and homogeneous protein sample is available, how to proceed in structural biology is straightforward. Vapor diffusion crystallization experiments will be used to obtain crystals. Several commercial crystallization screens are available, providing a wide range of conditions containing precipitants such as high salts or (poly)alcohols that reduce the solubility of the protein and provoke the loss of its hydrate shell. Furthermore, protein concentration, pH and temperature also impact the crystallization process. Ideally patches on the protein surface become contact areas between the protein molecules leading to nucleation. These specific and regular contacts initialize the piling up of protein molecules in a three dimensional lattice. The protein molecules are trapped in a certain conformation are immobilized in the crystal. The unit cell contains one or more molecules that can be related by crystallographic or non-crystallographic symmetry.

During data collection, crystals interact with high energy X-rays (0.5 – 1.5 Å) that can cause radiation damage. To reduce this effect the protein crystals are flash frozen in liquid nitrogen. Protein crystals contain around 50 % solvent and as water expands when frozen it has to be prevented from forming ice. Transferring the protein crystal in a cryo-protection solution containing (poly)alcohols such as glycerol or low molecular polyethylene glycols avoids this. There might be negative effects on the mosaicity or stability of the crystal when it has been transferred to a cryo-protection solution. However, after a suitable cryo-protection solution is found, the crystals will be irradiated with a high energy monochromatic X-ray beam, leading to scattering. All electrons of the atoms in the crystal contribute to the diffraction. The diffraction pattern recorded by a two dimensional charge-coupled device detector is a Fourier transformation of the repetitive planes of the three dimensional distribution of electrons in the crystal. The protein crystal is rotated during data collection, leading to a data set of images. The diffraction pattern is dependent on the orientation of the crystal to the beam. Positions and intensities of the spots appear in a reciprocal lattice, which are measured and used for space group determination. The origin of scattering, the location of the electrons in real space, cannot be determined directly. In small-molecule crystallography, basic assumptions about atomicity give rise to relationships between the amplitudes from which phase information can be extracted. In protein crystallography the phase information is lost during data collection and has to be determined separately.

The phase information can be obtained when homologous X-ray structures are available. In principle, molecular replacement uses the real space information of a known structure to estimate the phases of the new recorded diffraction experiment. Information about position and intensities of the reciprocal lattice are combined with the known location of electrons in real space of a homologous structure to calculate phases. If no homologous structures are

available or homologous structures are arranged differently in the crystal, the molecular replacement method is unlikely to succeed.

The wavelength-depended absorption effects of some heavier atoms can be used to solve the phase problem in protein crystallography. Methods such as MIR, MIRAS, SIR, SIRAS, MAD or SAD are commonly used to find the marker atom positions that are intrinsic to the protein or have been added. Soaking the protein crystal with compounds containing such atoms should preserve isomorphism, such the structural changes do not influence unit cell parameters or the orientation of the protein in the cell. . Alternatively, the incorporation of selenium in form of selenomethionine into the protein during expression overcome the problem of crystal damage caused by soaking. The isomorphous derivate give rise to measureable intensity changes that can be used to deduce the position of the heavy atoms. Once the heavy atom positions have been determined their phases can be calculated and subsequently the native phases can be estimated. The experimental phases are usually the starting point for phase improvement using a variety of density-modification methods such as solvent flattening or non-crystallographic averaging.

3.8. Ongoing research and outlook

Based on an X-ray structure of MurT/GatD, a detailed reaction mechanism how Lipid II is amidated, may be described. A crystal structure without bound ligands will probably not provide enough insights to address the questions. Therefore, MurT/GatD structures with bound ligands will be pursued. According to literature describing the GATase reaction, a sequential binding mode of ATP, glutamine and Lipid II can be expected for MurT/GatD. In cooperation with the AG Schneider and the AG Sahl in Bonn, soaking or co-crystallization experiments will be performed to obtain MurT/GatD structures with bound glutamine, ATP or analogues as well as Lipid II analogues with a shortened isoprenoid tail. Crystal structures of MurT/GatD protein complexes may provide the basis to understand the influence of an amidated stem peptide on increased growth rates and increased resistance to lysozyme. Additionally, structure based development of new drugs inhibiting MurT/GatD is desirable. Ideally, a detailed description of Lipid II binding to MurT/GatD allows to design specific antagonistic inhibitors. Fragment based screening and high throughput screening are two common methods to develop a new compound with desired affinity and stability. Preclinical and clinical studies are necessary to evaluated possible side effects on the patient. A MurT/GatD inhibitor might not cause cell death but promote the native immune system to defend against MRSA. An early appearance of resistance mechanisms can only be prevented by responsible usage!

4. References

1. Ogston A (1881) Report upon Micro-Organisms in Surgical Diseases. *British Medical Journal* 1(1054):369 b362-375.

2. Rosenbach FJ (1884) *Mikro-Organismen bei den Wund-Infections-Krankheiten des Menschen* (Bergmann, J.F., Wiesbaden).

3. Flügge C & Frosch P (1886) *Die Mikroorganismen : mit besonderer Berücksichigung der Ätiologie der Infektionskrankheiten* (Vogel, F.C.W., Leipzig).

4. Chapman GH, Berens C, & Stiles MH (1941) The Coagulation of Plasma by Staphylococci. *Journal of Bacteriology* 41(4):431-440.

5. Evans JB, Bradford Jr. WL, & Niven Jr. CF (1955) Comments concerning the taxonomy of the genera Micrococcus and Staphylococcus. *International Bulletin of Bacteriological Nomenclature and Taxonomy* 5:61-66.

6. Silvestri LG & Hill LR (1965) Agreement Between Deoxyribonucleic Acid Base Composition and Taxometric Classification of Gram-Positive Cocci. *Journal of Bacteriology* 90(1):136-140.

7. Götz F, Bannerman T, & Schleifer K-H (2006) The Genera Staphylococcus and Macrococcus. *The Prokaryotes*, eds Dworkin M, Falkow S, Rosenberg E, Schleifer K-H, & Stackebrandt E (Springer US), pp 5-75.

8. Prevost G, Jaulhac B, & Piemont Y (1992) DNA fingerprinting by pulsed-field gel electrophoresis is more effective than ribotyping in distinguishing among methicillin-resistant Staphylococcus aureus isolates. *Journal of Clinical Microbiology* 30(4):967-973.

9. Lindsay JA & Holden MT (2006) Understanding the rise of the superbug: investigation of the evolution and genomic variation of Staphylococcus aureus. *Functional and Integrative Genomics* 6(3):186-201.

10. Peacock SJ*, et al.* (2002) Virulent combinations of adhesin and toxin genes in natural populations of Staphylococcus aureus. *Infection and Immunity* 70(9):4987-4996.

11. Williams RE (1963) Healthy carriage of Staphylococcus aureus: its prevalence and importance. *Bacteriological Reviews* 27:56-71.

12. Parfentjev IA & Catelli AR (1964) Tolerance of Staphylococcus Aureus to Sodium Chloride. *Journal of Bacteriology* 88:1-3.

13. von Eiff C, Becker K, Machka K, Stammer H, & Peters G (2001) Nasal carriage as a source of Staphylococcus aureus bacteremia. Study Group. *The New England Journal of Medicine* 344(1):11-16.

14. Wertheim HF, Melles DC, Vos MC, van Leeuwen W, van Belkum A, Verbrugh HA, & Nouwen JL (2005) The role of nasal carriage in Staphylococcus aureus infections. *The Lancet. Infectious Diseases* 5(12):751-762.

15. Lowy FD (1998) Staphylococcus aureus infections. *The New England Journal of Medicine* 339(8):520-532.

16. Bagger JP, Zindrou D, & Taylor KM (2004) Postoperative infection with meticillin-resistant Staphylococcus aureus and socioeconomic background. *Lancet* 363(9410):706-708.

17. Otto M (2010) Basis of virulence in community-associated methicillin-resistant Staphylococcus aureus. *Annual Review of Microbiology* 64:143-162.

18. Lowy FD (2003) Antimicrobial resistance: the example of Staphylococcus aureus. *The Journal of Clinical Investigation* 111(9):1265-1273.

19. Lowy FD (2011) How Staphylococcus aureus adapts to its host. *The New England Journal of Medicine* 364(21):1987-1990.

20. Kock R, Mellmann A, Schaumburg F, Friedrich AW, Kipp F, & Becker K (2011) The epidemiology of methicillin-resistant Staphylococcus aureus (MRSA) in Germany. *Deutsches Arzteblatt international* 108(45):761-767.

21. Jenkins A*, et al.* (2015) Differential expression and roles of Staphylococcus aureus virulence determinants during colonization and disease. *MBio* 6(1):e02272-02214.

22. Engleberg NC, DiRita V, & Dermody TS (2013) *Schaechter's Mechanisme of Microbal Disease* (Lippincott Williams & Wilkins, Philadelphia PA) 5th Ed.

23. Patti JM, Allen BL, McGavin MJ, & Höök M (1994) MSCRAMM-mediated adherence of microorganisms to host tissues. *Annual Review of Microbiology* 48:585-617.

24. Foster TJ & Hook M (1998) Surface protein adhesins of Staphylococcus aureus. *Trends Microbiol* 6(12):484-488.

25. Gordon RJ & Lowy FD (2008) Pathogenesis of methicillin-resistant Staphylococcus aureus infection. *Clinical Infectious Diseases: an Official Publication of the Infectious Diseases Society of America* 46 Suppl 5:S350-359.

26. Foster TJ (2005) Immune evasion by staphylococci. *Nature Reviews Microbiology* 3(12):948-958.

27. Murdoch C & Finn A (2000) Chemokine receptors and their role in inflammation and infectious diseases. *Blood* 95(10):3032-3043.

28. de Haas CJ*, et al.* (2004) Chemotaxis inhibitory protein of Staphylococcus aureus, a bacterial antiinflammatory agent. *The Journal of Experimental Medicine* 199(5):687-695.

29. Bhakdi S & Tranum-Jensen J (1991) Alpha-toxin of Staphylococcus aureus. *Microbiological Reviews* 55(4):733-751.

30. Llewelyn M & Cohen J (2002) Superantigens: microbial agents that corrupt immunity. *The Lancet. Infectious Diseases* 2(3):156-162.

31. Proft T & Fraser JD (2003) Bacterial superantigens. *Clinical and Experimental Immunology* 133(3):299-306.

32. Dinges MM, Orwin PM, & Schlievert PM (2000) Exotoxins of Staphylococcus aureus. *Clinical Microbiology Reviews* 13(1):16-34, table of contents.

33. Pragman AA & Schlievert PM (2004) Virulence regulation in Staphylococcus aureus: the need for in vivo analysis of virulence factor regulation. *FEMS Immunology and Medical Microbiology* 42(2):147-154.

34. Novick RP & Muir TW (1999) Virulence gene regulation by peptides in staphylococci and other Gram-positive bacteria. *Current Opinion in Microbiology* 2(1):40-45.

35. Recsei P, Kreiswirth B, O'Reilly M, Schlievert P, Gruss A, & Novick RP (1986) Regulation of exoprotein gene expression in Staphylococcus aureus by agar. *Molecular and General Genetics: MGG* 202(1):58-61.

36. Zhang L & Ji G (2004) Identification of a staphylococcal AgrB segment(s) responsible for group-specific processing of AgrD by gene swapping. *Journal of Bacteriology* 186(20):6706-6713.

37. Götz F (2002) Staphylococcus and biofilms. *Molecular Microbiology* 43(6):1367-1378.

38. Kong KF, Vuong C, & Otto M (2006) Staphylococcus quorum sensing in biofilm formation and infection. *International journal of medical microbiology: IJMM* 296(2-3):133-139.

39. Vuong C, Saenz HL, Götz F, & Otto M (2000) Impact of the agr quorum-sensing system on adherence to polystyrene in Staphylococcus aureus. *The Journal of Infectious Diseases* 182(6):1688-1693.

40. Yarwood JM, McCormick JK, & Schlievert PM (2001) Identification of a novel two-component regulatory system that acts in global regulation of virulence factors of Staphylococcus aureus. *Journal of Bacteriology* 183(4):1113-1123.

41. Lindsay JA (2010) Genomic variation and evolution of Staphylococcus aureus. *International journal of medical microbiology: IJMM* 300(2-3):98-103.

42. Clewell DB, An FY, White BA, & Gawron-Burke C (1985) Streptococcus faecalis sex pheromone (cAM373) also produced by Staphylococcus aureus and identification of a conjugative transposon (Tn918). *Journal of Bacteriology* 162(3):1212-1220.

43. Fleming A (2001) On the antibacterial action of cultures of a penicillium, with special reference to their use in the isolation of B. influenzae. 1929. *Bull World Health Organ* 79(8):780-790.

44. Hodgkin DC (1949) The X-ray analysis of the structure of penicillin. *Advancement of Science* 6(22):85-89.

45. Sheehan J & Henery-Logan K (1957) THE TOTAL SYNTHESIS OF PENICILLIN V. *Journal of the American Chemical Society* 79(5):1262–1263.

46. Kirby WM (1944) Extraction of a Highly Potent Penicillin Inactivator from Penicillin Resistant Staphylococci. *Science* 99(2579):452-453.

47. Rosenstein R, Nerz C, Biswas L, Resch A, Raddatz G, Schuster SC, & Götz F (2009) Genome analysis of the meat starter culture bacterium Staphylococcus carnosus TM300. *Applied and Environmental Microbiology* 75(3):811-822.

48. Götz F (1990) Staphylococcus carnosus: a new host organism for gene cloning and protein production. *Society for Applied Bacteriology Symposium Series* 19:49S-53S.

49. Gill SR*, et al.* (2005) Insights on evolution of virulence and resistance from the complete genome analysis of an early methicillin-resistant Staphylococcus aureus strain and a biofilm-producing methicillin-resistant Staphylococcus epidermidis strain. *Journal of Bacteriology* 187(7):2426-2438.

50. Rosenstein R & Götz F (2010) Genomic differences between the food-grade Staphylococcus carnosus and pathogenic staphylococcal species. *International journal of medical microbiology: IJMM* 300(2-3):104-108.

51. Aras RA, Kang J, Tschumi AI, Harasaki Y, & Blaser MJ (2003) Extensive repetitive DNA facilitates prokaryotic genome plasticity. *Proceedings of the National Academy of Sciences of the United States of America* 100(23):13579-13584.

52. van de Guchte M*, et al.* (2006) The complete genome sequence of Lactobacillus bulgaricus reveals extensive and ongoing reductive evolution. *Proceedings of the National Academy of Sciences of the United States of America* 103(24):9274-9279.

53. Corbiere Morot-Bizot S, Leroy S, & Talon R (2007) Monitoring of staphylococcal starters in two French processing plants manufacturing dry fermented sausages. *Journal of Applied Microbiology* 102(1):238-244.

54. Neubauer H & Götz F (1996) Physiology and interaction of nitrate and nitrite reduction in Staphylococcus carnosus. *Journal of Bacteriology* 178(7):2005-2009.

55. Neubauer H, Pantel I, & Götz F (1999) Molecular characterization of the nitrite-reducing system of Staphylococcus carnosus. *Journal of Bacteriology* 181(5):1481-1488.

56. Tielens AG, Rotte C, van Hellemond JJ, & Martin W (2002) Mitochondria as we don't know them. *Trends in Biochemical Sciences* 27(11):564-572.

57. Richardson DJ (2000) Bacterial respiration: a flexible process for a changing environment. *Microbiology* 146 (Pt 3):551-571.

58. Vargas M, Kashefi K, Blunt-Harris EL, & Lovley DR (1998) Microbiological evidence for Fe(III) reduction on early Earth. *Nature* 395(6697):65-67.

59. Fearnley IM & Walker JE (1992) Conservation of sequences of subunits of mitochondrial complex I and their relationships with other proteins. *Biochimica et Biophysica Acta* 1140(2):105-134.

60. Yagi T (1993) The bacterial energy-transducing NADH-quinone oxidoreductases. *Biochimica et Biophysica Acta* 1141(1):1-17.

61. Carroll J, Fearnley IM, Skehel JM, Shannon RJ, Hirst J, & Walker JE (2006) Bovine complex I is a complex of 45 different subunits. *The Journal of Biological Chemistry* 281(43):32724-32727.

62. Brandt U (2006) Energy converting NADH:quinone oxidoreductase (complex I). *Annual Review of Biochemistry* 75:69-92.

63. Yagi T & Matsuno-Yagi A (2003) The proton-translocating NADH-quinone oxidoreductase in the respiratory chain: the secret unlocked. *Biochemistry* 42(8):2266-2274.

64. Steffen W & Steuber J (2013) Cation transport by the respiratory NADH:quinone oxidoreductase (complex I): facts and hypotheses. *Biochemical Society Transactions* 41(5):1280-1287.

65. Mayer S, Steffen W, Steuber J, & Götz F (2015) The Staphylococcus aureus NuoL-like protein MpsA contributes to the generation of membrane potential. *Journal of Bacteriology* 197(5):794-806.

66. Mitchell P (1961) Coupling of phosphorylation to electron and hydrogen transfer by a chemi-osmotic type of mechanism. *Nature* 191:144-148.

67. Mitchell P (1973) Performance and conservation of osmotic work by proton-coupled solute porter systems. *Journal of Bioenergetics* 4(1):63-91.

68. Mitchell P (1976) Possible molecular mechanisms of the protonmotive function of cytochrome systems. *Journal of Theoretical Biology* 62(2):327-367.

69. Harold FM (1972) Conservation and transformation of energy by bacterial membranes. *Bacteriological Reviews* 36(2):172-230.

70. Boonstra J & Konings WN (1977) Generation of an electrochemical proton gradient by nitrate respiration in membrane vesicles from anaerobically grown Escherichia coli. *European Journal of Biochemistry / FEBS* 78(2):361-368.

71. Hamilton WA (1998) Bioenergetics of sulphate-reducing bacteria in relation to their environmental impact. *Biodegradation* 9(3-4):201-212.

72. Lie TJ, Godchaux W, & Leadbetter ER (1999) Sulfonates as terminal electron acceptors for growth of sulfite-reducing bacteria (Desulfitobacterium spp.) and sulfate-reducing bacteria: effects of inhibitors of sulfidogenesis. *Applied and Environmental Microbiology* 65(10):4611-4617.

73. Berks BC, Ferguson SJ, Moir JW, & Richardson DJ (1995) Enzymes and associated electron transport systems that catalyse the respiratory reduction of nitrogen oxides and oxyanions. *Biochimica et Biophysica Acta* 1232(3):97-173.

74. Czjzek M, Dos Santos JP, Pommier J, Giordano G, Mejean V, & Haser R (1998) Crystal structure of oxidized trimethylamine N-oxide reductase from Shewanella massilia at 2.5 A resolution. *Journal of Molecular Biology* 284(2):435-447.

75. Lovley DR, Holmes DE, & Nevin KP (2004) Dissimilatory Fe(III) and Mn(IV) reduction. *Advances in Microbial Physiology* 49:219-286.

76. Philippot L & Hojberg O (1999) Dissimilatory nitrate reductases in bacteria. *Biochimica et Biophysica Acta* 1446(1-2):1-23.

77. MacGregor CH (1976) Biosynthesis of membrane-bound nitrate reductase in Escherichia coli: evidence for a soluble precursor. *Journal of Bacteriology* 126(1):122-131.

78. Sodergren EJ, Hsu PY, & DeMoss JA (1988) Roles of the narJ and narI gene products in the expression of nitrate reductase in Escherichia coli. *The Journal of Biological Chemistry* 263(31):16156-16162.

79. Fedtke I, Kamps A, Krismer B, & Götz F (2002) The nitrate reductase and nitrite reductase operons and the narT gene of Staphylococcus carnosus are positively controlled by the novel two-component system NreBC. *Journal of Bacteriology* 184(23):6624-6634.

80. Pantel I, Lindgren PE, Neubauer H, & Götz F (1998) Identification and characterization of the Staphylococcus carnosus nitrate reductase operon. *Molecular and General Genetics: MGG* 259(1):105-114.

81. Clegg S, Yu F, Griffiths L, & Cole JA (2002) The roles of the polytopic membrane proteins NarK, NarU and NirC in Escherichia coli K-12: two nitrate and three nitrite transporters. *Molecular Microbiology* 44(1):143-155.

82. Fast B, Lindgren P, & Götz F (1996) Cloning, sequencing, and characterization of a gene (narT) encoding a transport protein involved in dissimilatory nitrate reduction in Staphylococcus carnosus. *Archives of Microbiology* 166(6):361-367.

83. Schlag S*, et al.* (2008) Characterization of the oxygen-responsive NreABC regulon of Staphylococcus aureus. *Journal of Bacteriology* 190(23):7847-7858.

84. Niemann V, Koch-Singenstreu M, Neu A, Nilkens S, Gotz F, Unden G, & Stehle T (2014) The NreA protein functions as a nitrate receptor in the staphylococcal nitrate regulation system. *Journal of Molecular Biology* 426(7):1539-1553.

85. Nilkens S, Koch-Singenstreu M, Niemann V, Gotz F, Stehle T, & Unden G (2014) Nitrate/oxygen co-sensing by an NreA/NreB sensor complex of Staphylococcus carnosus. *Molecular Microbiology* 91(2):381-393.

86. Kamps A, Achebach S, Fedtke I, Unden G, & Gotz F (2004) Staphylococcal NreB: an O(2)-sensing histidine protein kinase with an O(2)-labile iron-sulphur cluster of the FNR type. *Molecular Microbiology* 52(3):713-723.

87. Koshland DE, Jr. (2002) Special essay. The seven pillars of life. *Science* 295(5563):2215-2216.

88. Galperin MY (2004) Bacterial signal transduction network in a genomic perspective. *Environmental Microbiology* 6(6):552-567.

89. Stock AM, Robinson VL, & Goudreau PN (2000) Two-component signal transduction. *Annual Review of Biochemistry* 69:183-215.

90. Jung K, Fried L, Behr S, & Heermann R (2012) Histidine kinases and response regulators in networks. *Current Opinion in Microbiology* 15(2):118-124.

91. Foussard M*, et al.* (2001) The molecular puzzle of two-component signaling cascades. *Microbes and Infection / Institut Pasteur* 3(5):417-424.

92. West AH & Stock AM (2001) Histidine kinases and response regulator proteins in two-component signaling systems. *Trends in Biochemical Sciences* 26(6):369-376.

93. Gao R & Stock AM (2009) Biological insights from structures of two-component proteins. *Annual Review of Microbiology* 63:133-154.

94. Buelow DR & Raivio TL (2010) Three (and more) component regulatory systems - auxiliary regulators of bacterial histidine kinases. *Molecular Microbiology* 75(3):547-566.

95. Szurmant H, White RA, & Hoch JA (2007) Sensor complexes regulating two-component signal transduction. *Current Opinion in Structural Biology* 17(6):706-715.

96. Martinez-Hackert E & Stock AM (1997) Structural relationships in the OmpR family of winged-helix transcription factors. *Journal of Molecular Biology* 269(3):301-312.

97. Galperin MY (2006) Structural classification of bacterial response regulators: diversity of output domains and domain combinations. *Journal of Bacteriology* 188(12):4169-4182.

98. Saito H (2001) Histidine phosphorylation and two-component signaling in eukaryotic cells. *Chemical Reviews* 101(8):2497-2509.

99. Taylor BL & Zhulin IB (1999) PAS domains: internal sensors of oxygen, redox potential, and light. *Microbiology and Molecular Biology Reviews : MMBR* 63(2):479-506.

100. Möglich A, Ayers RA, & Moffat K (2009) Structure and signaling mechanism of Per-ARNT-Sim domains. *Structure* 17(10):1282-1294.

101. Aravind L & Ponting CP (1997) The GAF domain: an evolutionary link between diverse phototransducing proteins. *Trends in Biochemical Sciences* 22(12):458-459.

102. Crosson S & Moffat K (2001) Structure of a flavin-binding plant photoreceptor domain: insights into light-mediated signal transduction. *Proceedings of the National Academy of Sciences of the United States of America* 98(6):2995-3000.

103. Ho YS, Burden LM, & Hurley JH (2000) Structure of the GAF domain, a ubiquitous signaling motif and a new class of cyclic GMP receptor. *The EMBO journal* 19(20):5288-5299.

104. Galperin MY, Nikolskaya AN, & Koonin EV (2001) Novel domains of the prokaryotic two-component signal transduction systems. *FEMS Microbiology Letters* 203(1):11-21.

105. Hurley JH (2003) GAF domains: cyclic nucleotides come full circle. *Science's STKE : Signal Transduction Knowledge Environment* 2003(164):PE1.

106. Ninfa AJ & Magasanik B (1986) Covalent modification of the glnG product, NRI, by the glnL product, NRII, regulates the transcription of the glnALG operon in Escherichia coli. *Proceedings of the National Academy of Sciences of the United States of America* 83(16):5909-5913.

107. Ninfa AJ, Ninfa EG, Lupas AN, Stock A, Magasanik B, & Stock J (1988) Crosstalk between bacterial chemotaxis signal transduction proteins and regulators of transcription of the Ntr regulon: evidence that nitrogen assimilation and chemotaxis are controlled by a common phosphotransfer mechanism. *Proceedings of the National Academy of Sciences of the United States of America* 85(15):5492-5496.

108. Chardin C, Girin T, Roudier F, Meyer C, & Krapp A (2014) The plant RWP-RK transcription factors: key regulators of nitrogen responses and of gametophyte development. *Journal of Experimental Botany* 65(19):5577-5587.

109. Vollmer W, Blanot D, & de Pedro MA (2008) Peptidoglycan structure and architecture. *FEMS Microbiology Reviews* 32(2):149-167.

110. van Heijenoort J (2001) Formation of the glycan chains in the synthesis of bacterial peptidoglycan. *Glycobiology* 11(3):25R-36R.

111. Holtje JV (1998) Growth of the stress-bearing and shape-maintaining murein sacculus of Escherichia coli. *Microbiology and Molecular Biology Reviews : MMBR* 62(1):181-203.

112. Coico R (2001) Gram staining. *Current Protocols in Immunology* Appendix 3:Appendix 3O.

113. Schleifer KH & Kandler O (1972) Peptidoglycan types of bacterial cell walls and their taxonomic implications. *Bacteriological Reviews* 36(4):407-477.

114. Bertsche U, Mayer C, Gotz F, & Gust AA (2015) Peptidoglycan perception--sensing bacteria by their common envelope structure. *International journal of medical microbiology: IJMM* 305(2):217-223.

115. Snowden MA & Perkins HR (1990) Peptidoglycan cross-linking in Staphylococcus aureus. An apparent random polymerisation process. *European Journal of Biochemistry / FEBS* 191(2):373-377.

116. Tipper DJ, Tomoeda M, & Strominger JL (1971) Isolation and characterization of -1,4-N-acetylmuramyl-N-acetylglucosamine and its O-acetyl derivative. *Biochemistry* 10(25):4683-4690.

117. Davis KM & Weiser JN (2011) Modifications to the peptidoglycan backbone help bacteria to establish infection. *Infection and Immunity* 79(2):562-570.

118. Brown ED, Vivas EI, Walsh CT, & Kolter R (1995) MurA (MurZ), the enzyme that catalyzes the first committed step in peptidoglycan biosynthesis, is essential in Escherichia coli. *Journal of Bacteriology* 177(14):4194-4197.

119. Du W*, et al.* (2000) Two active forms of UDP-N-acetylglucosamine enolpyruvyl transferase in gram-positive bacteria. *Journal of Bacteriology* 182(15):4146-4152.

120. Skarzynski T, Mistry A, Wonacott A, Hutchinson SE, Kelly VA, & Duncan K (1996) Structure of UDP-N-acetylglucosamine enolpyruvyl transferase, an enzyme essential for the synthesis of bacterial peptidoglycan, complexed with substrate UDP-N-acetylglucosamine and the drug fosfomycin. *Structure* 4(12):1465-1474.

121. Schönbrunn E, Sack S, Eschenburg S, Perrakis A, Krekel F, Amrhein N, & Mandelkow E (1996) Crystal structure of UDP-N-acetylglucosamine enolpyruvyltransferase, the target of the antibiotic fosfomycin. *Structure* 4(9):1065-1075.

122. Smith CA (2006) Structure, function and dynamics in the mur family of bacterial cell wall ligases. *Journal of Molecular Biology* 362(4):640-655.

123. Benson TE, Filman DJ, Walsh CT, & Hogle JM (1995) An enzyme-substrate complex involved in bacterial cell wall biosynthesis. *Nature Structural Biology* 2(8):644-653.

124. Benson TE, Harris MS, Choi GH, Cialdella JI, Herberg JT, Martin JP, Jr., & Baldwin ET (2001) A structural variation for MurB: X-ray crystal structure of Staphylococcus aureus UDP-N-acetylenolpyruvylglucosamine reductase (MurB). *Biochemistry* 40(8):2340-2350.

125. Benson TE, Walsh CT, & Hogle JM (1996) The structure of the substrate-free form of MurB, an essential enzyme for the synthesis of bacterial cell walls. *Structure* 4(1):47-54.

126. Lovering AL, Safadi SS, & Strynadka NC (2012) Structural perspective of peptidoglycan biosynthesis and assembly. *Annual Review of Biochemistry* 81:451-478.

127. Patin D*, et al.* (2010) Purification and biochemical characterization of Mur ligases from Staphylococcus aureus. *Biochimie* 92(12):1793-1800.

128. Fan C, Moews PC, Walsh CT, & Knox JR (1994) Vancomycin resistance: structure of D-alanine:D-alanine ligase at 2.3 A resolution. *Science* 266(5184):439-443.

129. Mol CD*, et al.* (2003) Crystal structures of active fully assembled substrate- and product-bound complexes of UDP-N-acetylmuramic acid:L-alanine ligase (MurC) from Haemophilus influenzae. *Journal of Bacteriology* 185(14):4152-4162.

130. Bouhss A, Crouvoisier M, Blanot D, & Mengin-Lecreulx D (2004) Purification and characterization of the bacterial MraY translocase catalyzing the first membrane step of peptidoglycan biosynthesis. *The Journal of Biological Chemistry* 279(29):29974-29980.

131. Al-Dabbagh B*, et al.* (2008) Active site mapping of MraY, a member of the polyprenyl-phosphate N-acetylhexosamine 1-phosphate transferase superfamily, catalyzing the first membrane step of peptidoglycan biosynthesis. *Biochemistry* 47(34):8919-8928.

132. van Heijenoort Y, Gomez M, Derrien M, Ayala J, & van Heijenoort J (1992) Membrane intermediates in the peptidoglycan metabolism of Escherichia coli: possible roles of PBP 1b and PBP 3. *Journal of Bacteriology* 174(11):3549-3557.

133. Hu Y*, et al.* (2003) Crystal structure of the MurG:UDP-GlcNAc complex reveals common structural principles of a superfamily of glycosyltransferases. *Proceedings of the National Academy of Sciences of the United States of America* 100(3):845-849.

134. Unligil UM & Rini JM (2000) Glycosyltransferase structure and mechanism. *Current Opinion in Structural Biology* 10(5):510-517.

135. Biarrotte-Sorin S, Maillard AP, Delettre J, Sougakoff W, Arthur M, & Mayer C (2004) Crystal structures of Weissella viridescens FemX and its complex with UDP-MurNAc-pentapeptide: insights into FemABX family substrates recognition. *Structure* 12(2):257-267.

136. Benson TE*, et al.* (2002) X-ray crystal structure of Staphylococcus aureus FemA. *Structure* 10(8):1107-1115.

137. Bera A, Herbert S, Jakob A, Vollmer W, & Götz F (2005) Why are pathogenic staphylococci so lysozyme resistant? The peptidoglycan O-acetyltransferase OatA is the major determinant for lysozyme resistance of Staphylococcus aureus. *Molecular Microbiology* 55(3):778-787.

138. Figueiredo TA*, et al.* (2012) Identification of genetic determinants and enzymes involved with the amidation of glutamic acid residues in the peptidoglycan of Staphylococcus aureus. *PLoS Pathogens* 8(1):e1002508.

139. Gally D & Archibald AR (1993) Cell wall assembly in Staphylococcus aureus: proposed absence of secondary crosslinking reactions. *Journal of General Microbiology* 139(8):1907-1913.

140. Münch D, Roemer T, Lee SH, Engeser M, Sahl HG, & Schneider T (2012) Identification and in vitro analysis of the GatD/MurT enzyme-complex catalyzing lipid II amidation in Staphylococcus aureus. *PLoS Pathogens* 8(1):e1002509.

141. Nakel M, Ghuysen JM, & Kandler O (1971) Wall peptidoglycan in Aerococcus viridans strains 201 Evans and ATCC 11563 and in Gaffkya homari strain ATCC 10400. *Biochemistry* 10(11):2170-2175.

142. Mouilleron S & Golinelli-Pimpaneau B (2007) Conformational changes in ammonia-channeling glutamine amidotransferases. *Current Opinion in Structural Biology* 17(6):653-664.

143. Zalkin H (1993) The amidotransferases. *Advances in Enzymology and Related Areas of Molecular Biology* 66:203-309.

144. Massiere F & Badet-Denisot MA (1998) The mechanism of glutamine-dependent amidotransferases. *Cell Mol Life Sci* 54(3):205-222.

145. Zalkin H & Smith JL (1998) Enzymes utilizing glutamine as an amide donor. *Advances in Enzymology and Related Areas of Molecular Biology* 72:87-144.

146. Tesmer JJ, Klem TJ, Deras ML, Davisson VJ, & Smith JL (1996) The crystal structure of GMP synthetase reveals a novel catalytic triad and is a structural paradigm for two enzyme families. *Nature Structural Biology* 3(1):74-86.

Acknowledgements

Appendix

License for the reuse of
Nilkens S, Koch-Singenstreu M, Niemann V, Götz F, Stehle T, & Unden G (2014) Nitrate/oxygen co-sensing by an NreA/NreB sensor complex of *Staphylococcus carnosus*. *Molecular Microbiology* 91(2):381-393. doi:10.1111/mmi.12464 in this thesis/dissertation (Ref. 85):

Licensee: Volker Niemann
License Date: Jul 28, 2015
License Number: 3677551363848
Publication: Journal of Molecular Biology
Title: Nitrate/oxygen co-sensing by an NreA/NreB sensor complex of *Staphylococcus carnosus*

License for the reuse of
Niemann V, Koch-Singenstreu M, Neu A, Nilkens S, Götz F, Unden G, & Stehle T (2014) The NreA protein functions as a nitrate receptor in the staphylococcal nitrate regulation system. *Journal of Molecular Biology* 426(7):1539-1553. doi:10.1016/j.jmb.2013.12.026 in this thesis/dissertation (Ref. 84):

Licensee: Volker Niemann
License Date: Jul 28, 2015
License Number: 3677551509476
Publication: Molecular Microbiology
Title: The NreA Protein Functions as a Nitrate Receptor in the Staphylococcal Nitrate Regulation System

Molecular Microbiology (2014) 91(2), 381–393 ■
doi:10.1111/mmi.12464
First published online 6 December 2013

Nitrate/oxygen co-sensing by an NreA/NreB sensor complex of *Staphylococcus carnosus*

Stephanie Nilkens,[1] Mareike Koch-Singenstreu,[1] Volker Niemann,[2] Friedrich Götz,[3] Thilo Stehle[2,4] and Gottfried Unden[1]*

[1]*Institute for Microbiology and Wine Research, Johannes Gutenberg University of Mainz, Germany.*
[2]*Interfaculty Institute of Biochemistry, and* [3]*Microbial Genetics, Interfaculty Institute for Microbiology and Infection Medicine Tübingen (IMIT), University of Tübingen, Germany.*
[4]*Department of Pediatrics, Vanderbilt University School of Medicine, Nashville, Tennessee, USA.*

Summary

In Staphylococci maximal induction of nitrate reductase (*narGHJI* genes) requires anaerobic conditions, the presence of nitrate, and the NreABC regulatory system. Aerobic regulation is effected by the NreB/NreC two-component system. The role of the nitrate receptor NreA in nitrate induction and its relation to aerobic regulation was analysed in *Staphylococcus carnosus*. Nitrate induction of a *narG-lip* reporter gene required presence of NreB/NreC. When *nreA* was deleted, nitrate was no longer required for maximal induction, suggesting that NreA is a nitrate regulated inhibitor of NreB/NreC. *In vitro*, NreA and mutant NreA(Y95A) decreased NreB phosphorylation in part or completely, which was due to the inhibition of the autophosphorylating activity rather than an increase of phosphatase activity. Inhibition of phosphorylation was relieved completely when the nitrate-bound NreA was used instead of the nitrate-free form. In the bacterial two-hybrid BACTH system and HPINE interaction assays, NreA interacted with NreB, but not with NreC, and the interaction was diminished by nitrate. In summary, NreA interacts with NreB and controls its phosphorylation level in a nitrate dependent manner. In this way nitrate and NreA modulate the function of the oxygen sensor NreB, resulting in nitrate/oxygen co-sensing by an NreA/NreB sensor unit as part of the NreABC-system.

Accepted 19 November, 2013. *For correspondence. E-mail unden@uni-mainz.de; Tel. (+49) 6131 3923550; Fax (+49) 6131 3922695.

Introduction

Staphylococcus carnosus grows preferentially by aerobic respiration, but in the absence of oxygen nitrate can be used as an electron acceptor to support anaerobic respiration and growth. The nitrate is reduced to ammonia, with nitrite being formed as an intermediate. Nitrate and nitrite reduction are catalysed by the membrane bound nitrate reductase of the NarG type (*narGHJI* genes) and cytoplasmic nitrite reductase (*nirBRD* genes) respectively (Fedtke *et al.*, 2002; Schlag *et al.*, 2008). Uptake of nitrate is effected by the NarT transporter (*narT* gene). Full induction of nitrate respiration requires anaerobic conditions and presence of nitrate (Fedtke *et al.*, 2002), but the contributions of anaerobic conditions and nitrate to the induction of nitrate respiration have not been quantified in detail due to the lack of a suitable reporter gene system.

Regulation of nitrate respiration by oxygen is effected in *S. carnosus* by the NreBC two-component system (*nreBC* genes) (Fedtke *et al.*, 2002; Kamps *et al.*, 2004). The cytoplasmic sensor kinase NreB is a direct O_2 sensor and uses a $[4Fe\text{-}4S]^{2+}$ cluster for O_2 sensing and control of kinase activity (Müllner *et al.*, 2008). Under anoxic conditions, NreB ligates a $[4Fe\text{-}4S]^{2+}$ cluster and the protein is then in the active state catalysing NreB autophosphorylation. The phosphoryl group is transferred to the response regulator NreC. Phosphorylated NreC (NreC-P) binds to DNA and stimulates the expression of *narG* and other target genes. Under anaerobic conditions, the presence of nitrate further stimulates the expression of *narG* (Fedtke *et al.*, 2002).

NreA of *S. carnosus* is a cytoplasmic protein consisting only of a GAF domain. The GAF domain is named after cGMP-specific phosphodiesterases, adenylyl cyclases and FhlA, three proteins in which the domain was originally identified (Aravind and Ponting, 1997). The recently solved crystal structure of NreA shows that the protein binds one molecule of nitrate at the binding site of the GAF domain (V. Niemann *et al.*, pers. comm.). The nitrate receptor NreA is found in most bacteria featuring NreBC of the Staphylococcus type, that is NreB with four conserved cysteine residues (Unden *et al.*, 2013). The respective group of bacteria comprises the *Staphylococci, Bacillus clausii, Paenibacillus spec.*, *Listeria grayi* and some other bacteria (Unden *et al.*, 2013). Mutations at the

binding site for nitrate profoundly affect the function of NreA *in vivo* and indicate that NreA is directly involved in nitrate dependent regulation of *S. carnosus* (V. Niemann *et al.*, pers. comm.). NreA shares no similarities with nitrate sensors or receptors known from other bacteria, such as the membrane bound sensor kinase NarX of proteobacteria (Williams and Stewart, 1997; Cheung and Hendrickson, 2009), the periplasmic nitrate binding protein NrtA from *Synechocystis sp.* (Koropatkin *et al.*, 2006), or the cytoplasmic RNA binding protein and translational regulator NasR (Boudes *et al.*, 2012). Nitrate sensors of these types are not encoded by *S. carnosus* (Rosenstein *et al.*, 2009) which, together with the physiological effects of NreA deletion, suggests that NreA is responsible for nitrate sensing and regulation in *S. carnosus*.

Structural and other data gave no indication on how NreA effects nitrate regulation. The organization of the *nre* genes in the *nreABC* gene cluster and the effects of NreA deletion on *narG* expression suggest that NreA is closely linked in function to the NreB-NreC two-component system, and that NreA inhibits in some way the transcriptional activation of *narG* when no nitrate is present. In order to investigate in which way NreA regulates the expression of nitrate respiratory genes, here *in vivo* and *in vitro* studies were performed. The *in vivo* studies should demonstrate the significance of NreA in the expression of *narG* in response to nitrate, and differentiate the function of NreA and NreB in nitrate and oxygen regulation. *In vitro*, purified NreA, NreB and NreC proteins were used to identify the role of NreA in nitrate regulation and its functional relation to NreB and NreC. It turned out that NreA does not directly interact with *narG* promoter DNA. Instead, NreA interacts with NreB and modulates the kinase activity of NreB in response to nitrate, suggesting that NreA/NreB form a sensor complex that responds to nitrate and oxygen.

Results

Control of narG-lip expression by nitrate requires nreA, nreB and nreC

For quantitative studies on the effect of the NreA and NreB proteins on nitrate reductase (*narG*) expression *in vivo* in *S. carnosus*, a reporter gene system was established with the lipase gene *lip* from *S. hyicus* as the reporter. The lipase is secreted by the cells and is not sensitive to adverse parameters such as oxygen or nitrate. The amount produced was quantified in the supernatant with a colorimetric assay (Rosenstein *et al.*, 1992). The reporter gene *narG-lip* is under the transcriptional control of the *narG* promoter, which possesses the GC-rich palindromic NreC binding site (Fedtke *et al.*, 2002). The expression test plasmid pMW1040 carries in addition to the reporter gene *narG-lip* the *nreABC* operon. This plasmid was used in a strain with the chromosomal deletion Δ*nreABC*, to study the role of NreB-NreC or NreA (and variants thereof) in transcriptional regulation of *narG-lip* in response to nitrate or oxygen. Figure 1 shows *narG-lip* expression during aerobic and anaerobic mid-exponential growth. In strain *S. carnosus* m1 pMW1040 (white bars), which is positive for *nreA, nreB* and *nreC*, the low lipase activity was slightly increased by nitrate during aerobic growth but by a factor of 13.3 by applying anaerobic conditions. The anaerobic expression was further increased 2.3-fold by nitrate.

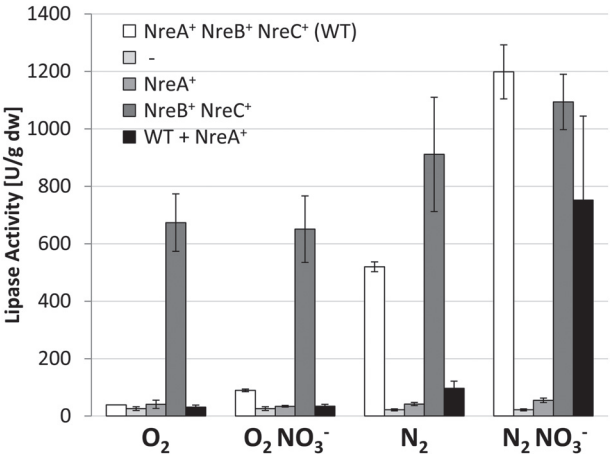

Fig. 1. Quantification of *narG-lip* expression *in vivo*. The effect of O_2 and NO_3^- on *narG-lip* expression was tested in the Δ*nreABC S. carnosus* mutant m1 that was complemented with various *nre* genes on plasmid: *S. carnosus* m1 pMW1040 encoding *nreA nreB nreC*, *S. carnosus* m1 pMW1001 encoding no *nreABC* (–), *S. carnosus* m1 pMW1532 encoding *nreA*, and *S. carnosus* m1 pMW1393 encoding *nreB nreC*. In addition a strain with chromosomal *nreABC* and an additional plasmid encoded *nreA* (*S. carnosus* TM300 pMW1532) was tested (wild-type and plasmid encoded *nreA*). The *narG-lip* expression was quantified by measuring the lipase activity photometrically at 415 nm. Supernatant of a culture grown to an OD_{578} of 0.5 was used. The graphs show averages of three independent growth experiments each of which was measured in triplicate; error bars indicate the standard deviation.

A strain lacking the *nreABC* operon (*S. carnosus* m1 pMW1001, light grey bars) produced only very low lipase activity under all conditions. Comparably low activities were obtained with the strain lacking *nreBC* but containing *nreA* (*S. carnosus* m1 pMW1532). The *nreA* deficient strain (*S. carnosus* m1 pMW1393) that contains intact *nreB* and *nreC*, was used to identify the role of NreA for control of *narG-lip* expression. The strain showed high lipase activity during aerobic growth, which was further increased (1.4-fold) under anaerobic conditions. Under aerobic and anaerobic conditions there was no significant nitrate effect visible.

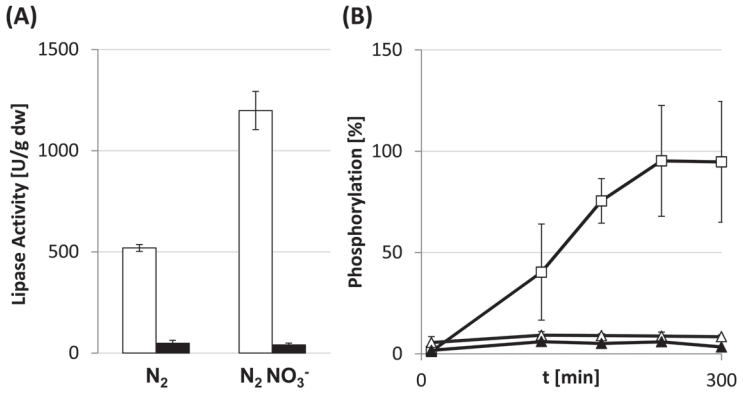

Fig. 2. Effect of NreA(Y95A) on *narG-lip* expression (A) and NreB autophosphorylation (B) with and without nitrate.
A. The effect of the mutation Y95A in NreA on *narG* expression was tested with the strain *S. carnosus* m1 pMW1298 encoding NreA(Y95A) NreBC (black bars) in comparison to the *S. carnosus* m1 pMW1040 encoding wild-typic NreABC (white bars) under anaerobic conditions. The *narG-lip* expression was quantified as described above. The graphs show averages of three independent growth experiments, where each independent experiment was repeated three times; the error bars indicate the standard deviation.
B. NreA(Y95A) or NreA(Y95A)·[NO_3^-] were added at a concentration of 600 μM to the reaction mixture before starting the phosphorylation of anaerobically isolated NreB (15 μM) by the addition of [γ-^{33}P] ATP. The graphs show NreB phosphorylation (–□–) in presence of NreA(Y95A) (–△–) and NreA(Y95A)·[NO_3^-] (–▲–) with averages of two independent experiments, each of which was measured in triplicate. The error bars indicate the standard deviation.

Strain *S. carnosus* TM300 pMW1532 carries plasmid encoded *nreA* in addition to the *nreABC* encoded chromosomal genes for over-production of NreA. Under aerobic conditions very low activities of lipase were found, and nitrate caused no significant induction. Interestingly, anaerobic conditions caused only a weak induction in contrast to the wild-type, and only addition of nitrate raised *narG-lip* expression to high levels, which was, however, still below the corresponding expression of the wild-type. The higher concentration of *nreA* (and presumably NreA) in the cell led to an increase in difference between expression under anaerobic conditions with nitrate and those without nitrate (8-fold increase).

Related studies have shown that mutation NreA(Y95A) has a profound effect on nitrate induction by NreA. The NreA(Y95A) variant exhibits a more solvent-accessible binding pocket with reduced nitrate affinity (V. Niemann *et al.*, pers. comm.). In Fig. 2A the effect of the variant NreA(Y95A) on *narG-lip* expression was tested in the strain *S. carnosus* m1 pMW1298 which produces NreA(Y95A) instead of NreA (in addition to NreB-NreC). The expression of *narG-lip* was similar to that obtained with the *nreABC* deletion strain *S. carnosus* m1 pMW1001. Under all conditions tested (aerobic, anaerobic, with and without nitrate) there were only low lipase activities, demonstrating that NreA(Y95A) has a strong negative effect on *narG* expression, even in the presence of nitrate. In the *S. carnosus* mutant where *nreA* was replaced by a variant encoding NreA(Y95A), anaerobic growth rate on nitrate was decreased by a factor of 2 or more (not shown). Overall, the quantitative data obtained with the *narG-lip* reporter are compatible with an interpretation that the (O_2-sensitive) expression of *narG-lip* is modulated by NreA in a negative manner in the absence of nitrate.

NreA controls NreB autophosphorylation in response to nitrate availability

In a first approach for identifying the site and mode of NreA action, the protein was overproduced in *Escherichia coli* M15 pQE31nreA and purified. Purified NreA (with and without nitrate) was applied to gel shift experiments with a *narG* promoter fragment. Neither NreA nor NreA·[NO_3^-] caused a shift of the *narG* promoter fragment in mobility shift experiments (Fig. S1). This is in contrast to mobility shifts obtained with phosphorylated NreC (Fedtke *et al.*, 2002), indicating that NreA does not function by binding to the *narG* promoter DNA.

In a further experiment the conserved Asp residue of NreC that accepts the phosphoryl residue from NreB-P was mutated to a Glu residue. This mutation can either permanently activate NreC by simulating phosphorylation of the Asp residue, or inactivate the protein when the structural changes are inhibitory. Replacement of wild-typic NreC by the NreC(D53E) variant diminished *narG-lip* expression to near background levels even under anaerobic conditions, and the nitrate effect or induction was also mostly lost, suggesting that nitrate induction of *narG* requires NreC (not shown) similar to the anaerobic induction.

In an alternative approach the effect of NreA on NreB phosphorylation was tested *in vitro* with purified proteins. Phosphorylation of NreB was assessed by labelling with [^{33}P] phosphate derived from [γ-^{33}P] ATP. The amount of

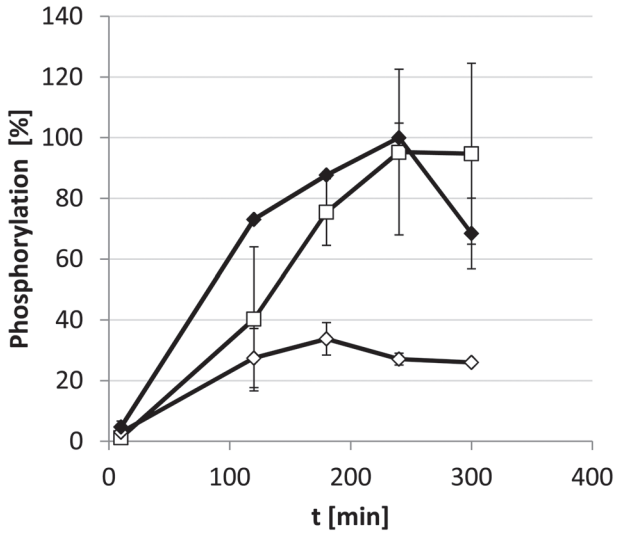

Fig. 3. The effect of NreA and NreA·[NO_3^-] on NreB autophosphorylation. Phosphorylation of a mixture of anaerobically isolated NreB (15 μM) and NreA was started by the addition of [γ-^{33}P] ATP. NreA or NreA·[NO_3^-] were present at a concentration of 600 μM. The graphs show NreB phosphorylation without (-□-) and in the presence of NreA (-◇-), and NreA·[NO_3^-] (-◆-), with averages of two independent experiments, each of which was measured in triplicate. The error bars indicate the standard deviation.

NreB-phosphorylation was measured by quantitative autoradiography after SDS-PAGE to remove phosphate from the protein which was not covalently bound. Anaerobically isolated NreB was phosphorylated after addition of [γ-^{33}P] ATP, and rapidly dephosphorylated at the expense of NreC when NreC was added (Fig. S2). This indicates that the phosphorylation and P-transfer cascade, including NreB phosphorylation, NreB/NreC phosphoryl transfer, and NreC dephosphorylation are intact in the isolated system.

To test whether NreA has a (direct) effect on NreB phosphorylation, labelling of NreB by [^{33}P] was performed under anoxic conditions, under conditions previously optimized for NreB (Müllner *et al.*, 2008), in the presence and absence of NreA (Fig. 3). Phosphorylation was slow but response of sensor kinases to their stimuli can be slow as observed for other sensor kinases (Janausch *et al.*, 2002; Sousa *et al.*, 2013). Phosphorylation of NreB occurred at constant rates during the first 100 min (Fig. S3).

The presence of NreA inhibited the rate and level of NreB phosphorylation (Fig. 3). NreA with bound nitrate (NreA·[NO_3^-]), on the other hand, no longer inhibited the phosphorylation. The rates of phosphorylation exceeded those of NreB alone, and the maximal levels were comparable to those obtained without NreA. The nitrate effect was only observed with NreA that was overproduced and isolated in the presence of nitrate. Mere addition of nitrate to the reaction mixture had no effect on NreB phosphorylation, demonstrating that NreA is required for the nitrate effect.

In vivo the variant NreA(Y95A) had a strong effect on *narG* expression (Fig. 2A) and growth (not shown) in the absence and in the presence of nitrate. NreA(Y95A) was overproduced and isolated in the absence and the presence of nitrate. Presence of the NreA(Y95A) protein in the phosphorylation experiment decreased NreB autophosphorylation to background levels (Fig. 2B); only 6% of the NreB phosphorylation obtained with wild-type NreA was reached. NreA(Y95A) prepared in the presence of nitrate showed the same inhibition of NreB phosphorylation as nitrate-free NreA(Y95A). It appears that the variant NreA(Y95A) inhibited phosphorylation of NreB much stronger than wild-typic NreA, and nitrate was not able to relieve the inhibitory effect. This is in agreement with the almost complete loss of *narG-lip* expression by this variant in the presence and absence of nitrate (Fig. 2A).

To elaborate the differences of NreA, NreA·[NO_3^-] and NreA(Y95A) on NreB phosphorylation, the initial rates of NreB phosphorylation were determined as a function of the concentrations of the NreA variants. The rate of NreB phosphorylation was set to 100% when no NreA was present (Fig. 4). With increasing concentrations of wild-typic NreA, the phosphorylation rate of NreB gradually decreased and reached 40% of the original activity in the presence of 550 μM NreA. NreA(Y95A) was a more efficient inhibitor and decreased the phosphorylation to 7% of the original activity in the presence of 550 μM protein. NreA·[NO_3^-] showed a smaller effect on NreB phosphor-

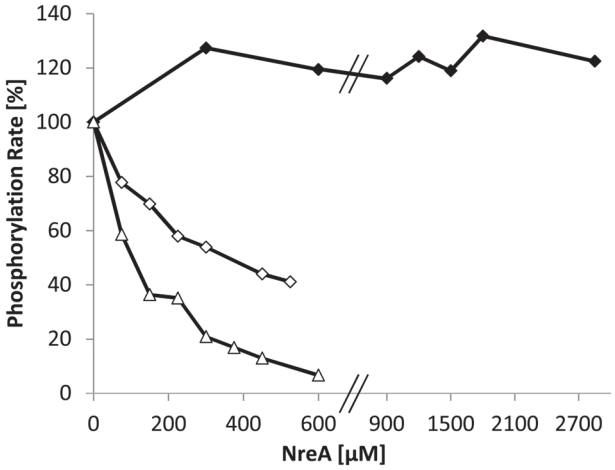

Fig. 4. Autophosphorylation of NreB with increasing NreA, NreA·[NO_3^-] and NreA(Y95A) concentrations. The phosphorylation rate (enzyme activity) was measured by determining the initial rate or amount of NreB phosphorylation after 100 min with different NreA concentrations. The phosphorylation rate of NreB without NreA was set to 100%. The graphs show the NreB phosphorylation rate in presence of NreA (-◇-), NreA·[NO_3^-] (-◆-) and NreA(Y95A) (-△-).

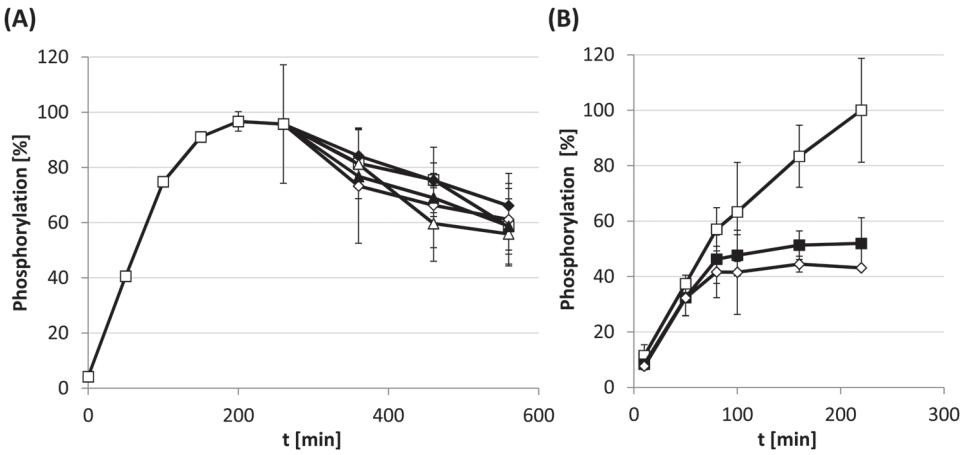

Fig. 5. The effect of NreA and NreA(Y95A) with or without nitrate on phosphorylated NreB in the absence of ATP.
A. The removal of ATP was performed by gel filtration chromatography. Anaerobically isolated NreB (27 μM) was phosphorylated for 200 min by [γ-^{33}P] ATP and then applied to a gel filtration matrix Sephadex G50 Superfine to remove residual [γ-^{33}P] ATP. The NreB-[^{33}P] (10 μM) without [γ-^{33}P] ATP from the column was incubated with NreA (-◇-), NreA·[NO_3^-] (-◆-), NreA(Y95A) (-△-), or NreA(Y95A)·[NO_3^-] (-▲-). The NreA proteins were added at a concentration of 400 μM. For comparison NreB phosphorylation was monitored without the addition of NreA protein (-□-). The phosphorylation state was detected by SDS-PAGE followed by phosphoimaging. The graphs show averages of two independent experiments. The error bars indicate the standard deviation.
B. The removal of ATP was performed by glucose and hexokinase. Anaerobically isolated NreB (15 μM) was phosphorylated with [γ-^{33}P] ATP in presence of glucose (0.4 μM). After 49 min hexokinase (40 U l^{-1}) was added to the reaction mixture for ATP dephosphorylation. After 85 min NreA (400 μM) was added. The graphs show the NreB phosphorylation without hexokinase and without NreA (-□-), with hexokinase (-■-), and with hexokinase and NreA (-◇-). Averages of three independent experiments were measured; error bars indicate the standard deviation.

ylation and stimulated NreB phosphorylation activity by up to approx. 20%. This level of stimulation remained constant for levels up to 2700 μM NreA·[NO_3^-]. Therefore NreA and in particular NreA(Y95A) have an inhibitory effect on NreB phosphorylation that is lost for wild-typic NreA in the nitrate bound form.

Overall, the data show that NreA has an effect on NreB phosphorylation that is most explicit and unequivocal for NreA(Y95A), which leads to a full inhibition of NreB phosphorylation. The concentrations of the NreA proteins used here were in the medium (75 μM) to high (600 μM) micromolar range. The concentrations of the proteins in the bacteria are not known, and the relatively high concentrations required here might be due to the *in vitro* conditions that not fully meet *in vivo* conditions.

NreA and NreA·[NO_3^-] *do not effect NreB-P dephosphorylation*

The negative effect of NreA on NreB phosphorylation can be explained by an inhibition of NreB phosphorylation, but on the contrary, there is also the possibility that NreA stimulates dephosphorylation of NreB-P. When NreA was added to NreB that was already phosphorylated to a large extent, further phosphorylation was hampered (Fig. S4). The inhibition of NreB phosphorylation by the late addition of NreA is in line with an inhibitory effect of NreA, but a competition by NreA dephosporylation and NreB autophosphorylation with residual ATP (resulting in constant phosphorylation levels) had to be excluded.

To obtain clean experimental conditions, NreB-P was first produced, and then residual ATP was removed by gel filtration chromatography to adjust conditions in which no further phosphorylation by ATP can take place. Under these conditions a very slow decrease of NreB phosphorylation was observed (Fig. 5A) which is compatible with the spontaneous dephosphorylation due to intrinsic lability of histidyl phosphate (Krell *et al.*, 2010). There was no stimulation of NreB-P dephosphorylation, however, when NreA or NreA(Y95A) were added, either with or without nitrate. Therefore NreA or NreA(Y95A) do not stimulate dephosphorylation of NreB-P.

In a similar experiment residual ATP was consumed after phosphorylation of NreB-P by the addition of hexokinase and glucose, which results in rapid and complete consumption of ATP by the exergonic hexokinase reaction. When this experimental set was supplemented again with NreA there was no stimulation of NreB-P dephosphorylation (Fig. 5B). Therefore both experiments show that NreA has no significant phosphatase activity, and does not stimulate such an activity.

NreA interacts with NreB in a nitrate dependent manner in vivo

The experimental data suggest that NreA interacts with NreB to control phosphorylation. The BACTH (bacterial

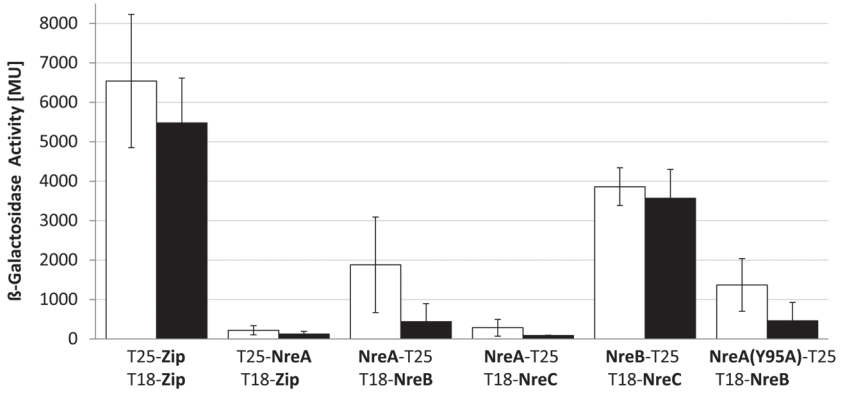

Fig. 6. Interaction study of the Nre proteins by BACTH. *E. coli* BTH101 was co-transformed with plasmid pairs. In each pair one plasmid encoded a T25 fusion and the other a T18 fusion of an Nre protein. NreA-T25 (pMW1775), T25-NreA (pMW1423), NreA(Y95A)-T25 (pMW2065), NreB-T25 (pMW1776) were the T25 fusions, and T18-NreB (pMW1424) and T18-NreC (pMW1425) were the T18 fusions. The β-galactosidase activity was determined after growth to an OD_{570} of 0.25 to 0.5. The interaction was tested in absence (white bars) and in presence (black bars) of 10 mM $NaNO_3$.The strain expressing the pair of leucine zipper proteins, T25-Zip (pKT25) and T18-Zip (pUT18C), was used as a positive control. The background for non-interacting proteins is represented by the interaction level of the pair T25-NreA and T18-Zip.

two-hybrid system) was used to assess whether the components of the NreA-NreB-NreC system interact *in vivo*. NreA, NreB and NreC were fused to the T25 or T18 domains of adenylate cyclase, and interaction of the proteins was tested pairwise by their ability to reconstitute active adenylate cyclase from the fusion proteins in the *E. coli* test strain BTH101. Reconstitution depends on reuniting the domains by the interaction of the Nre proteins. For each of the Nre proteins 4 types of fusions were produced (i.e. NreX-T25, NreX-T18, T25-NreX, T18-NreX), and for any of the pairs (NreA/NreB, NreA/NreC, NreB/NreC) each of the eight combinations was tested for interaction. When for a pair three or more combinations showed a positive reaction, it was assumed that the pairs interact; only one of the representative pairs is shown in Fig. 6. The data are compared with positive (interaction of two zipper proteins T18-zip/T25-zip) and negative (interaction T18-zip/T25-NreA) control pairs. The NreA/NreB pair showed significant β-galactosidase activity after anaerobic growth that amounted to 29% of the positive control of the Zip protein, and was clearly (by a factor of 8) above the background of non-interacting proteins (zip/NreA). The value for the NreA/NreC pair, however, was below the background level. The pair NreB/NreC showed very high β-galactosidase activity, amounting to 61% of the positive control, which is in agreement with the function of NreB and NreC as cognate pair of a two-component system. Overall, the data present evidence for interactions of NreB with either NreA or NreC, while NreA and NreC did not interact directly in this assay.

When the BACTH experiments were repeated in bacteria grown anaerobically in the presence of nitrate, the β-galactosidase activity for the NreA/NreB pair decreased to 24% of the activity during nitrate deficient growth, but the nitrate value was still above background. In the other pairs (NreB/NreC, and NreA/NreC) there was only a small decrease in the presence of nitrate and in the same range as observed for the control pair (Zip/Zip). These data indicate that the interaction of NreB with NreA but not with NreC is specifically decreased in the presence of nitrate. When the same experiment was performed with the pair NreA(Y95A)/NreB, the interaction or β-galactosidase activity was generally lower, but there was also a response to nitrate which was also observed for other fusions of the NreA(Y95A)/NreB pair. The BACTH data therefore suggest that nitrate binding to NreA(Y95A) has an effect on NreA/NreB interaction even though nitrate no longer controls the function of NreA(Y95A). Interaction of NreB with Nre(Y95A) is compatible with the experiment of Fig. 2B which shows inhibition of NreB by NreA(Y95A). The bacteria are expected to take up nitrate under the respective growth conditions (anaerobic with nitrate), and therefore the nitrate effect is presumably effected in the cytoplasm of the bacteria.

In a second approach, direct interaction of NreA and NreB was studied using HPINE (His-Protein Interaction Experiment). The HPINE assay (S. Graf *et al.*, pers. comm.) is based on the coexpression of two potential interaction partners in *E. coli* cells, and only one of the proteins carries a His_6-tag for affinity purification on a Ni-NTA column. Interacting proteins are cross-linked in the bacteria by the addition of the permeant cross-linker formaldehyde. The supernatant of the cell homogenate is then tested for binding of the non-His-tagged protein to the Ni-NTA column. In the experiment of Fig. 7A, *E. coli*

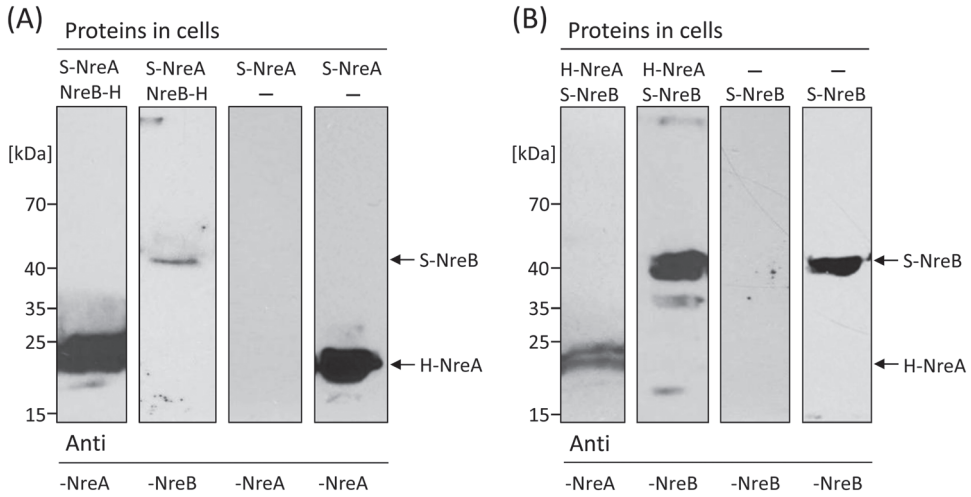

Fig. 7. Binding of NreA by NreB-His_6 (A) and NreB by His_6-NreA (B) to a Ni-NTA column (HPINE assay) after *in vivo* cross-linking of the proteins. Strep-NreA (S-NreA) encoded by pMW1243 and NreB-His_6 (NreB-H) encoded by pMW1950, or H-NreA (encoded by pMW1949) and S-NreB (encoded by pMW1192), respectively, were coexpressed in *E. coli* JM109. Formaldehyde (0.6% v/v) was added to the suspension of the bacteria at the end of growth. The cleared cell homogenate (170 mg protein) was applied to a Ni-NTA column. The flow-through and the eluate were collected, incubated for 5 min at 95°C, and applied to SDS-PAGE and Western blotting.
A. Eluate (lanes I, II, III) and flow-through (lane IV) of *E. coli* JM109 with S-NreA and NreB-H, or JM109 with S-NreA after Ni-NTA chromatography, tested with anti-NreA or anti-NreB as indicated.
B. Eluate (lanes I, II, III) and flow-through (lane IV) of *E. coli* JM109 with H-NreA and S-NreB or JM109 with S-NreB after Ni-NTA chromatography, tested with anti-NreA or anti-NreB as indicated.

coexpressing His_6-tagged NreB (NreB-H) and NreA with a Strep-tag (S-NreA) were treated with formaldehyde. The proteins of the cytoplasmic cell-fraction were applied to a Ni-NTA column. After extensive washing the bound proteins were eluted by imidazole, and the eluate was tested by SDS-PAGE and immunoblotting for the presence of NreA and NreB. As expected, the eluate contained NreB-H, but in addition also S-NreA. When bacteria were used that produced only S-NreA but no NreB-H, S-NreA was found in the flow-through of the Ni-NTA column, whereas the imidazole eluate contained no S-NreA (Fig. 7A), demonstrating that NreB-H is required to retain S-NreA on the column. The experiment was also performed in the reverse way (Fig. 7B), that means NreA was equipped with the His_6-tag (H-NreA), and NreB with the Strep-tag (S-NreB). The Western blot (Fig. 7B) shows after the corresponding treatment of the bacteria that NreB-S was retained on the Ni-NTA column in the presence of NreA-H (and only in its presence). H-NreA showed a double-band of proteins in the eluate with slightly differing molar mass; both bands responded to anti-NreA serum confirming the identity of the bands. The HPINE experiments of Fig. 7 therefore demonstrate that NreA and NreB can be cross-linked by formaldehyde which allows their binding via the His_6-tagged partner to a Ni-NTA column. In a similar way, isolated NreA and NreB were cross-linked *in vitro* by formaldehyde (not shown).

Discussion

The nitrate receptor NreA controls kinase activity of NreB in a nitrate-dependent manner

The nitrate receptor NreA is found in most bacteria featuring NreBC of the *Staphylococcus* type that contains NreB with four conserved cysteine residues (Unden *et al.*, 2013). The *nreA* gene is colocalized with the *nreBC* genes in the *nreABC* operon (Schlag *et al.*, 2008) suggesting that the NreBC two-component system is used in the bacteria for regulating genes that respond to O_2 and nitrate (Unden *et al.*, 2013), such as the *narGHJI* and *narT* genes for nitrate reductase and the nitrate transporter respectively. Expression of *narG* responds to O_2 and nitrate. Regulation in response to O_2 is effected by the NreB-NreC two-component system (Kamps *et al.*, 2004; Müllner *et al.*, 2008), whereas NreA is responsible for nitrate regulation together with the NreB-NreC proteins (Schlag *et al.*, 2008; this work). In agreement with the function of NreA as a novel nitrate receptor, *S. aureus* and *S. carnosus* contain neither homologues of the NarXL-like nitrate two-component systems known from *E. coli* (Williams and Stewart, 1997), nor of the periplasmic nitrate binding protein NrtA from *Synechocystis sp.* (Koropatkin *et al.*, 2006), or of the nitrate responsive RNA binding NasR functioning as a translational regulator (Boudes *et al.*, 2012).

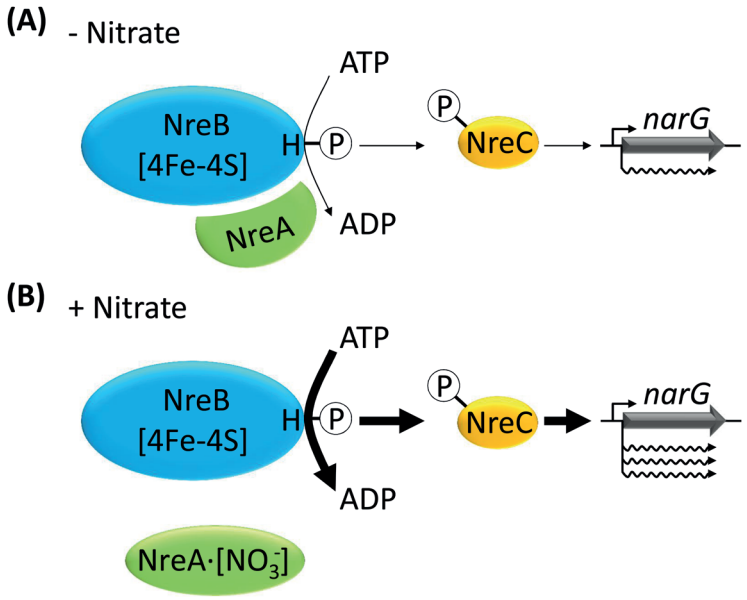

Fig. 8. Model for the function of NreA in nitrate regulation of *narG* expression under anaerobic conditions: Formation of an NreA/NreB sensor complex for response to O_2 and nitrate. In the absence of nitrate, NreA binds to NreB and inhibits NreB phosphorylation activity, leading to a decreased NreC phosphorylation and consequently to a decreased *narG*-expression. In the presence of nitrate, NreA·[NO_3^-] is formed and interaction with NreB is changed or decreased, and the inhibitory effect of NreA is lost. NreB shows full autokinase activity leading to a strong *narG* expression.

The *in vivo* and *in vitro* experiments show that NreA interacts physically and functionally with NreB in a nitrate dependent manner. The physical interaction is evident from the BACTH and the HPINE interaction analyses, and by cross-linking of the isolated proteins. Purified NreA obviously inhibited autokinase activity of anaerobic (active) NreB, which was relieved in the presence of nitrate. At the same time the interaction between NreA and NreB decreased in the presence of nitrate.

The negative effects of NreA on the phosphorylation of NreB basically could be due to an inhibition of the NreB kinase, or by providing phosphatase activity for NreB-P dephosphorylation. The data exclude the latter option because the phosphorylation state of NreB-P was constant or not decreased compared with the background when NreB-P was incubated with NreA or NreA·[NO_3^-]. This also applies for NreA(Y95A) for which high phosphatase activity would be required due to the strong decrease or inhibition of NreB phosphorylation. The postulated function as an inhibitor of the kinase is also compatible with the strong NreA and NreB interaction. PAS domains are often used for recruiting co-sensors or co-activators in order to enable signal-integration and -confluence (Razeto *et al.*, 2004; Partch and Gardner, 2010; Witan *et al.*, 2012). It seems likely that the interaction between NreB and NreA represents a further example for a PAS/GAF domain interaction. Future experiments will have to characterize the NreB/NreA interaction in detail in order to understand the mode of interaction and regulation on a molecular level.

The inhibitory function of NreA is relieved by nitrate binding and formation of the NreA·[NO_3^-] complex. The NreA(Y95A) mutation exhibits a more solvent-accessible binding pocket with reduced nitrate affinity (V. Niemann *et al.*, pers. comm.). This diminishes efficient expression of *narG* under anaerobic conditions either with or without nitrate, suggesting that the variant is permanently in the inhibitory form, and represents a more efficient inhibitor than wild-typic NreA. These *in vitro* data are in agreement with the nearly complete loss of *narG-lip* expression in the NreA(Y95A) mutant.

Overall, it can be concluded that the nitrate receptor NreA inhibits NreB phosphorylation and activity, and this inhibition is relieved by nitrate. Thus nitrate regulation in *S. carnosus* is closely intertwined with O_2 sensing by NreB, and the nitrate receptor NreA modulates the NreB kinase. The close link between both systems is reflected on the genetic level by organizing *nreA* with *nreBC* in the same operon.

A model for the control of narG expression by NreA-NreB in response to nitrate and O_2

NreA functions as the nitrate receptor, and interacts with NreB in a nitrate dependent manner which appears to be the basis for NreA function in context with NreB. *In vivo* and *in vitro* NreA interacts with NreB and modulates in this way the kinase activity of anaerobic NreB (Kamps *et al.*, 2004; Müllner *et al.*, 2008), as indicated in Fig. 8. The following scheme for the function of NreA in nitrate sensing arises. Under anaerobic conditions NreB binds a $[4Fe\text{-}4S]^{2+}$ cluster and autophosphorylates His_{159} in the kinase domain. The phosphoryl group is transferred to Asp_{53} on the response regulator NreC that then activates the transcription of target genes including the *narG* operon.

NreA binds to NreB in the absence of nitrate (Fig. 8A). In this state, NreA inhibits the kinase activity of NreB, and

NreB autophosphorylation is decreased even though NreB is in the active form. Experimentally this situation is characterized by NreA/NreB interaction in the BACTH, HPINE and cross-link experiments, and by the inhibition of NreB autophosphorylation *in vitro*.

In the presence of nitrate an NreA·[NO_3^-] complex is formed (Fig. 8B). NreA·[NO_3^-] shows decreased interaction with NreB, and no longer inhibits phosphorylation of NreB. *In vivo* under these conditions maximal expression of the *narG-lip* reporter is observed. A similar situation is achieved in an *nreA* deletion strain where the inhibiting effect of NreA is missing and increased expression of *narG-lip* is observed. *narG-lip* is then expressed even under aerobic conditions where NreB is mostly inactive (Müllner *et al*., 2008).

It is obvious that nitrate and aerobic regulation in *S. carnosus* differ fundamentally from NarX-NarL containing bacteria such as *E. coli*. Nitrate and aerobic regulation are exerted by two independent systems in *E. coli*, that is NarX-NarL (or NarQ-NarP) for nitrate and FNR (or ArcB-ArcA) for O_2 sensing. The nitrate and O_2 systems detect and transmit the signals independently to target genes such as *narG* of *E. coli*. The promoter of $narG_{Ec}$ is subject to transcriptional regulation by NarL and FNR, and there are binding sites for both regulators. The NreA-NreB-NreC system for nitrate and O_2 sensing, on the other hand, contains the NreB-NreC two-component system that responds to O_2, and the nitrate receptor NreA that modulates the function of the basic regulatory system NreB-NreC in response to nitrate. NreA is not able to regulate *narG* expression directly. In this way the NreA/NreB proteins represent a system for co-sensing of nitrate and O_2 that integrates the presence of two biochemically different stimuli. Control of aerobic and anaerobic respiration or fermentation is often very efficiently co-ordinated resulting in hierarchical control of expression (Gunsalus, 1992; Unden and Bongaerts, 1997). In the NreA-NreB-NreC system the joint regulation is verified in a new manner where one joint signal (NreC phosphorylation) is derived from two separate stimuli (nitrate and O_2 availability) and transferred to the target promoter. This mode of signal-integration and -confluence represents an efficient mode for signal co-ordination.

Experimental procedures

Growth and bacteria

The bacterial strains and plasmids used in this study are listed in Table 1. For the lipase kinetic analysis cells were grown in modified B(basic)-broth (BM) (10 g l^{-1} peptone, 5 g l^{-1} yeast extract, 5 g l^{-1} NaCl, 1 g l^{-1} glucose, pH 7.4 (Götz and Schumacher, 1987), without the addition of Na_2HPO_4 to avoid precipitate formation during the lipase assay. The medium was supplemented with chloramphenicol (10 µg ml^{-1}). For expression studies the bacteria were grown aerobically or anaerobically with and without nitrate as indicated. For aerobic growth an overnight culture was grown aerobically in a test tube on a rotary shaker. For the inoculation of the main culture, the bacteria were sedimented and washed in modified BM medium. The main culture (40 ml modified BM) was inoculated to an OD_{578} of 0.1 and grown in baffled flasks (300 ml) on a rotary shaker to an OD_{578} of 0.5. Then the growth was stopped by centrifuging (12 000 *g*, 5 min at RT), and the supernatant was stored on ice until determination of lipase activity. Anaerobic growth was performed equally except for the following variations. The overnight culture was grown in standing test tubes without agitation in an incubator at 37°C and the main culture was grown in rubber stoppered flasks (Müller-Krempel, Bülach, Switzerland) after replacing the gas phase with N_2 (99.99%). To test the effect of nitrate on *narG* expression under aerobic or anaerobic conditions, the overnight cultures as well as the main cultures were supplemented with 10 mM sodium nitrate.

For isolation of aerobic NreB-His_6 the strain *S. carnosus* m1 pCQE1nreB was used. On plasmid pCQE1nreB the *nreB* gene is cloned behind an inducible *xylA* promoter and before a His_6 encoding, C-terminal tag (Wieland *et al*., 1995; Fedtke *et al*., 2002). This strain was grown in yeast extract production medium YEP (45 g l^{-1} yeast extract, 50 mM sodium phosphate buffer pH 7.2, 40 mM glycerol) at 37°C on a rotary shaker at 200 r.p.m. to an OD_{578} of 10. Then the cells were induced with 150 mM xylose for 6 h until reaching an OD_{578} of about 30–40 (Müllner *et al*., 2008). For anaerobic isolation of NreB-His_6, anaerobic growth of the strain was performed in YEP medium supplemented with 10 mM sodium nitrate, 10 mM ammonium iron(III) citrate and 1 mM L-cysteine hydrochloride. First the cells were grown and induced aerobically as described above to reach a high OD_{578} of 18. After growth to an OD_{578} of 35, the culture was transferred to anaerobic flasks (Müller-Krempel, Bülach, Switzerland). The flasks were filled to the top leaving no air inside after sealing, and incubated by constant stirring (magnetic mixer) for 16 h at 4°C (Müllner *et al*., 2008).

For the isolation of His_6-NreA and His_6-NreA(Y95A) the strains *E. coli* M15 pQE31nreA and *E. coli* M15 pQE31nreA(Y95A) were used. On these plasmids *nreA* stands under the control of IPTG inducible T5 promoter. These strains were grown in lysogeny broth (LB; Bertani, 1951) medium (10 g l^{-1} peptone, 5 g l^{-1} yeast extract and 5 g l^{-1} NaCl) to an OD_{578} of 0.5. Then the cultures were induced by the addition of 1 mM IPTG for 5 h (Qiagen manual). For the isolation of His_6-NreA with bound nitrate (His_6-NreA·[NO_3^-] and His_6-NreA(Y95A)·[NO_3^-]) the medium was supplemented with 10 mM sodium nitrate at the beginning of growth and again 1 h and 4 h after induction. For the isolation of NreC-Strep the strain *E. coli* JM109 pMW1617, which carries a *tetA* promoter upstream of *nreC*, was grown in LB medium to an OD_{578} of 0.5. Then the culture was induced by the addition of 200 ng ml^{-1} anhydrotetracyclin for 5 h (IBA manual).

Preparation of proteins

Preparation of aerobic NreB-His_6 was performed after aerobic growth and induction of strain *S. carnosus* m1

Table 1. *S. carnosus* and *E. coli* strains and plasmids.

Strains and plasmids	Genotype	Reference or source
Strain		
S. carnosus TM300	WT	Schleifer and Fischer (1982)
S. carnosus m1	Δ*nreABC*::*ermB*	Fedtke *et al.* (2002)
E. coli XL1-Blue	*recA1*, *supE44*, *endA1*, *hsdR17*, *gyrA96*, *relA1*, *thi-1*, *lac*, [*F'*, *proAB*, *lacIqZΔM15*, *Tn10 (tet^R)*]	Stratagene
E. coli M15	[[pREP4], *Nal^S*, *Str^S*, *Rif^S*, *Thi$^-$*, *Lac$^-$*, *Ara$^+$*, *Gal$^+$*, *Mtl$^-$*, *F$^-$*, *RecA$^+$*, *Uvr$^+$*, *Lon$^+$*	Quiagen
E. coli JM109	*recA1*, *supE44*, *endA1*, *hsdR17*, *gyrA96*, *relA1*, thi-1, Δ(lac-proAB), [F', *traD36*, *proAB*, lacIqZΔM15]	Yanisch-Perron *et al.*, (1985)
E. coli BTH101	*Rec$^+$*, *F- cya-99*, *araD139*, *galE15*, *galK16*, *hsdR2*, *mcrA1*, *mcrB1 rpsL1* (str^R),	Karimova *et al.*, (1998)
Plasmid		
pPS44	staphylococcal promoter probe vector, *lip* (*Staphylococcus hyicus*), pC194 origin, *cam^R*	Peschel *et al.*, (1993)
pMW1001	pPS44 derivative with *narG* promoter introduced into the single BamHI site in front of lipase gene	This study
pRB473	*E. coli*/*S. carnosus* shuttle vector with *amp^R* for *E. coli* and *cam^R* for *S. carnosus*	Brückner (1992)
pRB473nreABC	pRB473 with *nreABC* and native promoter	Müllner *et al.*, (2008)
pCQE1nreB	pCQE1 derivative carrying *nreB*, staphylococcal His_6-tag (C-terminal) expression vector, xylose inducible, glucose repressible *xylA* promoter, *cam^R*	Fedtke *et al.*, (2002)
pQE31nreA	*nreA* with N-terminal His_6-tag, cloning by insertion of BamHI/HindIII restriction sites, *kan^R*, *amp^R*, IPTG inducible promoter	This study
pMW1733	pQE31nreA derivative with *nreA* coding NreA(Y95A)	This study
pMW1040	*nreABC, narG-lip, cam^R*	This study
pMW1298	pMW1040 derivative with *nreA* coding NreA(Y95A)	This study
pMW1393	pMW1040 derivative with *nreA* deletion	This study
pMW1532	pMW1040 derivative with *nreBC* deletion	This study
pKT25	C-terminal T25 protein fusion plasmid, pSU40 derivative, *kan^R*	Karimova *et al.* (1998)
pKNT25	N-terminal T25 protein fusion plasmid, pSU40 derivative, *kan^R*	Karimova *et al.* (1998)
pUT18	N-terminal T18 protein fusion plasmid, pUC19 derivative, *amp^R*	Karimova *et al.* (1998)
pT25-zip	T25-Zip expression plasmid, pKT25 derivative, *kan^R*	Karimova *et al.* (1998)
pT18C-zip	T18-Zip expression plasmid, pUT18C derivative, *amp^R*	Karimova *et al.* (1998)
pMW1423	T25-NreA expression plasmid, pKT25 derivative, *kan^R*	This study
pMW1425	T18-NreC expression plasmid, pUT18C derivative, *amp^R*	This study
pMW1424	T18-NreB expression plasmid, pUT18C derivative, *amp^R*	This study
pMW1775	NreA-T25 expression plasmid, pKNT25 derivative, *amp^R*	This study
pMW1776	NreB-T25 expression plasmid, pKNT25 derivative, *kan^R*	This study
pMW2065	NreA(Y95A)-T25 expression plasmid, pKNT25 dervative, *kan^R*	This study
pASK-IBA3plus	Strep-tag (C-terminal) expression vector, anhydrotetracyclin inducible, *tet*-promoter, *amp^R*	IBA
pMW1617	pASK-IBA3plus derivative with *nreC* introduced into the single BsaI site, C-terminal Strep-tag, *amp^R*	This study
pASK-IBA13plus	Strep-tag (N-terminal) expression vector, anhydrotetracyclin inducible, *tet*-promoter, *amp^R*	IBA
pMW1243	pASK-IBA13plus derivative with *nreA* introduced into XhoI and EcoRV site, N-terminal Step-tag, *amp^R*	This study
pMW1192	pASK-IBA13plus derivative with *nreB* introduced into BamHI and HindIII site, N-terminal Strep-tag, *amp^R*	This study
pMW400	NreB-His, pet28a derivate (NcoI; HindIII), C-terminal His_6-tag, *kan^R*	This study
pMW1949	pBAD33 derivate for overexpression of NreA with His_6-tag, anhydrotetracycline inducible, His_6-*nreA* cloned from pQE31nreA (PstI; HindIII), *cam^R*	This study
pMW1950	pBAD33 derivate for overexpression of NreB with His_6-tag, anhydrotetracycline inducible, *nreB*-His cloned from pMW400 (KpnI; XbaI), *cam^R*	This study

pCQE1nreB by addition of xylose. The procedure for preparation of anaerobic NreB-His_6 from the anaerobic culture of *S. carnosus* m1 pCQE1nreB was performed equally, except that all steps were performed under anoxic conditions in an anaerobic chamber (Coy) using anoxic buffers. To handle the anaerobic bacteria or solutions outside the chamber air tight sealed containers were used. Anaerobic NreB-His_6 was isolated as described by Müllner *et al.* (2008).

NreB fractions of 1 ml were obtained with protein concentrations of up to 16 mg ml^{-1}.

The preparation of His_6-NreA and His_6-NreA(Y95A) was performed as recommended (Qiagen) after aerobic growth and induction of strain *E. coli* M15 pQE31nreA and pMW1733 respectively. The disruption of *E. coli* cells was done aerobically with a French pressure cell press (3 passages, $13.8{\cdot}10^7$ kg s^{-2} m^{-1}). Cell debris was separated from solvent by centrifugation (20 000 *g*, 20 min and 4°C). The proteins were isolated from the cleared supernatant by chromatography via His-tag on a Ni-NTA column. The column was washed with wash buffer (20 mM imidazole, 1 M NaCl, 50 mM sodium phosphate pH 7.2, 20% glycerol) followed by eluting the protein from the column with elution buffer (150 mM imidazole, 300 mM NaCl, 50 mM sodium phosphate pH 7.2, 20% glycerol).

For the isolation of His_6-NreA·[NO_3^-] and His_6-NreA(Y95A)·[NO_3^-] all steps were performed equally except that the cells were grown in $NaNO_3$-containing medium (as described above), the lysis and wash buffers were supplemented with 100 mM sodium nitrate and the elution buffer with 20 mM sodium nitrate.

Preparation of NreC-Strep was performed as recommended (IBA manual) after aerobic growth and induction of strain *E. coli* JM109 pMW1617. The cells were pelleted (5000 *g* for 20 min and 4°C) and suspended in buffer W (100 mM Tris/HCl pH 8, 150 mM NaCl and 1 mM EDTA). Cells were disrupted in a French pressure cell press (3 passages, $13.8{\cdot}10^7$ kg s^{-2} m^{-1}) and cell debris was separated from solvent by centrifugation (20 000 *g*, 20 min and 4°C). The proteins were isolated by chromatography via Strep-tag of the clear supernatant on Strep-Tactin Sepharose. The

column was washed with buffer W followed by eluting the protein from the column by buffer E (buffer W with 2.5 mM desthiobiotin).

Genetic methods

The staphylococcal promoter probe vector pPS44 was used to construct the plasmid pMW1001, carrying the reporter gene fusion *narG-lip*. The promoter of *narG* was amplified by PCR using primers pnarG-BamH1-F and pnarG-BamHI-R (Table S1) from genomic DNA of *S. carnosus* TM300 and inserting BamHI restriction sites. The amplified *narG* promoter sequence comprises region −389 to +185, including two NreC recognition sites. The promoter was inserted into the single BamHI restriction site of pPS44. The plasmid pMW1001 was then transferred into *S. carnosus* TM300 by electroporation (Löfblom *et al*., 2007). For construction of plasmid pMW1040 the reporter gene fusion *narG-lip* from pMW1001 was amplified by PCR using primers narGlip-SbfI-F and narGlip-NheI-R to insert SbfI and NheI restriction sites. The fragment was inserted into the vector pRB473nreABC at the SbfI and NheI restriction sites. pRB473nreABC is a derivative of the *E. coli*/*S. carnosus* shuttle vector pRB473 carrying the *nreABC* operon with its native promoter (Brückner, 1992; Müllner *et al*., 2008). pMW1040 was amplified in *E. coli*, isolated and transformed into *S. carnosus* m1 by electroporation (Löfblom *et al*., 2007). The plasmid pMW1393 is a pMW1040 derivative with an *nreA* deletion. This deletion was performed by amplification of the plasmid pMW1040 without *nreA* with primers Del-nreA-F and Del-nreA-R, inserting a BglII restriction site. The fragment was then religated resulting in an *nreA* deletion, except for the four first amino acids of NreA and a deletion of the first two amino acids of NreB. *nreB* is put in frame with the beginning of *nreA*, being positioned under control of the native promoter. This plasmid was transformed into *S. carnosus* m1. The plasmid pMW1532 is a pMW1040 derivative with an *nreBC* deletion, encoding only *nreA*. The *nreBC* deletion was performed by amplification of the plasmid pMW1040 without *nreBC*, with primers Del-nreBC-F and Del-nreBC-R, inserting a BglII restriction site. The fragment was then religated resulting in an *nreBC* deletion and *nreA* receiving the terminator sequence of the operon. This plasmid was transformed into *S. carnosus* TM300 and *S. carnosus* m1. To create the plasmid pMW1298 encoding NreA(Y95A) the residue tyrosine 95 of NreA was mutated to alanine on plasmid pMW1040 by the site-directed mutagenesis kit (Stratagene) and primers nreA-Y95A-F and nreA-Y95A-R. This plasmid was amplified in *E. coli* and transformed into *S. carnosus* m1.

For over-production of His_6-NreA(Y95A) the plasmid pMW1733, a pQE31nreA derivative, was created. By site directed mutagenesis the residue tyrosine 95 was mutated to alanine with the primers nreA-Y95A-F and nreA-Y95A-R. This plasmid was transferred into *E. coli* M15. For over-production of NreC the pASK-IBA3plus expression vector was used and *nreC* inserted by primers NreC-BsaI-F and NreC-BsaI-R into the BsaI site of the multiple cloning site. This way the plasmid pMW1617 with *nreC* carrying a C-terminal Strep-tag was created and transformed into *E. coli* JM109.

For *in vivo* protein interaction studies BACTH was used (Karimova *et al*., 1998; 2005). For this purpose the T25 and T18 domains were fused to the N- or C-termini of NreA, NreB and NreC. The fusions were produced by cloning the *nreA, nreB* or *nreC*-genes after PCR amplification (A_BamHI-for A^{-1}-EcoRI-rev for *nreA*, B_XbaI-for/B_EcoRI-rev for *nreB*, and C_XbaI_for/C_KpnI-rev for *nreC*) into the pKT25 and pUT18C, or (pUT18nreA-for-2/pUT18nreA-rev-2 for *nreA*, pUT18nreB-for/pUT18nreB-rev for *nreB*) into pKNT25 and pUT18C vectors. The control gene fusions T25-*zip* and T18-*zip* were obtained from the BACTH-kit (Karimova *et al*., 1998).

For *in vivo* cross-links between NreA and NreB in the HPINE assay, the plasmid pMW1243 for production of NreA with an N-terminal Strep-tag was constructed by amplification of *nreA* with primers NreA(XhoI)-F and NreA(EcoRV)-R and insertion into the MCS of pASK-IBA13plus. For production of NreB with an N-terminal Strep-tag plasmid pMW1192 was constructed by amplification of *nreB* with primers NreB(BamHI)-F and NreB(HindIII)-R and insertion into the MCS of pASK-IBA13plus. The plasmid pBAD33-NreA (pMW1949) with NreA carrying an N-terminal His_6-tag was constructed by amplification of *nreA* from pQE31nreA with primers nreA-PstI-F and nreA-HindIII-R and insertion into the MCS of pBAD33. The plasmid pBAD33-NreB (pMW1950) with *nreB* carrying a C-terminal His_6-tag was constructed by amplification of *nreB* from pMW400 with primers NreB-XbaI-F and NreB-KpnI-R and insertion into the MCS of pBAD33. For cross-link experiments the plasmids were transformed into *E. coli* JM109.

All constructed plasmids were confirmed by sequencing. The medium for selection of transformants *of E. coli* contained 100 μg ml^{-1} ampicillin and those of *S. carnosus* 10 μg ml^{-1} chloramphenicol.

Lipase reporter gene assays

For the lipase reporter gene assays strains carrying plasmid encoded *narG-lip* (plasmid pMW1040 and derivatives) were used. The lipase is excreted and is quantified in the supernatant without having to disrupt the cells. Lipase activity was assessed by hydrolysis of p-nitrophenyl caprylate in a 96-well plate assay. The test buffer contained 5 mM p-nitrophenyl caprylate, 10 mM $CaCl_2$, 0.1% Triton X-100 and 20 mM Tris/HCl pH 9.0 (Rosenstein *et al*., 1992). A volume of 225 μl of the buffer was added to each well together with 25 μl supernatant. The production of p-nitrophenolate was measured by absorbance at 415 nm using an extinction coefficient of $16.97 \cdot 10^3$ M^{-1} cm^{-1}. The specific lipase activity (U g^{-1} dry weight) was determined by calculating p-nitrophenyl caprylate hydrolysis per min (1 U corresponds to the hydrolysis of 1 μmol p-nitrophenyl caprylate per min) and the cell density of the culture (1 ml culture with an OD_{578} of 1 corresponds to a dry weight of 0.245 mg).

Autophosphorylation assay of NreB

Autophosphorylation of NreB was assayed with isolated NreB. For anaerobically prepared NreB all steps were performed under anoxic conditions in an anaerobic chamber (Coy). NreB (15 μM) was diluted with reaction buffer consisting of 50 mM HEPES (pH 8), 50 mM KCl, 5 mM $MgCl_2$, 0.5 mM EDTA and 2 mM DTT. The reaction mixture was adjusted to 45 μl by the addition of the protein elution buffer

(see above). To start the reaction 3 µl of [γ-^{33}P]-ATP (0.22 µM with 5.5 TBq mmol^{-1}) were added. After starting the reaction, 8 µl samples were taken from the reaction mixture at different time intervals (5–300 min) and mixed with 14 µl stop solution (SDS sample buffer). The samples were then subjected to SDS-PAGE on 12.5% polyacrylamide gels. Subsequently the gels were folded in saran wrap, put on a phosphor imaging plate (FUJIFILM BAS 2040 imaging plate) with an exposure time of 18 h at 4°C. The β-irradiation was then detected by evaluating the plate in the FUJI BAS 1500 bioimaging analyser. The relative contents of radioactivity were determined with Gel-Pro Analyzer 6.0 after subtracting the background of the imager plate (Müllner *et al.*, 2008).

For testing the effects of NreA, NreA·[NO_3^-], NreA(Y95A) and NreA(Y95A)·[NO_3^-] the proteins were added at concentrations of 600 µM, or as indicated, to the reaction mixture before or after the addition of [γ-^{33}P]-ATP. For control, the same volume of protein elution buffer was added.

To monitor the phosphotransfer from NreB (30 µM) to NreC (30 µM), NreB was autophosphorylated as described above, but the reaction volume was increased to 120 µl. The reaction was started by the addition of 20 µl of [^{33}P]-ATP (0.22 µM with 5.5 TBq mmol^{-1}). One hundred and fifty minutes after the addition of [^{33}P]-ATP NreC was added at the same concentration as NreB. Volumes containing equivalent amounts of NreB and NreC in all experiments were withdrawn for testing phosphorylation.

Gel-filtration (GF) chromatography

To separate phosphorylated NreB from residual ATP GF was performed using the porous matrix Sephadex G50 Superfine. First, 1 ml of anaerobically prepared NreB (27 µM) was phosphorylated with [γ-^{33}P]-ATP (0.22 µM, 5.5 TBq mmol^{-1}) in reaction buffer (see above) in an anaerobic chamber. A column (1 cm^2 × 10 cm) filled with Sephadex G50 was equilibrated with anaerobic buffer (50 mM sodium phosphate buffer pH 7.2, 300 mM NaCl, 20% glycerol). After phosphorylation for 200 min, NreB in 1 ml buffer was applied to the matrix and eluted by rinsing with anaerobic buffer on the column. Fractions of 1 ml were collected and the fraction with the highest NreB concentration was used for testing the effect of NreA, NreA·[NO_3^-], NreA(Y95A) and NreA(Y95A)·[NO_3^-] on the phosphorylation state. The proteins were added at a concentration of 400 µM to isolated phosphorylated NreB (10 µM). The state of phosphorylation of NreB was determined after SDS-PAGE and phosphoimaging as described above.

Protein interaction using BACTH

Interaction of the Nre proteins was studied *in vivo* using BACTH (Karimova *et al.*, 1998; 2005). The T25 and the T18 domains were each fused to the target genes *nreA*, *nreA*(Y95A), *nreB* and *nreC*. T25-*zip* and T18-*zip* were obtained as part of the BACTH system for use as a positive control (Karimova *et al.*, 2005). *E. coli* BTH101 was co-transformed with 15 ng of plasmids encoding the T25- and T18-protein fusions. After growth for 40 h on agar plates at 30°C, an overnight culture was inoculated. The overnight culture was used to inoculate the main culture (1.5%, v/v) for the β-galactosidase assay. The *E. coli* cells were grown anaerobically at 30°C in deep well plates in LB medium supplemented with ampicillin (50 µg ml^{-1}), kanamycin (25 µg ml^{-1}), 500 µM IPTG and 20 mM dimethylsulphoxide. The effect of nitrate on interaction was tested by the addition of 10 mM $NaNO_3$. The β-galactosidase assay (Sambrook and Russell, 2001) was performed in 96-well plates at an OD_{570} of 0.25 to 0.5. Each strain was prepared by two or more independent co-transformations, and three cultures of each strain were assayed in quadruplicates.

In vivo *binding assays of NreA and NreB (HPINE)*

The HPINE *in vivo* interaction studies were performed according to Graf *et al.* (unpublished). The plasmids pBAD33-NreA (pMW1949) and pASK-IBA13plus-nreB (pMW1192) or pBAD33-NreB (pMW1950) and pASK-IBA13plus-nreA (pMW1243) were co-transformed into *E. coli* JM109. Bacteria were grown in 400 ml LB medium supplemented with 100 mM glucose in a baffled flask (2 l). His_6-NreA and Strep-NreB or NreB-His_6 and Strep-NreA were coexpressed. For induction of protein expression 200 ng ml^{-1} anhydrotetracycline (Strep-NreA, Strep-NreB), and 0.01% arabinose (His-NreA, NreB-His) were added at an OD_{578} of 0.3–0.5. For chemical cross-linking of interacting proteins 0.6% (v/v) formaldehyde was added at an OD_{578} of 1.3–1.5, and the culture was incubated for 20 min at 37°C. After cell harvest and resuspension in 16 ml lysis buffer [0.3 M NaCl, 5% (v/v) glycerol, 0.01 M imidazole, 0.05 M sodium phosphate buffer pH 7.2], cells were disrupted in a French pressure cell press (3 passages, 13.8·10^7 kg s^{-2} m^{-1}). Cell debris was separated from solvent by centrifugation (7740 *g*, 4°C, 1 h) and the proteins were isolated from supernatant by chromatography via His_6-Tag from clear supernatant on a Ni-NTA column (Machery Nagel). The column was washed with 13 ml wash buffer [1 M NaCl, 5% (v/v) glycerol, 0.02 M imidazole, 0.05 M sodium phosphate buffer pH 7.2]. For elution 8 ml elution buffer [0.3 M NaCl, 5% (v/v) glycerol, 0.15 M imidazole, 0.05 M sodium phosphate buffer pH 7.2] were used. The first four elution fractions of approximately 1.5 ml were concentrated to a total volume of 0.5 ml. SDS loading buffer was added to the samples before heating them to 99°C for 5 min to reverse the cross-linking of the proteins. These were separated by SDS-PAGE and analysed by Western blot and immunostaining using anti-NreA and anti-NreB antibodies.

Acknowledgements

We are grateful to R. Brückner (Kaiserslautern) for supplying plasmid pRB473, and S. Schlag (Tübingen) for providing plasmid pQE31nreA, F. Reinhart (Mainz) for performing DNA mobility shift experiments with NreA, A. Kretzschmar (Mainz) for support and helpful discussions, and the Deutsche Forschungsgemeinschaft for supplying funding to GU. TS, FG and VN acknowledge support from SFB-TR34.

References

Aravind, L., and Ponting, C.P. (1997) The GAF domain: an evolutionary link between diverse phototransducing proteins. *Trends Biochem Sci* **22:** 458–459.

Bertani, G. (1951) Studies on lysogenesis. I. The mode of phage liberation by lysogenic *Escherichia coli*. *J Bacteriol* **62:** 293–300.

Boudes, M., Lazar, N., Graille, M., Durand, D., Gaidenko, T.A., Stewart, V., and van Tilbeurgh, H. (2012) The structure of the NasR transcription antiterminator reveals a one-component system with a NIT nitrate receptor coupled to an ANTAR RNA-binding effector. *Mol Microbiol* **85:** 431–444.

Brückner, R. (1992) A series of shuttle vectors for *Bacillus subtilis* and *Escherichia coli*. *Gene* **122:** 187–192.

Cheung, J., and Hendrickson, W.A. (2009) Structural analysis of ligand stimulation of the histidine kinase NarX. *Structure* **17:** 190–201.

Fedtke, I., Kamps, A., Krismer, B., and Götz, F. (2002) The nitrate reductase and nitrite reductase operons and the *narT* gene of *Staphylococcus carnosus* are positively controlled by the novel two-component system NreBC. *J Bacteriol* **184:** 6624–6634.

Götz, F., and Schumacher, B. (1987) Improvement of protoplast transformation in *Staphylococcus carnosus*. *FEMS Microbiol Lett* **40:** 285–288.

Gunsalus, R.P. (1992) Control of electron flow in *Escherichia coli*: coordinated transcription of respiratory pathway genes. *J Bacteriol* **174:** 7069–7074.

Janausch, I.G., Garcia-Moreno, I., and Unden, G. (2002) Function of DcuS from *Escherichia coli* as a fumarate-stimulated histidine protein kinase *in vitro*. *J Biol Chem* **277:** 39809–39814.

Kamps, A., Achebach, S., Fedtke, I., Unden, G., and Götz, F. (2004) Staphylococcal NreB: an O_2-sensing histidine protein kinase with an O_2-labile iron-sulphur cluster of the FNR type. *Mol Microbiol* **52:** 713–723.

Karimova, G., Pidoux, J., Ullmann, A., and Ladant, D. (1998) A bacterial two-hybrid system based on a reconstituted signal transduction pathway. *Proc Natl Acad Sci USA* **95:** 5752–5756.

Karimova, G., Dautin, N., and Ladant, D. (2005) Interaction network among *Escherichia coli* membrane proteins involved in cell division as revealed by bacterial two-hybrid analysis. *J Bactoriol* **187:** 2233–2243.

Koropatkin, N.M., Pakrasi, H.B., and Smith, T.J. (2006) Atomic structure of a nitrate-binding protein crucial for photosynthetic productivity. *Proc Natl Acad Sci USA* **103:** 9820–9825.

Krell, T., Lacal, J., Busch, A., Silva-Jiménez, H., Guazzaroni, M.E., and Ramos, J.L. (2010) Bacterial sensor kinases: diversity in the recognition of environmental signals. *Annu Rev Microbiol* **64:** 539–559.

Löfblom, J., Kronqvist, N., Uhlén, M., Ståhl, S., and Wernérus, H. (2007) Optimization of electroporation-mediated transformation: *Staphylococcus carnosus* as model organism. *J Appl Microbiol* **102:** 736–747.

Müllner, M., Hammel, O., Mienert, B., Schlag, S., Bill, E., and Unden, G. (2008) A PAS domain with an oxygen labile $[4Fe\text{-}4S]^{2+}$ cluster in the oxygen sensor kinase NreB of *Staphylococcus carnosus*. *Biochemistry* **47:** 13921–13932.

Partch, C.L., and Gardner, K.H. (2010) Coactivator recruitment: a new role for PAS domains in transcriptional regulation by the bHLH-PAS family. *J Cell Pysiol* **223:** 553–557.

Peschel, A., Augustin, J., Kupke, T., Stevanovic, S., and Götz, F. (1993) Regulation of epidermin biosynthetic genes by EpiQ. *Mol Microbiol* **9:** 31–39.

Razeto, A., Ramakrishnan, V., Litterst, C.M., Giller, K., Griesinger, C., Carlomagno, T., *et al*. (2004) Structure of the NCoA-1/SRC-1 PAS-B domain bound to the LXXLL motif of the STAT6 transactivation domain. *J Mol Biol* **336:** 319–329.

Rosenstein, R., Peschel, A., Wieland, B., and Götz, F. (1992) Expression and regulation of the antimonite, arsenite, and arsenate resistance operon of *Staphylococcus xylosus* plasmid pSX267. *J Bacteriol* **174:** 3676–3683.

Rosenstein, R., Nerz, C., Biswas, L., Resch, A., Raddatz, G., Schuster, S.C., and Götz, F. (2009) Genome analysis of the meat starter culture bacterium *Staphylococcus carnosus* TM300. *Appl Environ Microbiol* **75:** 811–822.

Sambrook, J., and Russell, D.W. (2001) *Molecular Cloning: A Laboratory Manual*, 3rd edn, Vol. 3. New York: Cold Spring Harbor Laboratory Press.

Schlag, S., Fuchs, S., Nerz, C., Gaupp, R., Engelmann, S., Liebeke, M., *et al*. (2008) Characterization of the oxygen-responsive NreABC regulon of *Staphylococcus aureus*. *J Bacteriol* **190:** 7847–7858.

Schleifer, K.H., and Fischer, U. (1982) Description of a new species of the genus *Staphylococcus*: *Staphylococcus carnosus*. *Int J Syst Bacteriol* **32:** 153–156.

Sousa, E.H.S., Tuckerman, J.R., Gondium, A.C.S., Gonzalez, G., and Gilles-Gonzalez, M. (2013) Signal transduction and phosphoryl transfer by a FixL hybrid kinase with low oxygen affinity: importance of the vicinal PAS domain and receiver aspartate. *Biochemistry* **52:** 456–465.

Unden, G., and Bongaerts, J. (1997) Alternative respiratory pathways of *Escherichia coli*: energetics and transcriptional regulation in response to electron acceptors. *Biochim Biophys Acta* **1320:** 217–234.

Unden, G., Nilkens, S., and Singenstreu, M. (2013) Bacterial sensor kinases using Fe-S cluster binding PAS or GAF domains for O_2 sensing. *Dalton Trans* **42:** 3082–3087.

Wieland, K.P., Wieland, B., and Götz, F. (1995) A promoter-screening plasmid and xylose-inducible, glucose-repressible expression vectors for *Staphylococcus carnosus*. *Gene* **158:** 91–96.

Williams, S.B., and Stewart, V. (1997) Discrimination between structurally related ligands nitrate and nitrite controls autokinase activity of the NarX transmembrane signal transducer of *Escherichia coli* K-12. *Mol Microbiol* **26:** 911–925.

Witan, J., Monzel, C., Scheu, P.D., and Unden, G. (2012) The sensor kinase DcuS of *Escherichia coli*: two stimulus input sites and a merged signal pathway in the DctA/DcuS sensor unit. *Biol Chem* **393:** 1291–1297.

Yanisch-Perron, C., Vieira, J., and Messing, J. (1985) Improved M13 phage cloning vectors and host strains: nucleotide sequences of the M13mp18 and pUC19 vectors. *Gene* **33:** 103–119.

Supporting information

Additional supporting information may be found in the online version of this article at the publisher's web-site.

The NreA Protein Functions as a Nitrate Receptor in the Staphylococcal Nitrate Regulation System

Volker Niemann [1,†], Mareike Koch-Singenstreu [2,†], Ancilla Neu [3], Stephanie Nilkens [2], Friedrich Götz [4], Gottfried Unden [2] and Thilo Stehle [1,5]

*1 - **Interfaculty Institute of Biochemistry,** Universität Tübingen, Hoppe-Seyler-Strasse 4, D-72076 Tübingen, Germany*
*2 - **Institute for Microbiology and Wine Research,** Universität Mainz, Johann-Joachim-Becherweg 15, D-55128 Mainz, Germany*
*3 - **Max Planck Institute for Developmental Biology,** Spemannstrasse 35, D-72076 Tübingen, Germany*
*4 - **Interfaculty Institute of Microbiology and Infection Medicine,** Universität Tübingen, Auf der Morgenstelle 28, D-72076 Tübingen, Germany*
*5 - **Department of Pediatrics,** Vanderbilt University School of Medicine, Nashville, TN 37232, USA*

***Correspondence to Gottfried Unden and Thilo Stehle:** T. Stehle is to be contacted at: Interfaculty Institute of Biochemistry, Universität Tübingen, Hoppe-Seyler-Strasse 4, D-72076 Tübingen, Germany. unden@uni-mainz.de; thilo.stehle@uni-tuebingen.de*
http://dx.doi.org/10.1016/j.jmb.2013.12.026
Edited by J. H. Naismith

Abstract

Staphylococci are able to use nitrate as an alternative electron acceptor during anaerobic respiration. The regulation of energy metabolism is dependent on the presence of oxygen and nitrate. Under anaerobic conditions, staphylococci employ the nitrate regulatory element (Nre) for transcriptional activation of genes involved in reduction and transport of nitrate and nitrite. Of the three proteins that constitute the Nre system, NreB has been characterized as an oxygen sensor kinase and NreC has been characterized as its cognate response regulator. Here, we present structural and functional data that establish NreA as a new type of nitrate receptor. The structure of NreA with bound nitrate was solved at 2.35 Å resolution, revealing a GAF domain fold. Isothermal titration calorimetry experiments showed that NreA binds nitrate with low micromolar affinity (K_D = 22 μM). Two crystal forms for NreA were obtained, with either bound nitrate or iodide. While the binding site is hydrophobic, two helix dipoles and polar interactions contribute to specific binding of the ions. The expression of nitrate reductase (NarGHI) was examined using a *narG-lip* (lipase) reporter gene assay *in vivo*. Expression was regulated by the presence of NreA and nitrate. Structure-guided mutations of NreA reduced its nitrate binding affinity and also affected the gene expression, thus providing support for the function of NreA as a nitrate receptor.

Introduction

Staphylococci are generally able to perform dissimilatory nitrate reduction under anaerobic conditions. As shown in *Staphylococcus carnosus* nitrate is reduced to ammonia in two steps. (i) Nitrate is taken up and reduced to nitrite, and nitrite is subsequently excreted. (ii) After depletion of nitrate, the accumulated nitrite is imported and reduced to ammonia, which again accumulates in the medium [1]. For a functional dissimilatory nitrate reduction, a number of gene clusters and proteins are necessary, such as the transmembrane nitrate reductase [2] and the cytoplasmic nitrite reductase, which reduces nitrite to ammonia using NADH + H^+ as the electron donor [3], the nitrate [4] and molybdate transporters [5], the molybdene biosynthesis gene cluster [6] and the nitrate regulatory element NreABC. The latter senses the absence of oxygen and presence of nitrate to fully induce the dissimilatory nitrate reduction system [7–10]. The corresponding genes and enzymes were largely characterized; the genes are also present in other staphylococcal genomes. Anaerobiosis presents the more important factor for induction, and nitrate serves as an additional inducer. Regulation by anaerobiosis is effected in

Table 1. Crystallographic statistics.

Parameter	Values		
	Nre-I	Nre-I	Nre-NO_3
	Data set for phasing	Data set for refinement	
Data collection			
Beamline	ID14-4, ESRF, Grenoble, France	ID14-4, ESRF, Grenoble, France	X06DA, SLS, Villigen, Switzerland
Wavelength (Å)	0.92	0.92	1.00
Space group	$P4_32_12$	$P4_32_12$	$P4_32_12$
Cell dimensions			
a, *b*, *c* (Å)	85.45, 85.45, 91.54	85.49, 85.49, 91.54	85.66, 85.66, 91.34
α, β, γ (°)	90.0, 90.0, 90.0	90.0, 90.0, 90.0	90.0, 90.0, 90.0
Resolution (Å)	29.3–2.5 (2.54–2.50)	40.4–2.2 (2.25–2.20)	42.8–2.35 (2.41–2.35)
R_{meas} (%)	12.6 (74.1)	15.0 (115.8)	17.5 (284.2)
$I/\sigma I$	15.26 (2.1)	5.86 (1.16)	14.66 (1.02)
CC1/2 (%)	99.7 (69.3)	98.7 (36.8)	99.9 (43.9)
Completeness (%)	99.9 (99.9)	99.1 (99.8)	99.9 (99.3)
Redundancy	10.35 (3.95)	2.74 (2.72)	12.24 (11.95)
Unique reflections	22,412	2418	1066
Wilson *B* ($Å^2$)	42.5	40.8	55.9
Refinement			
Resolution (Å)	—	2.20	2.35
R_{work}/R_{free}	—	20.25/25.03	21.28/25.24
No. of atoms			
Protein (chain A/B)	—	1116/1086	1096/1070
Water	—	117	39
Ligand (chain A/B)	—	1/1	4/4
B-factors (Å)			
Protein (chain A/B)	—	26.6/25.9	45.5/47.0
Water	—	31.7	42.3
Ligand (chain A/B)	—	16.7/18.1	35.8/43.7
rmsd			
Bond length (Å)	—	0.005	0.005
Bond angles (°)	—	0.854	0.854

S. carnosus by the NreBC two-component system that is encoded by the *nreBC* genes. This system consists of the cytoplasmic sensor histidine kinase NreB and the response regulator NreC [7,8]. NreB is a direct O_2 sensor using a labile $[4Fe\text{-}4S]^{2+}$ cluster for O_2 sensing and controlling kinase activity of NreB [11]. Under anoxic conditions, the $[4Fe\text{-}4S]^{2+}$ cluster remains stable and NreB autophosphorylates. Subsequently, the phosphoryl group is transferred to NreC, and phosphorylated NreC (NreC-P) binds to the DNA and stimulates expression of gene clusters necessary for dissimilatory nitrate reduction. Under anaerobic conditions and the presence of nitrate, the expression of the genes is stimulated to an even higher level. The protein responsible for nitrate sensing and nitrate regulation was not known [7]. Interestingly, nitrate sensors or receptors of types present in other bacteria, such as the membrane-bound sensor kinase NarX of proteobacteria [12,13], the periplasmic nitrate-binding protein NrtA from *Synechocystis* sp. [14] or the cytoplasmic RNA-binding protein and translational regulator NasR [15], are not encoded by *S. carnosus*. This indicates that sensing of nitrate by *S. carnosus* could be based on a different protein and mechanism.The *nreBC* genes from *S. carnosus* and all other staphylococci are part of the *nreABC* operon [7,16]. NreA was predicted to belong to the GAF domain protein family [7,16]. The GAF domain is named after some of the proteins it is found in: cGMP-specific phosphodiesterases, adenylyl cyclases and FhlA [17]. GAF domains are present in a large range of diverse proteins [18–23]. They define one of the largest protein families and are conserved in evolution across two billion years [20]. GAF domains can bind different types of small molecules, and they are found in signal transduction pathways in the whole tree of life, engaging a wide spectrum of different ligands [19]. GAF domains are well described functionally and structurally, although they differ widely in their function. Due to large commercial interests, the best-characterized GAF domain functions are those of eukaryotic phosphodiesterases (PDEs), which hydrolyze cNMPs. GAF domains of PDEs are typically arranged in tandem, forming dimers [22].

Genetic deletion studies suggest that the NreA protein is involved in nitrate regulation, and *in vitro* studies show that NreA is responsible for the nitrate effect in transcriptional regulation by the NreABC system. In an *nreA* deletion strain, expression of the controlled genes is derepressed under aerobic and anaerobic conditions, and the effect of nitrate (as

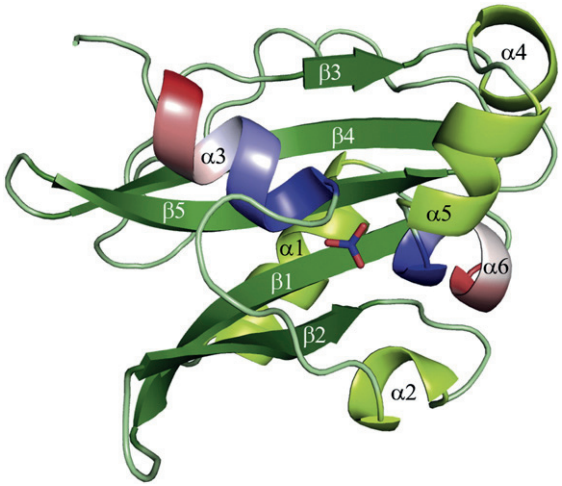

Fig. 1. Overall structure of NreA with bound nitrate. NreA structure is presented in ribbon drawing in complex with nitrate. Secondary structure elements are labeled, and the bound nitrate is shown in stick representation (nitrogen in blue and oxygens in red). The dipole moments of helices α3 and α6, which help to negate the negative charge of the nitrate, are indicated by colors, with blue and red indicating partial positive and negative charges, respectively.

well as part of the anaerobic induction) is mostly lost, indicating that NreA participates in some way in nitrate sensing and regulation [7,9,24]. *In vitro* studies identify NreA as the site for the nitrate response. NreA inhibited NreB phosphorylation and thus activation of NreB (and NreC), and nitrate relieved the NreA effect [24]. However, it was not known how nitrate influences NreA on a structural level.

To investigate structural and functional properties of NreA and provide some insight into its potential role in nitrate sensing or perception, we have determined the crystal structure of NreA demonstrating that NreA is a nitrate-binding GAF domain protein. Guided by the structural analyses and multiple alignments of *S. carnosus* NreA with homologue NreA proteins, we performed mutational and functional studies *in vivo* and *in vitro* to define the function of NreA in nitrate regulation. Our data support a model in which the NreA GAF domain serves as a nitrate receptor that is part of a nitrate/oxygen sensor complex composed of NreA and NreB. In this system, NreA interacts with the oxygen sensor NreB to form a new sensor system for joint sensing of nitrate and oxygen [24].

Results

Structure determination of NreA in two crystal forms

The structure of NreA was initially solved at 2.2 Å resolution in complex with iodide (NreA-I), using crystals that had been grown in the presence of

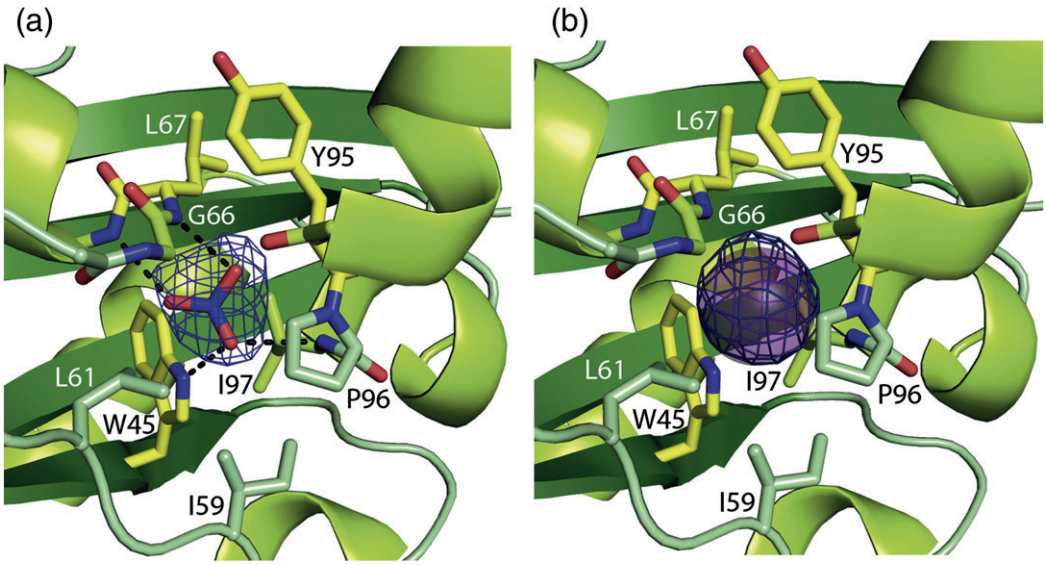

Fig. 2. Anion binding site of NreA. View into the binding sites of NreA with bound ligand. Amino acids coordinating the respective anion are arranged in the same orientation. Amino acids selected for mutagenesis experiments are colored yellow. In each case, a corresponding simulated annealing omit electron density map at a contour level of 3.0 σ is shown with a radius of 2.5 Å around the ligand. (a) Nitrate is shown in stick representation. Hydrogen bonds coordinating nitrate are depicted with black broken lines. (b) Iodide is shown as a sphere and is likely also contacted by hydrogen bonds, but due to the spherical nature of the ion, these cannot be assigned with confidence.

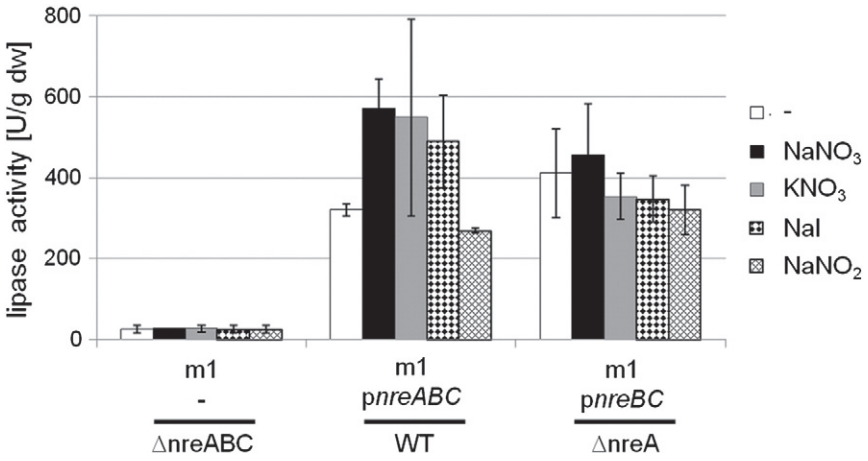

Fig. 3. Stimulation of *narG-lip* expression by nitrate, iodide and nitrite during anaerobic growth. *S. carnosus* strain m1 (Δ*nreABC*::ermB) containing either the plasmid pMW1001 with *narG-lip* but without *nreABC* (resulting genotype Δ*nre*ABC) or the plasmid pMW1040 encoding NreABC (resulting WT phenotype) or plasmid pMW1393 encoding NreB–NreC (resulting phenotype Δ*nreA*) was grown under anaerobic conditions to an OD_{578} of 0.5 and tested for lipase activity. Growth was performed in the presence (10 mM each) of $NaNO_3$, KNO_3, NaI or $NaNO_2$ as indicated. The control (–) carrying the plasmid pMW1040 encoding NreABC was also grown anaerobically, without supplement. The mean value of lipase activity is calculated form three independent experiments, each measured threefold. The standard deviation is indicated.

iodide (see Experimental Procedures). The NreA-I structure [Protein Data Bank (PDB) code: 4IUH] was determined via single anomalous dispersion using the single bound iodide as the anomalous scatterer. Several rounds of model building and refinement resulted in a model that has reliable statistics (R_{work} = 20.26% and R_{free} = 25.00%) (Table 1). As the location of the iodide indicated a functional role for an anion, crystals of NreA bound to nitrate were prepared (see Experimental Procedures). The structure of this complex, NreA-NO_3 (PDB code: 4IUK), was solved at 2.35 Å and revealed that nitrate and iodide bind, as expected, to the same site in the protein. Although the crystallographic *R*-factors for the NreA-NO_3 structure are somewhat higher compared with those for NreA-I (R_{work} = 21.26% and R_{free} = 25.20%) (Table 1), the structure nevertheless serves as a reliable platform for understanding the interactions with the anion as the electron density for nitrate and its surroundings is well defined. Both structures are highly similar, differing primarily in the bound ligand. A superimposition of NreA-I onto NreA-NO_3 yielded, as expected, a small C^{α} rmsd value of 0.36 Å. Both models contain at least amino acids 11–151. The histidine tags, the 10 N-terminal residues and the 4 C-terminal residues could not be built in either structure and are presumably disordered. In both structures, several solvent-exposed side chains were truncated (listed in the header of corresponding PDB file) because they lack density at the 1.0 σ level in the final electron density map. The truncations of surface-exposed residues do not reduce the scientific insights into the nitrate binding mechanism.

Overall structure of NreA

NreA folds into a single GAF domain, with a central, five-stranded antiparallel β-sheet (β1–β5) that is sandwiched between several α-helices (Fig. 1). The long helix α1, the N-terminus and the extended C-terminus cover one face of the β-sheet. The ligand binding pocket is located on the opposite face of the sheet and formed by a mixture of loops and five short α-helices. Some of the best-defined GAF domains bind cyclic nucleotides (cGMP or cAMP) in a central cavity, and other GAF domains have been found to engage other small molecules [23,25–27]. However, the NreA structure is the first example of a GAF domain that contains bound iodide or bound nitrate at this location. While this binding pocket is hydrophobic and mostly shielded from solvent, the negative charges of the ligands are partially compensated by partial positive charges from the dipole moments of helices α3 and α6 (Fig. 1). Together with hydrogen bonds to NreA residues, these two helices serve as anchors that fix the respective anion in the binding site (Fig. 2). Although the crystallization conditions for NreA-I and Nre-NO_3 contained iodide and nitrate, respectively, our structural and functional analysis indicates that the observed interactions are physiologically relevant and that nitrate is the physiologic ligand of NreA. Accordingly, although iodide was used to initially solve the structure of NreA-I, the description of the interactions will be focused on the NreA-NO_3 structure.

The nitrate binding pocket

The electron density for nitrate is well defined and allows the assignment of interactions with surrounding residues (Fig. 2a). The nitrate binds in a recessed pocket and is almost entirely shielded from solvent through interactions with hydrophobic residues (Ile59, Leu61, Gly66, Leu67 and Ile97). Nitrate is coordinated by only four hydrogen bonds, three of which involve the backbone amides of Leu67, Ala68 and Ile97. The fourth hydrogen bond is formed by the indole amide of Trp45. This side chain also serves as a spacer between the nitrate binding pocket and the central β-sheet. The side chain of Tyr95 acts as a lid, sealing the binding pocket. Pro96 introduces a kink in the chain between α-helices 5 and 6. As a result, the N-terminus of the α6-helix points toward the ligand and compensates the negative charge together with dipole moment of α3-helix. The residues that contact nitrate are highly conserved in the known NreA proteins from staphylococci (Fig. S1).

Nitrate and iodide serve as effectors of NreA function *in vivo*

The structural data demonstrate that NreA is able to bind nitrate or iodide as cofactors. *In vivo* studies were used to test which of the ligands or effectors are able to induce the plasmid-encoded *narG-lip* reporter gene under anaerobic conditions in an NreA-dependent manner. The experiments were performed in strains wild-typic for NreABC, deleted for NreA and producing only NreB–NreC or deleted of NreABC (Fig. 3). In the *narG-lip* reporter gene fusion, the lipase gene is cloned behind the *narG* promoter region. This gives rise to a construct in which the expression of lipase is subject to, and reports the transcriptional regulation of, the *narGHJI* operon [24]. The activity of lipase produced from the *narG-lip* reporter gene fusion correlates with the amount of lipase protein in the supernatant (Fig. S2). This demonstrates the suitability of the reporter gene assay, which has also been used earlier in similar form [24,28,29]. Under anaerobic conditions, expression of *narG-lip*

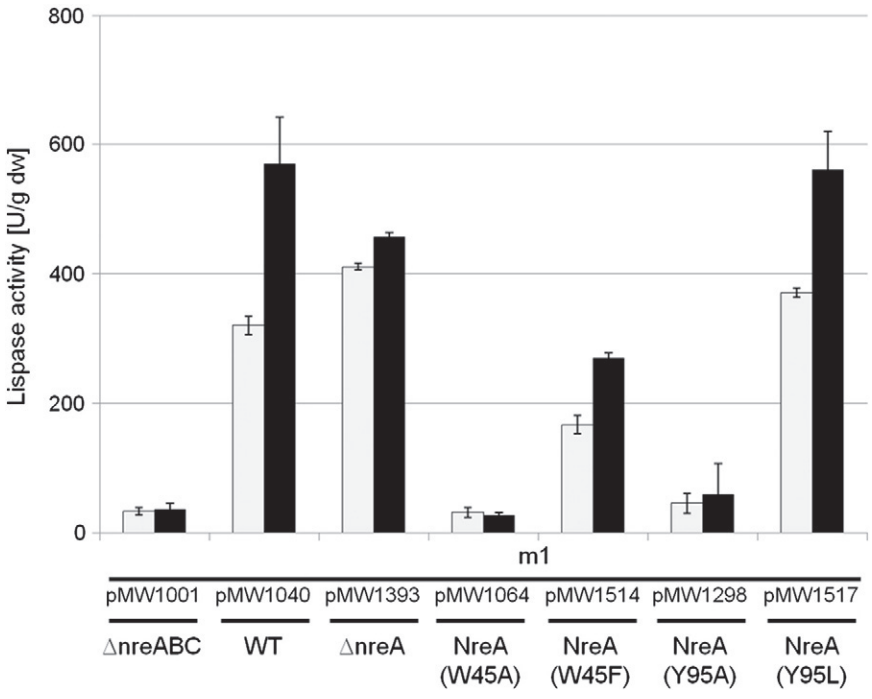

Fig. 4. Effect of mutations in NreA on *narG-lip* expression during anaerobic growth with and without nitrate. *S. carnosus* strain m1 (Δ*nreABC*::ermB) was complemented with various plasmids resulting in the production of NreA variants grown without (white bars) or with 10 mM sodium nitrate (black bars) under anaerobic conditions to an OD_{578} of 0.5 and tested for lipase activity. Strain m1 was complemented with plasmids derived from pMW1040 encoding variants of NreA (in addition to NreB, NreC and *narG-lip*). The relevant phenotype or genotype with respect to NreA (as well as NreB and NreC where deviating from WT situation) is given. The mean value of lipase activity is calculated form three independent experiments, each measured threefold. The standard deviation is indicated.

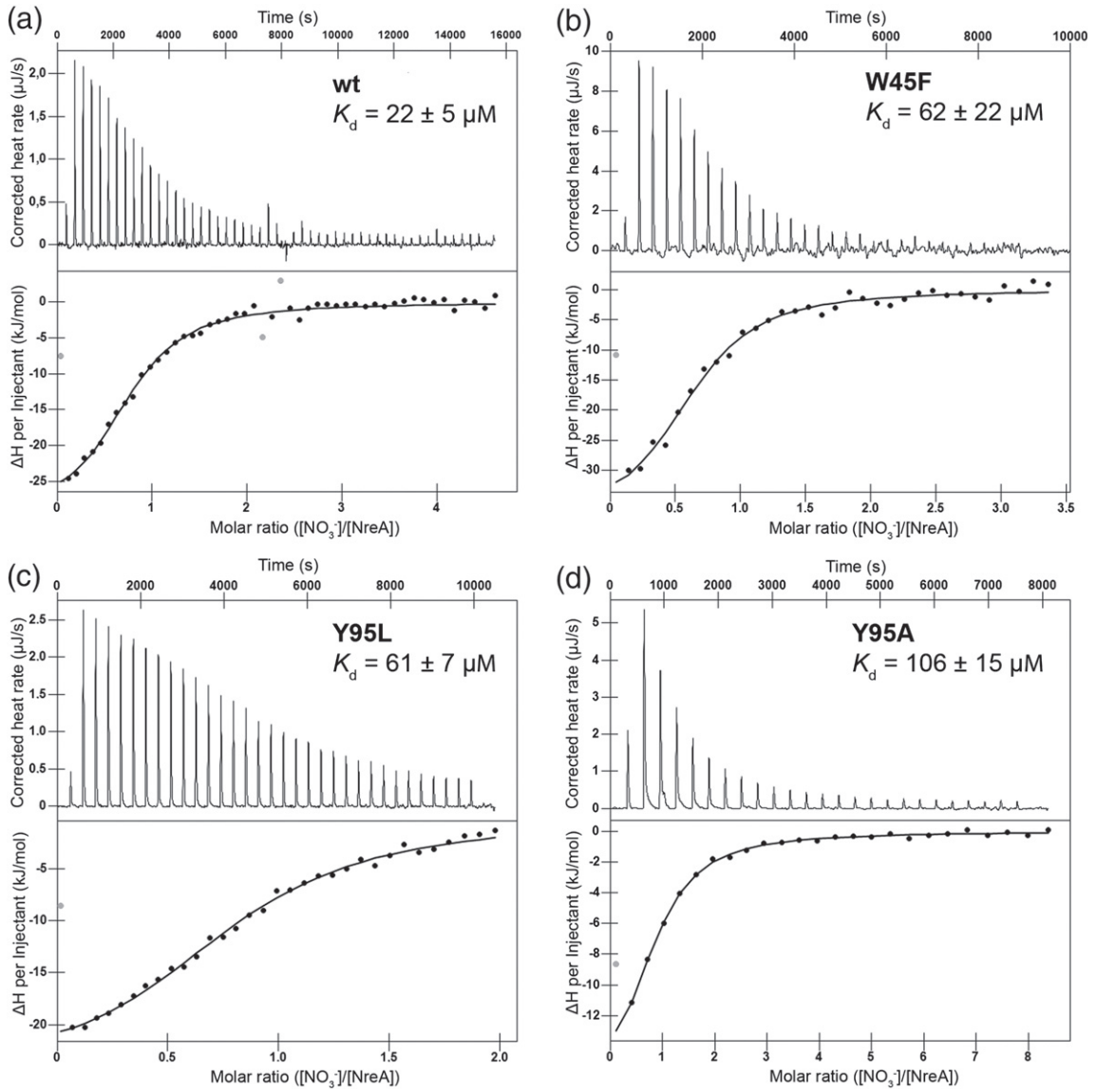

Fig. 5. ITC of ligand binding to WT and mutant NreA. In all experiments, nitrate was titrated into a reservoir of protein. The upper row of each panel shows the peaks of the corrected heat rate produced by the successive injection of nitrate to NreA over time. The lower row of each panel shows the curve fitted on the enthalpy change (Δ*H*) as a function of the molar ratio of NO_3^- to NreA. Affinities were calculated based on an independent binding model. (a) The WT form of NreA binds to nitrate with the highest affinity and a K_D value of 22 µM. (b) The mutation W45F leads to a reduction of K_D to 62 µM. (c) The Y95L mutation yields a K_D value of 61 µM. (d) The Y95A mutation shows the strongest reduction in affinity, with a K_D value of 106 µM.

was at a high level [320 U/g dry weight (dw)] compared to the NreABC lacking strain (36 U/g dw) and can further be induced by nitrate by a factor of 1.8 to maximal levels (569 U/g dw) in agreement with Nilkens *et al.* [24]. The stimulation of *narG-lip* expression in the presence of iodide (factor 1.5) was close to that obtained for nitrate, whereas nitrite had no stimulating effect. The data indicate that nitrate and iodide, which are both ligands for NreA, function as cofactors in induction, whereas the structurally related metabolite NO_2^- of nitrate metabolism showed no stimulation. The effect of nitrate and iodide depended on the anions, whereas the type of the cation (K^+ or Na^+) was not significant (Fig. 3), consistent with the structural data. The nitrate and iodide effects were only observed for bacteria carrying the wild-type (WT) NreA, but not for the strains lacking NreA (Fig. 3), and for a *nreABC* deletion strain, no expression of the reporter gene was observed.

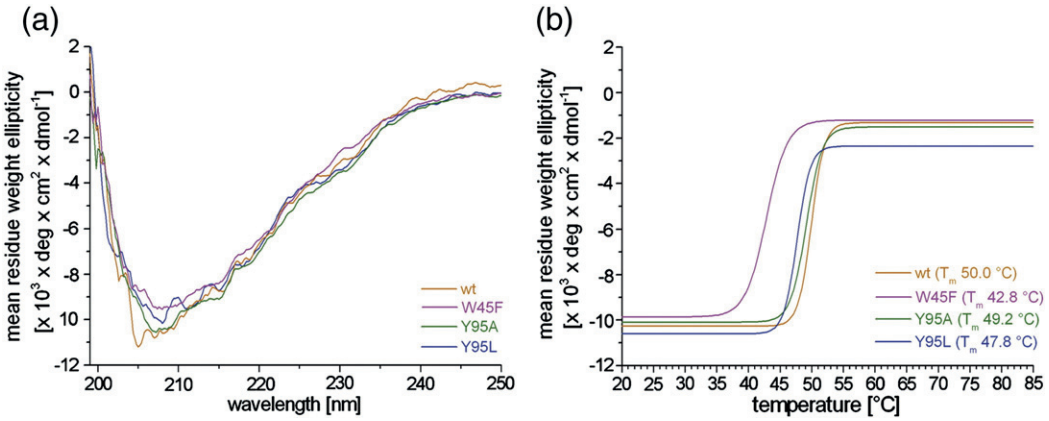

Fig. 6. CD spectroscopy measurements of WT and mutant NreA. (a) CD spectra measured from 250 to 199 nm at 20 °C show a mixture of α-helical and β-sheet secondary structure elements, consistent with the absence of the characteristic minima at 222 nm and 217 nm present in only α-helical and only β-sheet proteins, respectively. (b) Sigmoidal fit of melting curves of the WT and mutants of NreA measured at 208 nm, with linear temperature gradient from 20 to 85 °C. The melting points are calculated at the inflection points of the sigmoid fitting curves.

Mutations in the nitrate binding site of NreA

Based on the architecture of the binding site and sequence alignments of NreA with NreA homologues and related GAF domain proteins, amino acids involved in ligand binding were chosen for mutational analysis. The effect of these mutations was studied *in vivo* under anaerobic conditions by expressing the variants of *nreA* in a test strain of *S. carnosus* that was deleted for *nreABC* but contained the *nreABC* gene cluster including the mutated *nreA* on a plasmid. These constructs were used to prepare mutations of *nreA* and to retain the gene context of *nreA* within the gene cluster (Fig. 4). In addition, the plasmids encoded the *narG-lip* reporter gene fusion. Anoxic conditions caused strong expression of *narG-lip* in the *nreABC* WT. Nitrate stimulated the expression of *narG-lip* further to maximal levels. For the Δ*nreABC* mutation, only basal expression of the reporter gene was observed. In a strain lacking *nreA*, the expression of *narG-lip* requires no longer nitrate for full induction, demonstrating that nitrate regulation requires NreA and proving earlier suggestions that nitrate relieves repression by NreA [7]. The levels of *narG-lip* expression in the Δ*nreABC* and Δ*nreA* strain are in agreement with Nilkens *et al.* [24]. Mutations W45A and Y95A of NreA yielded permanently inactive phenotypes that were comparable to a Δ*nreABC* mutant that shows very low expression of the reporter gene. Replacing W45 and Y95 by other residues (mutations W45F and Y95L) restored expression of the reporter gene fusion and the response to nitrate derepression (factor 1.5). Mutants producing NreA(W45A), NreA(W45F), NreA(Y95A) and NreA(Y95L) were tested by immunoblotting with anti-NreA antibody. All extracts contained the NreA proteins, although the amount of protein varied somewhat (Fig. S3). Therefore, the main physiological effects of the mutations are most likely linked to a functional change of NreA. Taken together, the analysis of the mutants *in vivo* strongly supports the conclusion that NreA is the site responsible for nitrate stimulation and that binding of nitrate to the NreA binding pocket is physiologically relevant.

Affinity of WT and mutant NreA proteins for nitrate

Some of the point mutations in NreA show drastic effects on the phenotypes (Fig. 4), and it is tempting to speculate that these effects might be linked to reduced binding affinity of the mutant proteins for nitrate. We therefore determined dissociation constants (K_D) for the binding of nitrate to NreA and the W45F, Y95L and Y95A mutants using isothermal titration calorimetry (ITC) (Fig. 5). Independent binding models were chosen to fit the curves onto the enthalpy change (ΔH) per injectant (lower panel of Fig. 5a–d). While the K_D for WT NreA is 22 μM (Fig. 5a), the three point mutations have significantly reduced K_D values. Unsealing the binding pocket with the Y95A mutation yields a K_D value of 106 μM (Fig. 5d), consistent with the permanently inactive phenotype of this mutant (Fig. 4). The remaining two mutants, W45F and Y45L, have K_D values of 62 and 61 μM, respectively (Fig. 5b and c), in line with the more conservative nature of these exchanges. Both mutants also maintain the WT phenotype (Fig. 4). Our data therefore suggest that there is a stimulus threshold between about 60 μM and about 100 μM necessary for the nitrate effect.

Influence of mutations on protein stability

The insertion of the point mutations in NreA has an impact on nitrate binding affinities and on the phenotype of *S. carnosus*. In order to rule out that the mutations adversely affect the structure and stability of NreA, circular dichroism (CD) spectroscopy experiments were performed for WT and mutant proteins. The CD spectra show that all proteins contain a mixture of α-helical and β-sheet structures, in agreement with the mixed α/β fold of the NreA GAF domain (Fig. 6). The absence of typical minima at 222 nm for α-helical and at 217 nm for β-sheet proteins lead us to assign the spectra as mixed α/β fold structures. Jasco secondary structure estimation software (Jasco) was used to calculate the secondary structure content. In all NreA variants, the α-helical and β-sheet content is estimated to be 11–14% and 41–60%, respectively, with an rmsd of 22 ± 1.5. The spectra had to be truncated at 199 nm because of noisy signals below this wavelength. This limits the reliability of the secondary structure estimation. Both NreA-NO_3 and NreA-I crystal structures contain 26% α-helices and 27% β-strands.

The CD spectra furthermore confirm that the mutations do not disrupt the overall folding at room temperature. However, the calculated melting points show that the mutations lead to small differences in protein stability in some cases. The melting points are calculated at the inflection points of the sigmoid fitting curves (Fig. S4). The ligand-free WT form of NreA has a melting point of 50.0 °C, which can be taken as a reference point. Point mutations Y95A and Y95L reduce the melting temperature by about 0.8 and 2.2 °C, respectively, allowing for the correlation of the physiologic impact with the observed ligand binding properties. The W45F mutation shows a reduction of the melting temperature by 7.2 °C. We note that ligand-free NreA(W45F) begins to unfold at the 35 °C *in vitro* and the lipase assay was performed at 37 °C *in vivo*. NreA with bound ligand exhibit an increased melting temperature by 5–10 °C (Fig. S4), which is also described for other GAF domains [30]. Based on the binding affinities, the 100-fold excess ensures that at least 90% of NreA is bound to nitrate. The presence of 1 mM nitrate (100-fold excess) leads to noisy CD spectra in the far-UV range (<205 nm) (data not shown). Thus, it is difficult to compare the spectra of NreA with and without nitrate. The melting curves recorded at 208 nm have to be evaluated with care. However, even though this mutant is somewhat reduced in thermal stability, it had a phenotype similar to the WT protein. We therefore expect all three mutant proteins to be properly folded. Due the low expression level of NreA(W45A) in *Escherichia coli*, it was not possible to collect data *in vitro*. Furthermore, this rises the assumption that described phenotype is also caused by reduced amount of this variant.

Comparison with GAF domains

A search for structural homologues of NreA using the Dali server [31] unambiguously classifies NreA as a member of the GAF domain fold that is in agreement with earlier predictions [7]. The bulk of NreA (about 120 amino acids) aligns well with 20 different GAF domain structures, with C^{α} rmsd values ranging from 2.6 to 3.1 Å and *Z*-scores well above 10, indicating a highly significant match. The structural similarity is restricted to the five-stranded antiparallel β-sheet and the N-terminal α-helix. The highest-scoring structures are functionally diverse and distributed across the kingdoms of life, with examples from bacteria, fungi and mammals (Table S1). GAF domains form a conserved robust scaffold for small molecule ligand binding [18]. The binding site is formed by diverse loops and several α-helices. The binding site is lined with predominantly hydrophobic side chains in NreA, and with the exception of a hydrogen bond to the indole nitrogen of W45, all remaining polar interactions involve main-chain atoms only. The NKFDE motif, which has been discussed as being essential for specific cNMP binding in GAF domains of PDEs, is not present in NreA [32]. The phosphoryl group of cNMP is kept in position by a dipole moment of a helix in GAF domains of PDEs and adenylate cyclases, comparable to the arrangement in NreA [32–34]. All GAF domains therefore seem to compensate the negative charge of their ligands via the dipole moment of a helix at the binding site [27].

It is instructive to compare the NreA-NO_3 structure with structures of other GAF domains in complex with similar, small anions such as sulfate or phosphate. A search in the PDB[‡] yielded only one other GAF domain structure bound to such an anion: the N-terminal GAF domain of phosphoenolpyruvate-protein phosphotransferase (PtsP) in complex with phosphate (PDB code: 3TRC) (hit no. 5 in Table S1). A second GAF domain, Nlh1, has also been crystallized with a small, spherical ligand at its center, but the electron density was not sufficiently clear to reveal the identity of this ligand (PDB code: 4G3W) [23]. We therefore limit our comparison to the structure of PtsP, which exists as a dimer. The PtsP and NreA GAF domains can be superimposed using the SSM option in Coot [35] with an rmsd of only 2.2 Å (110 C^{α} atoms). The phosphorous and nitrogen atoms of the respective ligands are only 2.6 Å apart in the superposed structures. The comparison reveals an interesting conservation of structural features (Fig. 7). Similar to what is observed in NreA-NO_3, the negative charge of the phosphate bound to PtsP is also partially negated by a helix dipole moment (Fig. 7). Interestingly, the N-terminal residues of this helix are identical (G66 and

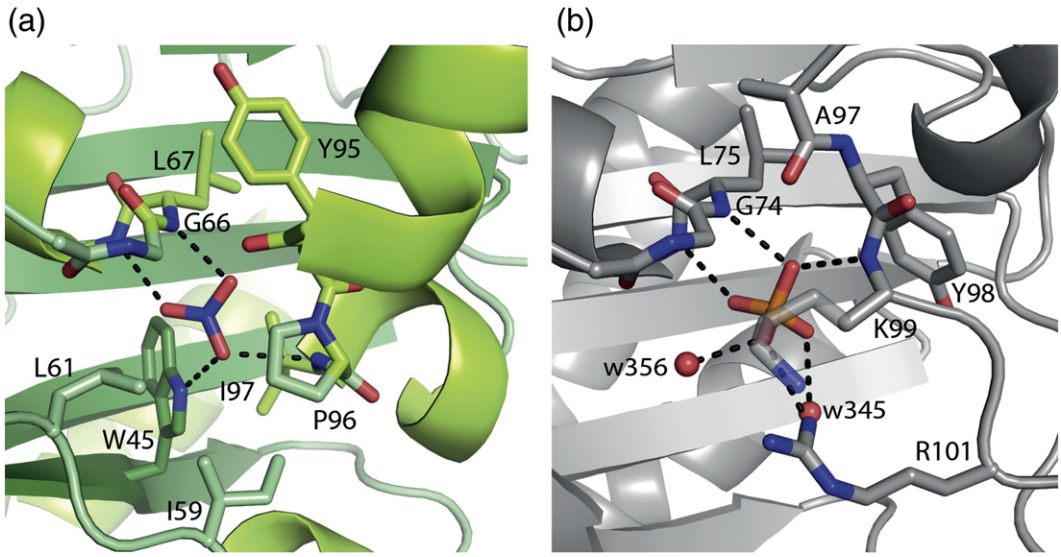

Fig. 7. Comparison of the ligand binding pockets of NreA-NO_3 and PtsP-PO_4. (a) Binding pocket of NreA-NO_3, with protein residues in green and key interactions with the bound nitrate shown in detail. (b) Similar view into the binding of PtsP-PO_4 (PDB code: 3TRC), with protein residues shown in gray and the phosphorous atom shown in orange. Similar features in both structures include a conserved helix (upper left) that contributes a dipole moment and identical contacts with the respective ligand with its N-terminal Gly-Leu sequence. A tyrosine (Y95 in NreA and Y98 in PtsP) seals the pocket in both cases.

L67 in NreA and G74 and L75 in PtsP), and they make similar contacts with two oxygen atoms of the respective ligand. The two residues are conserved in NreA proteins from different staphylococci (Fig. S1), and they seem to be important to arrange the small anion in the electric field of the helical dipole moment. The second helix (α6) of NreA, which lies on the opposite end of the nitrate binding site and also contributes to nitrate binding via its dipole moment, is missing in PtsP (Fig. 7). Instead, the negative charge of the phosphate is neutralized by the side chains of PtsP residues K99 and R101. The PtsP structure also contains a tyrosine residue, Y98, that creates a hydrophobic seal of the binding pocket, similar to the role of Y95 in NreA.

Dimerization of GAF domains

GAF domains in PDEs also provide an additional structural function by mediating homodimer formation [36]. While most GAF domains are dimeric [27], size-exclusion chromatography indicates that NreA is monomeric, at least under the conditions used for chromatography (Experimental Procedures and data not shown). Moreover, the presence or absence of nitrate did not influence the elution volume of NreA in size-exclusion chromatography (data not shown). It is of course possible that dimers of NreA only form at higher protein concentrations, including concentrations used for crystallization. Inspection of crystal packing can thus provide helpful clues about possible dimeric arrangements of crystallized proteins. The largest interface between two symmetry-related NreA molecules in the crystals covers an area of 607.4 $Å^2$. Analysis of this interface with PISA [37–39], which calculates the biological significance of macromolecular interfaces, yields a complexation significance score (CCS) of 0.000. This score indicates that the contact is unlikely to be a physiologic homodimer interface. Other smaller interfaces in the NreA crystal lattice show similar low CCS scores. It is of course possible that NreA could form another type of dimer that is not present in the crystal lattice. According to the PISA results, the related GAF domain protein SpoVT [40] of *Bacillus subtilis* forms a physiological homodimer (CCS of 1.000) despite its relatively small contact area of 620.7 $Å^2$ (hit no. 42 in Table S1). In SpoVT, helices α2 and α5 of each monomer assemble into a four-helix bundle that forms the dimer interface (Fig. 8). However, while the corresponding regions are present in NreA, the protein exhibits an unstructured but well-ordered region instead of forming a helix that would be similar to α5 of SpoVT (Fig. 8). Therefore, NreA cannot form a similarly large homodimeric interface. Thus, while we cannot rule out that NreA forms physiological dimers, analysis of the crystal structure does not provide clues as to how such a dimer might look like. We note that ligand binding can lead to secondary structure changes in GAF domains [23]. It is therefore possible that, in the absence of nitrate, the unstructured region at the C-terminus of ligand-bound NreA becomes helical and provides a new binding interface.

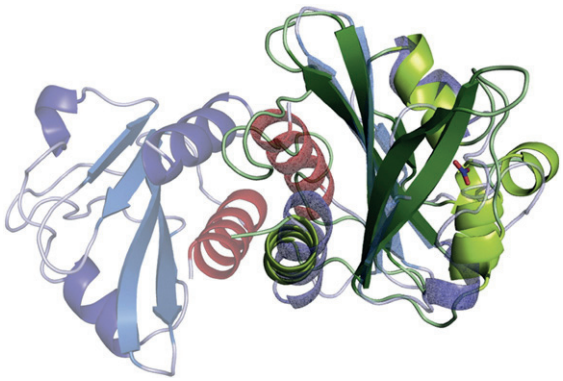

Fig. 8. Comparison of NreA with the dimeric structure of SpoVT. The GAF domain of NreA (green) was superimposed onto one of the two GAF domains of the SpoVT homodimer (blue; PDB code: 2W1R) [40]. Structural similarities between the two proteins are limited to the antiparallel β-sheet and the N-terminal helix. Dimerization of SpoVT is mediated by a four-helix bundle involving helices α2 and α5 of the GAF domain. The superimposition shows that helix α5 of SpoVT (red) overlays with the unstructured C-terminus of NreA. Therefore, NreA cannot dimerize using a similar mechanism.

Discussion

The Nre system in staphylococci consists of three proteins, termed NreA, NreB and NreC, which together regulate the uptake and reduction of nitrate and nitrite under anaerobic conditions. Oxygen sensing is effected by the histidine kinase NreB that phosphorylates NreC, a response regulator, under anaerobic conditions [8,11]. Phosphorylated NreC then binds to the DNA, enhancing transcription of the operon encoding nitrate reductase, nitrite reductase and a nitrate transporter. Nitrate sensing has been shown to depend on NreA [24]. The data presented here provide a molecular foundation for this finding by establishing NreA as a nitrate receptor that uses a new form of nitrate perception.

NreA engages nitrate with micromolar affinity in a recessed, hydrophobic binding pocket at the center of its GAF domain. Furthermore, results from the activity assay show that NreA has a negative effect on NreBC function in *narG* induction and is required for the nitrate effect. The deletion mutant Δ*nreABC* loses the ability of expressing the reporter gene for nitrate reductase. Deletion of *nreA* (Δ*nreA*) only leads to derepression of the nitrate reductase genes independent of the presence of nitrate even under aerobic conditions. The observation that *narG* expression levels cannot be modulated by nitrate in the Δ*nreA* mutant suggests that NreA serves in nitrate regulation. The presence of NreA reduces the basal expression under aerobic conditions, indicative of its function as a negative regulator [7,24]. The physiology resulting from point mutations in the binding site with diminished nitrate binding also supports the notion that NreA acts as a negative regulator. The phenotypes of these mutants are similar to the Δ*nreABC* mutant, indicating that unliganded mutant NreA represses *narG* expression completely. Ligand binding in the WT genotype leads to a higher expression of the *narG* gene under anaerobic conditions. Our structures thus show that NreA can bind nitrate and iodide, and both ions also lead to the induction of the *narG-lip* reporter gene in the presence of NreA. Several mutations were designed in order to probe the role of residues involved in nitrate binding. The W45A and Y95A mutants were permanently inactive in *narG-lip* expression, similar to the Δ*nreABC* mutant. The W45F mutation partially retained the WT phenotype. Taken together, the W45F and W45A mutations confirm the relevance of residue 45 for nitrate binding. The phenotype of the Y95A mutation shows a permanent loss of reporter gene expression [24]. Consistent with this observation, the Y95A mutation leads to significantly reduced affinity for nitrate and a leaky binding pocket. As a consequence, a higher ratio of permanent ligand-free NreA leads to the constitutive repression of reporter gene expression. The Y95L mutant has a phenotype comparable to the WT, likely because the larger leucine side chain is able to keep the ligand binding pocket mostly closed, thus maintaining sufficient affinity for nitrate. Connecting the *in vivo* and *in vitro* data allows us to propose a nitrate affinity threshold between 60 μM and 100 μM necessary to integrate the nitrate effect in NreABC signal transduction. Ongoing research establishing a purification protocol for a stable complex between NreA and NreB *in vitro* will clarify how the nitrate effect triggers the histidine kinase activity.

Our understanding of how proteins specifically recognize nitrate is still limited, mostly because very few structures of physiologically relevant protein–nitrate complexes exist. The comparison of NreA with the only two available structures of such complexes from bacteria, the periplasmic nitrate-binding protein NrtA [14] (PDB code: 2G29) and the periplasmic sensor domain of histidine kinase NarX [13] (PDB code: 3EZH) reveals not only profound differences in the overall structures as well as different mechanisms of nitrate binding but also some similar general strategies (Fig. 9). In all three cases, the bound nitrate is completely enveloped by protein residues and thus shielded from solvent. Both NarX and NrtA use multidomain structures to engage the nitrate ligand. In dimeric NarX, the nitrate is sandwiched between two monomers at the dimer interface [13], while in NrtA, the nitrate is sandwiched between two domains that are arranged as a C-clamp [14] (Fig. 9). The multidomain/multiprotein binding mode employed by both NarX and NrtA presumably allows nitrate access to the inaccessible binding site through changes at interfaces between

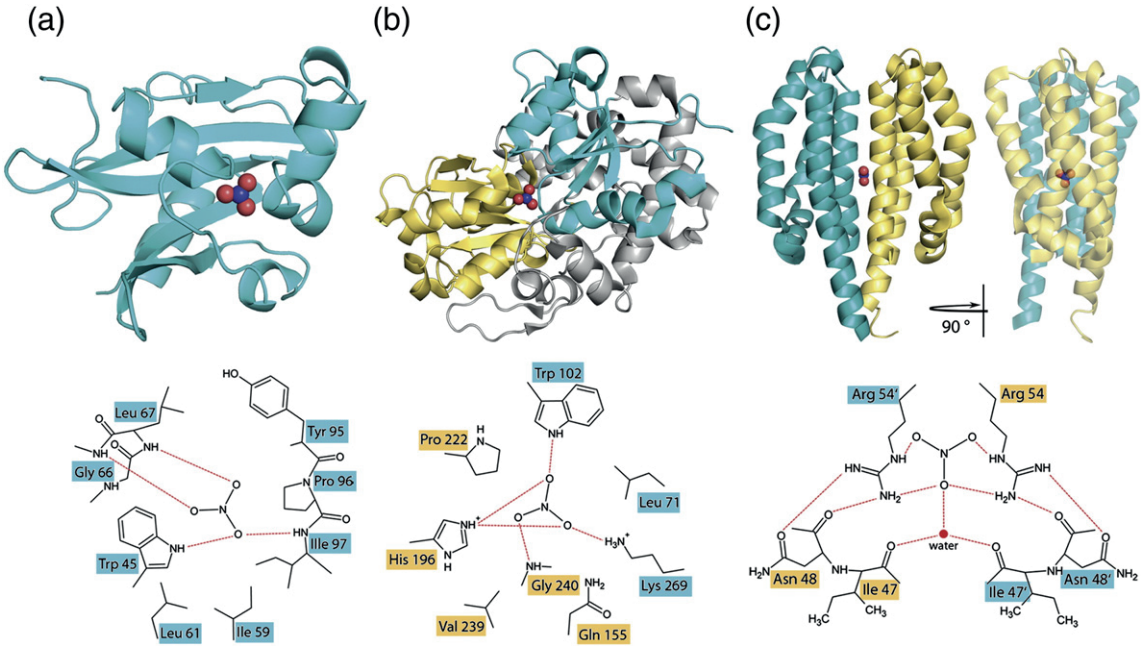

Fig. 9. Architectures of nitrate binding sites. Schematic drawings and detailed ribbon drawings are shown for three protein structures that bind nitrate physiologically. Possible hydrogen bonds and electrostatic interactions are depicted with red broken lines. (a) Cytoplasmic NreA of *S. carnosus*. (b) Periplasmic NrtA of *Synechocystis* sp. (PDB code: 2G29) [14]. (c) Periplasmic sensor domain of NarX of *E. coli* (PDB code: 3EZH) [13].

domains (either at the dimer interface in NarX or through alteration of the relative domain orientation in NrtA). Composed of only a single domain, NreA uses a different strategy to bind its ligand. As is the case in other GAF domains, flexibility in loop regions surrounding the ligands likely allows the ligands to access the binding site.

Both binding sites of NreA and NrtA feature hydrogen bonds to backbone amides and indole amides of a tryptophan coordinate the bound nitrate. However, the NrtA site is distinctly more polar, with lysine and histidine side chains forming salt bridges to the nitrate. NarX also uses highly polar interactions, including salt bridges to two arginines and a distinct network of hydrogen bonds, to engage its nitrate. The sensor domain of this histidine kinase dimerizes via a four-helix bundle that contains a highly conserved P-box region, located at helices H1 and H1′ and enables nitrate binding in the interface. In contrast to electrostatic interactions of amino acids with nitrate in NrtA and NarX, the compensation of the charge is achieved by the dipole moment of two α-helices pointing toward the nitrate in NreA.

Conclusion

NreA represents a new type of nitrate receptor that uses a new mode of nitrate perception. The mode of signal processing is clearly different from known examples. As described in more detail by Nilkens *et al.* [24], NreA cooperates with the O_2 sensor NreB physically and functionally in forming a sensor unit for the sensing of O_2 and nitrate. This functional model suggests that a joint signal output via NreC, the cognate response regulator of NreB, is achieved for the regulation of nitrate respiratory genes by O_2 and nitrate with one transcriptional regulator.

Experimental Procedures

Cloning

The bacterial strains and plasmids used in this study are listed in Table S2. Molecular genetics methods were performed according to standard procedures [41]. For the physiological studies, the *E. coli–S. carnosus* shuttle plasmid pMW1040 [24] was used (Table S2). The plasmid contains a *narG-lip* reporter gene fusion and the *nreABC* gene cluster under the control of the native *S. carnosus* promoter. The primer used for site-directed mutagenesis by PCR is listed in Table S3. This plasmid was transformed into *E. coli* JM109 and further into *S. carnosus* strain m1 for activity measurements by electrotransformation [42].

Protein expression and purification

To obtain protein for *in vitro* experiments and crystallization, we used the vector pQE31 containing full-length *nreA* of *S. carnosus* including an N-terminal His_6 tag [9]. The pQE31-nreA vector was transformed into *E. coli* M15 cells (Qiagen) and grown in Luria–Bertani broth at 37 °C to an OD_{600} of 0.4 before gene expression was induced with 0.5 mM isopropyl-β-thiogalactopyranoside. The temperature for expression of the target gene was adjusted to 20 °C at the time of induction. Bacteria were harvested by centrifugation (6000*g*, 30 min, 4 °C) after 20 h of incubation. The cell pellet was stored at −30 °C until use. The pellet was resuspended in buffer A [50 mM Hepes, 100 mM NaCl and 50 mM imidazole (pH 7.7)], and cells were disrupted with an EmulsiFlex-C3 system (Avestin). The lysate was centrifuged (28,000*g*, 30 min, 4 °C), and the filtered supernatant was loaded onto a 1-ml HisTrap HP column (GE Healthcare). After washing, we eluted the NreA protein with buffer B [10 mM Hepes, 100 mM NaCl and 150 mM imidazole (pH 7.7)]. Fractions containing NreA were pooled, concentrated and applied to Superdex 75 10/30 size-exclusion column (GE Healthcare) using buffer C [10 mM Hepes and 100 mM NaCl (pH 7.7)] to obtain protein for crystallization. In order to use NreA for CD measurements, we performed the size-exclusion chromatography with the lower-ionic-strength buffer D [5 mM Hepes and 50 mM NaCl (pH 7.7)]. For CD measurements in the presence of 100-fold excess nitrate, the size-exclusion chromatography was performed with buffer E [5 mM Hepes, 50 mM NaCl and 1 mM $NaNO_3$ (pH 7.7)].

WT NreA partly retains its ligand during purification from *E. coli*. Prior to the ITC experiments, NreA WT was subjected to denaturation and refolding to yield unliganded protein. Denaturation and refolding were performed as previously described[§], and the refolded protein was then concentrated and subjected to size-exclusion chromatography (Superdex 75 10/30; GE Healthcare) in buffer F [50 mM Hepes and 200 mM NaCl (pH 7.7)]. NreA-containing fractions eluting at the same volume as the natively purified protein were pooled and concentrated. To ensure a well-buffered mainly ligand free protein sample for ITC measurements, we then concentrated and extensively dialyzed nitrate-free purified NreA for 3 days at 4 °C (diluted 125,000×) against buffer G [50 mM Hepes and 200 mM NaCl (pH 7.7)].

Isothermal titration calorimetry

$NaNO_3$ solutions were prepared by dilution in buffer F used in the last dialysis step. ITC measurements were performed at 25 °C in a NanoITC low-volume calorimeter (TA Instruments) with a stirring speed of 200 rpm. The protein concentrations in the cell were 142 μM for NreA(WT), 296 μM for NreA(Y95A), 325 μM for NreA(Y95L) and 466 μM for NreA(W45F) with injection volumes of 1 or 2 μl. All data processing and analysis were carried out using the NanoAnalyze software suite (TA Instruments). Data were baseline corrected, integrated and corrected for dilutional heat by subtracting the average heat resulting from $NaNO_3$ injection into buffer. Affinities and thermodynamic parameters were calculated by fitting the data to a single binding site model. Errors in model parameters were obtained from Monte Carlo simulations.

CD spectroscopy

Fractions containing pure WT or mutant NreA were pooled, the protein concentration was adjusted to 1 mg/ml and aliquots were stored at −30 °C until use. For the measurements, the protein samples were diluted with buffer D or buffer E to 0.2 mg/ml and placed in a 1-mm-quartz cuvette. CD measurements were performed with a Jasco J-810 spectropolarimeter (Jasco) combined with thermoelectric temperature controller. Spectra were recorded at 20 °C, using a wavelength spectrum of 250–199 nm with a bandwidth of 1 nm, a scanning speed of 100 nm/min, a data pitch of 0.2 nm, a response time of 1 s and an accumulation of 10 spectra. Thermal stability was monitored at 208 nm between 20 and 85 °C with a temperature slope of 1 °C/min and a data pitch of 0.5 °C. For data processing and subtraction of the buffer baseline, the *Spectra Manager* was used. The noise of the CD data measured in the presence of nitrate was reduced by the smoothing function implemented in the spectra manager (Jasco). This function is based on the Savitzky–Golay smoothing algorithm [43]. Visualization of the data and the calculation of the melting temperature were performed with *Origin 6.0*. All measurements were performed in an identical manner for WT and mutant proteins.

Crystallization

Purified NreA in buffer C (11 mg/ml) was crystallized by the sitting-drop vapor diffusion at 20 °C, mixing equal amounts of the protein with the precipitant solution (300 nl). Crystals grew in two similar crystallization conditions, yielding closely related crystal forms of NreA that contained either iodide (NreA-I) or nitrate (NreA-NO_3). Crystal form NreA-I grew from 12.5% (w/v) polyethylene glycol (PEG) 1.000, 12.5% (w/v) PEG 3350, 12.5% (v/v) 2-methyl-2,4-pentanediol, 0.03 M sodium fluoride, 0.03 M sodium bromide, 0.03 M sodium iodide and 0.1 M Bicine [*N*,*N*-bis(2-hydroxyethyl)glycine]/Trizma base (pH 8.5) based on the Morpheus crystal screen. NreA-NO_3 crystallized with a precipitant solution composed of 12.5% (w/v) PEG 1.000, 12.5% (w/v) PEG 3350, 12.5% (v/v) 2-methyl-2,4-

pentanediol, 0.03 M sodium nitrate, 0.03 M disodium hydrogen phosphate, 0.03 M ammonium sulfate and 0.1 M Bicine/Trizma base (pH 8.5) based on the Morpheus crystal screen [44]. Crystals from both conditions grew within 3 days and were flash-frozen in liquid nitrogen for data collection at the European Synchrotron Radiation Facility (ESRF) (NreA-I) in Grenoble, France, and at the Swiss Light Source (SLS) (NreA-NO_3) in Villigen, Switzerland.

Structure determination and analysis

Both crystal forms belong to space group $P4_32_12$, have almost identical unit cell parameters and contain two copies of NreA in their asymmetric unit. The crystal forms differ primarily in the type of ion that is bound to the same site in NreA (iodide or nitrate). Three data sets from two NreA-I crystals were integrated with XDS and scaled and merged together with XSCALE [45] to obtain a 2.5-Å data set for phasing. These data were used to solve the structure with the single wavelength anomalous dispersion method implemented in SHARP/autoSHARP [46]. The experimental electron density map calculated with initial phases was suitable for tracing the chain and manual model building using Coot [35]. At a later stage, a complete data set with 2.2 Å resolution from one crystal was used for crystallographic refinement using refmac 5 [47] and PHENIX [48]. The resulting $F_o - F_c$ maps at 3 σ cutoff level indicated new density features that were subsequently added and refined to reasonable *R*-factors and geometries (Table 1). Residues that did not have sufficient electron density in the final $2F_o - F_c$ map at 1 σ were truncated at the appropriate side chain atom. Data collected from NreA-NO_3 crystals were processed with XDS in a similar manner. The resolution cutoffs were chosen based on the CC1/2 correlation, which describes the percentage of correlation between intensities from random half-data sets [49]. The final data set for NreA-NO_3 has CC1/2 values of 99.9% (overall) and 43.9% (highest-resolution bin). Furthermore, an $I/\sigma(I)$ value greater than 1 in the last bin was used to limit the resolution for data processing. A reliable electron density map was computed with molecular replacement using MOLREP [50]. The NreA-I structure, in which all ligands had been removed, was used as search model. This gave rise to a single solution that was subsequently modified and refined using Coot and PHENIX, respectively, as described above. Data collection and refinement statistics for NreA-I and NreA-NO_3 are given in Table 1. The structural similarities of NreA to known structures were investigated with Dali [31]. Whether the crystal contacts have an physiologic character were evaluated with PISA [37–39]. Conformational differences between the two models of NreA were analyzed with LSQMAN [51]. All figures depicting structures were prepared with PyMOL [52].

Lipase activity of reporter gene fusions *narG-lip*

For the measurement of reporter gene activities, plasmid pMW1040 and derivatives were transformed into *S. carnosus* strain m1 by electrotransformation [42]. The growth conditions for measurement of the reporter gene activities were kept constant for all strains. Each experiment is from three or more biological replicates, each measured threefold. The anaerobic cultures of *S. carnosus* m1 carrying plasmid pMW1040 or derivatives were incubated in screw-cap bottles at 37 °C in basic medium light without Na_2HPO_4 [53]. The medium was optionally supplemented with 10 mM $NaNO_3$, KNO_3, $NaNO_2$ or NaI, as indicated. The main cultures were inoculated with the corresponding preculture resulting in an OD_{578} of 0.1. Measurements were performed after the cells were harvested at OD_{578} of 0.5. Liquid cultures of the bacteria (OD_{578} = 0.5) were centrifuged (9.500*g*, 2 min, 20 °C), and activity of lipase that is secreted was determined from the supernatant. The substrate of the lipase *p*-nitrophenyl caprylate (pNPC; Sigma) was added in a concentration of 5 mM to buffer G [20 mM Tris–HCl, 10 mM $CaCl_2$ and 0.1% (v/v) Triton X-100 (pH 9)] and emulsified by vortexing for 15 s. The supernatant was mixed with buffer G in a 1:10 ratio for the measurements. The formation of *p*-nitrophenol ($\varepsilon_{415nm} = 15.188 \times 10^3 \times mol^{-1} \times cm^{-1}$) by hydrolysis of pNPC was monitored spectrophotometrically (BioTek) at 415 nm in 96-well plates for about 20 min. The activity was converted to specific lipase activity, with 1 U/g corresponding to the consumption of 1 μmol pNPC × min^{-1} × g^{-1} cell dw (1 ml culture with an OD_{578} of 1 corresponds to 0.254 mg cell dw).

Data deposition

The atomic coordinates for NreA-I and NreA-NO_3 have been deposited in the PDB [54] with the with the accession numbers 4IUH and 4IUK, respectively.

Acknowledgments

We thank Dr. Georg Zocher and Dr. Ursula Neu (Interfaculty Institute of Biochemistry, University of Tübingen) for advisory support in data processing and structure determination. We acknowledge Andreas Maurer (Interfaculty Institute of Biochemistry, University of Tübingen) and Dr. Silke Patzer (Max Planck Institute for Developmental Biology, Tübingen) for technical support in matrix-assisted laser desorption/ionization analysis and CD measurements, respectively. Great thanks to Sandra Zedler (Institute for Microbiology and Wine Research, University of Mainz) for experimental support. We are

grateful to the staff of beamline ID14-4 at the ESRF synchrotron and X06DA at the SLS synchrotron for assistance with data collection. This work was supported by transregional collaborative research grant SFB-TR34 of the German Research Foundation to T.S. and F.G. and by grant UN49/13-2 of the Deutsche Forschungsgemeinschaft to G.U.

Appendix A. Supplementary Data

Supplementary data to this article can be found online at http://dx.doi.org/10.1016/j.jmb.2013.12.026.

Received 4 September 2013;
Received in revised form 19 December 2013;
Accepted 23 December 2013
Available online 31 December 2013

Keywords:
GAF domain;
anaerobic respiration;
Staphylococcus;
nitrate binding;
X-ray structure

†V.N. and M.K.-S. contributed equally to this work.
‡www.rcsb.org
§http://openwetware.org/wiki/Sauer:Purification_of_His-tagged_proteins/Denaturing_prep

Abbreviations used:
PDE, phosphodiesterase; ITC, isothermal titration calorimetry; CCS, complexation significance score; PEG, polyethylene glycol; ESRF, European Synchrotron Radiation Facility; SLS, Swiss Light Source; pNPC, p-nitrophenyl caprylate; WT, wild type; PDB, Protein Data Bank; dw, dry weight.

References

[1] Neubauer H, Götz F. Physiology and interaction of nitrate and nitrite reduction in *Staphylococcus carnosus*. J Bacteriol 1996;178:2005–9.
[2] Pantel I, Lindgren PE, Neubauer H, Götz F. Identification and characterization of the *Staphylococcus carnosus* nitrate reductase operon. Mol Gen Genet 1998;259:105–14.
[3] Neubauer H, Pantel I, Götz F. Molecular characterization of the nitrite-reducing system of *Staphylococcus carnosus*. J Bacteriol 1999;181:1481–8.
[4] Fast B, Lindgren P, Götz F. Cloning, sequencing, and characterization of a gene (*narT*) encoding a transport protein involved in dissimilatory nitrate reduction in *Staphylococcus carnosus*. Arch Microbiol 1996;166:361–7.
[5] Neubauer H, Pantel I, Lindgren PE, Götz F. Characterization of the molybdate transport system ModABC of *Staphylococcus carnosus*. Arch Microbiol 1999;172:109–15.
[6] Neubauer H, Pantel I, Götz F. Characterization of *moeB*—part of the molybdenum cofactor biosynthesis gene cluster in *Staphylococcus carnosus*. FEMS Microbiol Lett 1998;164:55–62.
[7] Fedtke I, Kamps A, Krismer B, Götz F. The nitrate reductase and nitrite reductase operons and the *narT* gene of *Staphylococcus carnosus* are positively controlled by the novel two-component system NreBC. J Bacteriol 2002;184:6624–34.
[8] Kamps A, Achebach S, Fedtke I, Unden G, Götz F. Staphylococcal NreB: an O(2)-sensing histidine protein kinase with an O(2)-labile iron-sulphur cluster of the FNR type. Mol Microbiol 2004;52:713–23.
[9] Schlag S (2008). Dissimilatory nitrate and nitrite reduction in staphylococci: regulation and implication in biofilm formation. PhD Thesis, University of Tuebingen.
[10] Schlag S, Fuchs S, Nerz C, Gaupp R, Engelmann S, Liebeke M, et al. Characterization of the oxygen-responsive NreABC regulon of *Staphylococcus aureus*. J Bacteriol 2008;190:7847–58.
[11] Müllner M, Hammel O, Mienert B, Schlag S, Bill E, Unden G. A PAS domain with an oxygen labile [4Fe-4S](2+) cluster in the oxygen sensor kinase NreB of *Staphylococcus carnosus*. Biochemistry 2008;47:13921–32.
[12] Williams SB, Stewart V. Discrimination between structurally related ligands nitrate and nitrite controls autokinase activity of the NarX transmembrane signal transducer of *Escherichia coli* K-12. Mol Microbiol 1997;26:911–25.
[13] Cheung J, Hendrickson WA. Structural analysis of ligand stimulation of the histidine kinase NarX. Structure 2009;17:190–201.
[14] Koropatkin NM, Pakrasi HB, Smith TJ. Atomic structure of a nitrate-binding protein crucial for photosynthetic productivity. Proc Natl Acad Sci USA 2006;103:9820–5.
[15] Boudes M, Lazar N, Graille M, Durand D, Gaidenko TA, Stewart V, et al. The structure of the NasR transcription antiterminator reveals a one-component system with a NIT nitrate receptor coupled to an ANTAR RNA-binding effector. Mol Microbiol 2012;85:431–44.
[16] Unden G, Nilkens S, Singenstreu M. Bacterial sensor kinases using Fe-S cluster binding PAS or GAF domains for O(2) sensing. Dalton Trans 2013;42:3082–7.
[17] Aravind L, Ponting CP. The GAF domain: an evolutionary link between diverse phototransducing proteins. Trends Biochem Sci 1997;22:458–9.
[18] Anantharaman V, Koonin EV, Aravind L. Regulatory potential, phyletic distribution and evolution of ancient, intracellular small-molecule-binding domains. J Mol Biol 2001;307:1271–92.
[19] Ho YS, Burden LM, Hurley JH. Structure of the GAF domain, a ubiquitous signaling motif and a new class of cyclic GMP receptor. EMBO J 2000;19:5288–99.
[20] Martinez SE, Beavo JA, Hol WG. GAF domains: two-billion-year-old molecular switches that bind cyclic nucleotides. Mol Interv 2002;2:317–23.
[21] Schultz J, Milpetz F, Bork P, Ponting CP. SMART, a simple modular architecture research tool: identification of signaling domains. Proc Natl Acad Sci USA 1998;95:5857–64.
[22] Zoraghi R, Corbin JD, Francis SH. Properties and functions of GAF domains in cyclic nucleotide phosphodiesterases and other proteins. Mol Pharmacol 2004;65:267–78.
[23] Batchelor JD, Lee PS, Wang AC, Doucleff M, Wemmer DE. Structural mechanism of GAF-regulated sigma(54) activators from *Aquifex aeolicus*. J Mol Biol 2013;425:156–70.
[24] Nilkens S, Koch-Singenstreu M, Niemann V, Gotz F, Stehle T, Unden G. Nitrate/oxygen co-sensing by an NreA/NreB

sensor complex of *Staphylococcus carnosus*. Mol Microbiol 2013. http://dx.doi.org/10.1111/mmi.12464.
[25] Badger J, Sauder JM, Adams JM, Antonysamy S, Bain K, Bergseid MG, et al. Structural analysis of a set of proteins resulting from a bacterial genomics project. Proteins 2005;60:787–96.
[26] Essen LO, Mailliet J, Hughes J. The structure of a complete phytochrome sensory module in the Pr ground state. Proc Natl Acad Sci USA 2008;105:14709–14.
[27] Gruez A, Libiad M, Boschi-Muller S, Branlant G. Structural and biochemical characterization of free methionine-*R*-sulfoxide reductase from *Neisseria meningitidis*. J Biol Chem 2010;285:25033–43.
[28] Peschel A, Augustin J, Kupke T, Stevanovic S, Gotz F. Regulation of epidermin biosynthetic genes by EpiQ. Mol Microbiol 1993;9:31–9.
[29] Rosenstein R, Peschel A, Wieland B, Gotz F. Expression and regulation of the antimonite, arsenite, and arsenate resistance operon of *Staphylococcus xylosus* plasmid pSX267. J Bacteriol 1992;174:3676–83.
[30] Martinez SE, Heikaus CC, Klevit RE, Beavo JA. The structure of the GAF A domain from phosphodiesterase 6C reveals determinants of cGMP binding, a conserved binding surface, and a large cGMP-dependent conformational change. J Biol Chem 2008;283:25913–9.
[31] Holm L, Rosenstrom P. Dali server: conservation mapping in 3D. Nucleic Acids Res 2010;38:W545–9.
[32] Heikaus CC, Pandit J, Klevit RE. Cyclic nucleotide binding GAF domains from phosphodiesterases: structural and mechanistic insights. Structure 2009;17:1551–7.
[33] Turko IV, Haik TL, McAllister-Lucas LM, Burns F, Francis SH, Corbin JD. Identification of key amino acids in a conserved cGMP-binding site of cGMP-binding phosphodiesterases. A putative NKXnD motif for cGMP binding. J Biol Chem 1996;271:22240–4.
[34] Wu AY, Tang XB, Martinez SE, Ikeda K, Beavo JA. Molecular determinants for cyclic nucleotide binding to the regulatory domains of phosphodiesterase 2A. J Biol Chem 2004;279:37928–38.
[35] Emsley P, Cowtan K. Coot: model-building tools for molecular graphics. Acta Crystallogr Sect D Biol Crystallogr 2004;60:2126–32.
[36] Martinez SE, Wu AY, Glavas NA, Tang XB, Turley S, Hol WG, et al. The two GAF domains in phosphodiesterase 2A have distinct roles in dimerization and in cGMP binding. Proc Natl Acad Sci USA 2002;99:13260–5.
[37] Krissinel E, Henrick K. Inference of macromolecular assemblies from crystalline state. J Mol Biol 2007;372:774–97.
[38] Krissinel E, Henrick K. Detection of protein assemblies in crystals. In: Berthold MR, Glen R, Diederichs K, Kohlbacher O, Fischer I, editors. Computational life sciences, 3695. Berlin Heidelberg: Springer; 2005. p. 163–74.
[39] Krissinel E. Crystal contacts as nature's docking solutions. J Comput Chem 2010;31:133–43.
[40] Asen I, Djuranovic S, Lupas AN, Zeth K. Crystal structure of SpoVT, the final modulator of gene expression during spore development in *Bacillus subtilis*. J Mol Biol 2009;386:962–75.
[41] Sambrook J, Russell DW. Molecular cloning: a laboratory manual. 3rd ed. New York: Cold Spring Harbor Laboratory Press; 2001.
[42] Löfblom J, Kronqvist N, Uhlen M, Stahl S, Wernerus H. Optimization of electroporation-mediated transformation: *Staphylococcus carnosus* as model organism. J Appl Microbiol 2007;102:736–47.
[43] Savitzky A, Golay MJE. Smoothing and differentiation of data by simplified least squares procedures. Anal Chem 1964;36:1627–39.
[44] Gorrec F. The MORPHEUS protein crystallization screen. J Appl Crystallogr 2009;42:1035–42.
[45] Kabsch W. Xds. Acta Crystallogr Sect D Biol Crystallogr 2010;66:125–32.
[46] Vonrhein C, Blanc E, Roversi P, Bricogne G. Automated structure solution with autoSHARP. Methods Mol Biol 2007;364:215–30.
[47] Murshudov GN, Vagin AA, Dodson EJ. Refinement of macromolecular structures by the maximum-likelihood method. Acta Crystallogr Sect D Biol Crystallogr 1997;53:240–55.
[48] Adams PD, Afonine PV, Bunkoczi G, Chen VB, Davis IW, Echols N, et al. PHENIX: a comprehensive Python-based system for macromolecular structure solution. Acta Crystallogr Sect D Biol Crystallogr 2010;66:213–21.
[49] Karplus PA, Diederichs K. Linking crystallographic model and data quality. Science 2012;336:1030–3.
[50] Vagin A, Teplyakov A. Molecular replacement with MOLREP. Acta Crystallogr Sect D Biol Crystallogr 2010;66:22–5.
[51] Kleywegt GJ, Jones TA. A super position. CCP4/ESF-EACBM Newsletter on Protein Crystallography 1994;31:9–14.
[52] Schrodinger LLC. The PyMOL Molecular Graphics System, version 1.3r1. LLC Schrödinger; 2010.
[53] Götz F, Schumacher B. Improvements of protoplast transformation in *Staphylococcus carnosus*. FEMS Microbiol Lett 1987;40:285–8.
[54] Berman HM, Westbrook J, Feng Z, Gilliland G, Bhat TN, Weissig H, et al. The Protein Data Bank. Nucleic Acids Res 2000;28:235–42.

The NreA protein functions as a nitrate receptor in the staphylococcal nitrate regulation system

Volker Niemann[1]*, Mareike Koch-Singenstreu[2]*, Ancilla Neu[3], Stephanie Nilkens[2], Friedrich Götz[4], Gottfried Unden[2+], Thilo Stehle[1,5+]

[1] Interfaculty Institute of Biochemistry, Universität Tübingen,

Hoppe-Seyler-Str. 4, D-72076 Tübingen, Germany

[2] Institute for Microbiology and Wine Research, Universität Mainz,

Johann-Joachim-Becherweg 15, D-55128 Mainz, Germany

[3] Max Planck Institute for Developmental Biology, Spemannstrasse 35, D-72076 Tübingen,

Germany

[4] Interfaculty Institute of Microbiology and Tropical Medicine, Universität Tübingen,

Auf der Morgenstelle 28, D-72076 Tübingen, Germany

[5] Department of Pediatrics, Vanderbilt University School of Medicine,

Nashville, TN 37232, United States of America

* contributed equally

[+] To whom correspondence should be addressed:

e-mail: thilo.stehle@uni-tuebingen.de

telephone: +49 7071 29-73043

fax: +49 7071 29-5565

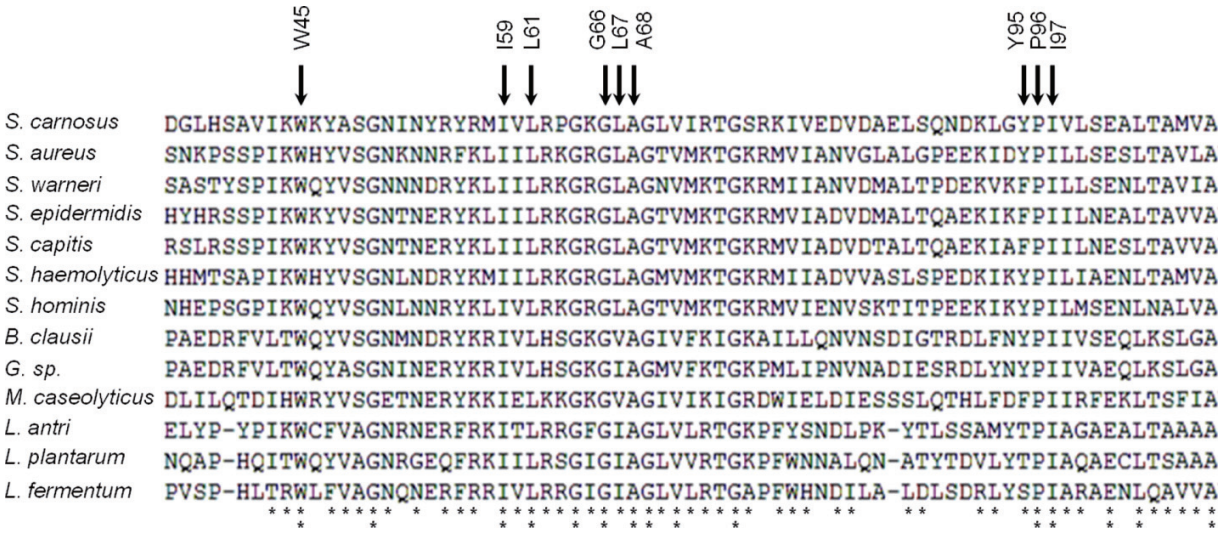

Fig S1. Sequence alignment of the binding region of NreA proteins.

Sequence alignment was performed for the region corresponding to residues 36 to 108 of NreA of *S. carnosus* including all residues involved in nitrate binding of NreA (labeled by arrows). The NreA proteins are predicted from the genomic sequence and are encoded in *nreABC* gene clusters (Unden *et al.*, 2013). Two asterisk: residues in all NreA proteins conserved (100%); one asterisk: conservative replacements (>60% conserved). Evaluation of conservation was done using similarity group-option of GeneDoc Verion 2.7. (http://www.nrbsc.org/gfx/genedoc/) (Nicholas *et al*., 1997). Bacteria shown (in addition to *Staphylococcus* (*S.*) *carnosus* TM300): *S. aureus* TW20, *S. warneri* L37603, *S. epidermidis* M23864:W1, *S. capitis* SK14, *S. haemolyticus* JCS1435, *S. hominis* SK119, *Bacilllus* (*B.*) *clausii* KSM-K16, *Geobacillus* (G.) *sp.* Y412MC10, Macrococcus (*M.*) *caseolyticus* JCSC5402, *Lactobacillus* (*L.*) *antri* DSM16041, *L. plantarum*, *L. fermentum* 28-3-CHN.

Unden, G., Nilkens, S., and Singenstreu, M., (2013) Bacterial sensor kinases using Fe-S cluster binding PAS or GAF domains for O(2) sensing. *Dalton Trans* 42: 3082-3087.

Nicholas, K.B., Nicholas H.B. Jr., and Deerfield, D.W. II. 1997 GeneDoc: Analysis and Visualization of Genetic Variation, EMBNEW.NEWS 4:14

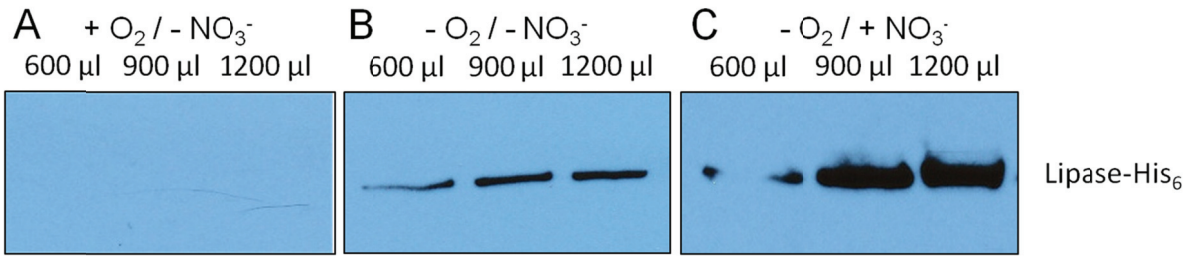

Fig. S2 Correlation of lipase activity with the amount of produced lipase. To verify experimentally that the lipase reporter gene activity correlates with the amount of lipase enzyme a western blot against His-tag was performed. In the experiment, wild type *S. carnosus* carrying plasmid pMW2094 (Table S2) was grown in BML medium with glucose and chloramphenicol. The growth conditions were aerobic (A), anaerobic (B) and anaerobic with nitrate (C). At an OD_{578} of 0.5 bacteria samples (600 µl, 900 µl and 1200 µl) were taken and sedimented by centrifugation. The Lipase in the supernatant was precipitated by addition of TCA (1 M final concentration). After centrifugation and discarding TCA, the pellets were washed twice with ice cold acetone. The lipase was resolved in 1 M Tris-HCl pH 9 samples were subjected on SDS-PAGE and subsequently the proteins blotted and incubated with mouse anti-His IgG. After washing, the blot was incubated with rabbit anti-mouse IgG coupled to horse radish peroxidase. The blots were developed using the chemiluminescence method. Clear signals depending on growth conditions and samples size are visible. The correlated specific lipase activities (A 31.5 U/g dw, B 383 U/g dw, C 699 U/g dw) are similar to those obtained in wild type strain m1 pMW1040 (A 37.5 U/g dw, B 320 U/g dw, C 570 U/g dw) (Figure 3).

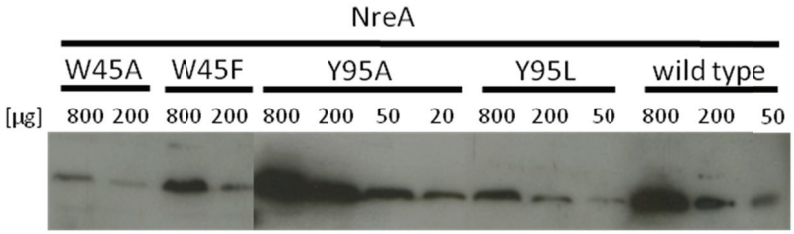

Fig. S3. Immunoblots of cell-homogenates of *S. carnosus* m1 carrying plasmid encoded variants of NreA.

The bacteria were grown for 3 h under aerobic conditions in the presence of 10 mM $NaNO_3$. The bacteria were sedimented, broken by glass beads and after centrifugation 800µg, 200µg or 50 µg protein of the supernatant was subjected to SDS-PAGE, and NreA was detected by immunoblotting using anti-NreA serum from rabbit (Eurogentec) and goat anti-rabbit IgG coupled to horse radish peroxidase. The following strains and proteins were tested m1 pMW1064 (NreA-W45A), m1 pMW1298 (NreA-Y95A), m1 pMW1514 (NreA-W45F), m1 pMW1517 (NreA-Y95L), m1 pMW1040 (wild type NreA) (Table S2).

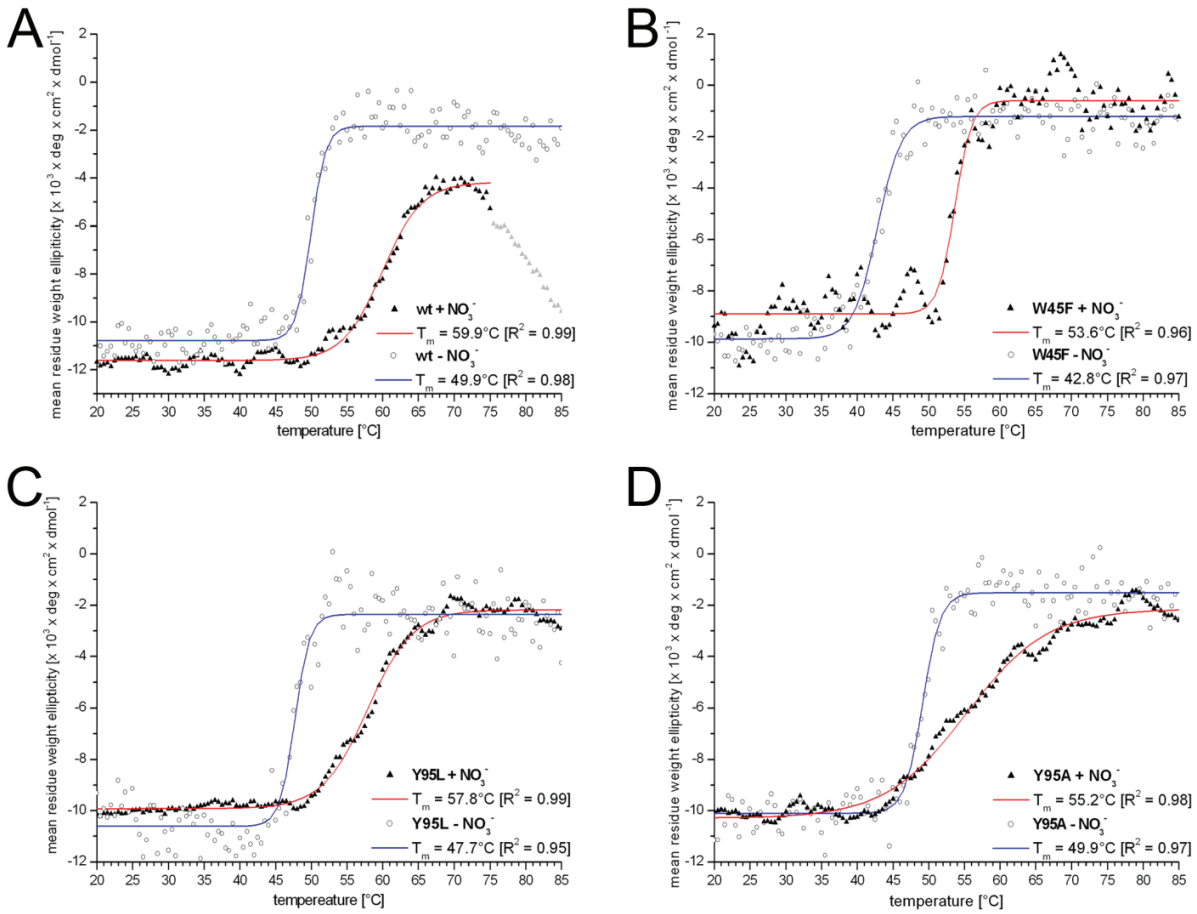

Fig, S4. Melting curves were determined for wt and mutant NreA proteins in the presence (+ NO_3^-, filled triangles) and absence (-NO_3^-, open circles) of nitrate using CD spectroscopy. The data measured in the presence of nitrate lead to a noisy signal. The sigmoid curves without nitrate (blue) and with nitrate (red) are fitted on the data based on the Boltzmann equation using origin 6.0 (OriginLab, Northampton, MA). The error values (R^2) indicate a reliable curve fitting. Based on the curve equation, the x-values of the inflection points determine the melting point in each case.

A. The melting temperature of wild type NreA increases form 49.9°C without ligand to 59°C with bound nitrate. The CD data measured in the presence of nitrate above 75°C were excluded from the curve fitting because of noisy signal.

B. The W45F mutant shows an increased melting temperature when nitrate is bound. The temperature rises from 42.8°C to 53.6°C.

C. When nitrate is bound to the Y95L mutant, the melting temperature rises from 47.7°C to 57.8°C.

D. The melting temperature is increased from 49.9°C to 55.2°C when the Y95A mutant is 90 % saturated with nitrate.

Table S1 DALI results with corresponding PISA results

Shown is condensed information from output generated by the DALI-server (http://ekhidna.biocenter.helsinki.fi/dali_server/start) (structural homology search) and the PISA-server (http://www.ebi.ac.uk/msd-srv/prot_int/cgi-bin/piserver) (evaluation of biological significance of crystal contacts). Results of the structure homology search on NreA are listed depending on the Z-score[a]. The root mean square deviation (rmsd) describes the distance between the Cα-atoms of the aligned amino acids in the structures. The number of amino acids in the native protein indicates whether the aligned GAF domain is part of a multi domain protein or an only GAF domain protein. The protein name and the organism describe the biological background. SCC[b] is a value evaluating the crystal contact of the proteins whereby 1.0 represents a likely physiological interaction and 0.0 a non-physiologic crystal contact.

Holm, L. & Rosenstrom, P. (2010). Dali server: conservation mapping in 3D. Nucleic acids research **38**, W545-9.

Krissinel, E. & Henrick, K. (2007). Inference of macromolecular assemblies from crystalline state. *Journal of molecular biology* **372**, 774-97.

Krissinel, E. & Henrick, K. (2005). Detection of Protein Assemblies in Crystals. In *Computational Life Sciences* (R. Berthold, M., Glen, R., Diederichs, K., Kohlbacher, O. & Fischer, I., eds.), Vol. 3695, pp. 163-174. Springer Berlin Heidelberg.

Krissinel, E. (2010). Crystal contacts as nature's docking solutions. *Journal of computational chemistry* **31**, 133-43.

Table S1. DALI results with corresponding PISA results

No	PDB-chain	Z-score[a]	rmsd	Aligned positions	Residues in matched structure	Residues in native protein	Protein name	Organism	SSC[b]	Interface area [Å^2]	Ligand in structure
1	3ci6-B	13,1	2,7	129	166	764	Phosphoenolpyruvate-protein phosphotransferase	*Acinetobacter sp.*	1,000	1478,3	N/A
2	3o5y-A	12,4	2,8	128	142	502	Two-component sensor histidine kinase	*Bacillus halodurans*	0,000	530,2	N/A
4	2qyb-A	12,2	2,8	126	151	910	Putative membrane protein, putative	*Geobacter sulfurreducens*	1,000	810,3	N/A
5	3trc-A	12,1	2,9	126	168	766	Phosphoenolpyruvate-protein phosphotransferase	*Coxiella burnetii*	0,287	1067,2	Phosphate
6	1ykd-A	11,9	2,8	125	383	860	Adenylate cyclase	*Anabaena sp.*	0,830	3694,1	cAMP
7	3oov-A	11,8	3,1	130	164	663	Putative Methyl-accepting chemotaxis protein	*Geobacter sulfurreducens*	0,000	778,2	N/A
9	3dba-B	11,7	2,9	122	171	862	Cone cGMP-specific 3',5'-cyclic phosphodiesterase	*Gallus gallus*	0,420	869,1	cGMP
10	2vjw-A	11,6	2,6	117	138	571	GAF family protein	*Mycobacterium smegmatis*	0,000	504,1	N/A
11	2zmf-B	11,6	2,9	122	172	779	3',5'-cyclic phosphodiesterase 10A	*Homo sapiens*	0,817	1530,9	cAMP
16	3ksi-A	11,6	2,6	120	152	154	Putative uncharacterized protein	*Staphylococcus aureus*	0,322	930,9	2-propanol
17	1vhm-A	11,5	2,6	121	159	165	Free methionine-R-sulfoxide reductase	*Escherichia coli*	1,000	1138,9	MES[c]
21	3mmh-A	11,4	2,7	124	168	167	Putative uncharacterized protein	*Neisseria meningitidis*	0,210	1117,2	methionine sulfoxide
22	3rfb-B	11,4	2,7	120	164	165	Putative uncharacterized protein	*Streptococcus pneumoniae*	1,000	1418,4	methionine sulfoxide
26	3eea-A	11,4	2,8	127	153	550	GAF domain/HD domain protein	*Geobacter sulfurreducens*	0,000	823,6	N/A
30	2vea-A	11,3	3,0	124	500	748	Phytochrome-like protein cph1	*Synechocystis sp.*	0,451	2504,7	phycocyanobilin
31	3hcy-B	11,3	2,8	120	143	907	Two-component sensor histidine kinase protein	*Rhizobium meliloti*	1,000	1008,0	N/A
42	2w1r-A	10,8	2,7	111	117	178	Stage V sporulation protein T	*Bacillus subtilis*	1,000	620,7	N/A
44	1f5m-A	10,7	2,8	124	176	180	Free methionine-R-sulfoxide reductase	*Saccharomyces cerevisiae*	0,910	1386,2	N/A
45	3eoy-B	10,7	2,7	111	152	455	Outer capsid protein sigma-1	Reovirus type 3	1,000	1121,8	N/A
46	2ool-B	10,7	3,1	123	298	775	Bacteriophytochrome	*Rhodopseudomonas palustris*	0,508	1260,0	RpBphP3[d]

a Z-score, i.e., strength of structural similarity in standard deviations above expected. The matched structures are sorted by Z-score.

b CSS stands for the Complexation Significance Score, which indicates how significant for assembly formation the interface is. The score is defined as a maximal fraction of the total free energy of binding that belongs to the interface in stable assemblies.

c 2-(N-morpholino)ethanesulfonic acid

d 3-[2-[(Z)-[3-(2-carboxyethyl)-5-[(Z)-(4-ethenyl- 3-methyl-5-oxidanylidene-pyrrol-2-ylidene)methyl]- 4-methyl-pyrrol-1-ium-2-ylidene]methyl]-5- [(Z)-[(3E)-3-ethylidene-4-methyl-5-oxidanylidene- pyrrolidin-2-ylidene]methyl]-4-methyl-1H- pyrrol-3-yl]propanoic acid

Table S2. Strains of *S. carnosus* and *E. coli* and plasmids

Bacterial strains	**Genotype and characteristics**	**Source**
E. coli JM109	*recA1 supE44 endA1 hsdR17 gyrA96 relA1 thi e14*$^-$ F' *traD36 proAB*$^+$ *lacI*^{q} Δ*(lacZ)*M15Δ*(lac-proAB)*	[1]
E. coli XL1-Blue	*recA1 endA1 gyrA96 thi-1 hsdR17 (rK*$^-$ mκ$^+$*) supE44 relA* λ$^-$ *lac* [F' *proAB lacI*^{q} *Z*ΔM15 *Tn10(Tet*^{r}*)*]	Stratagene
E. coli M15 (pREP4)	K12 derivate with Nal^S Str^S Rif^S Thi$^-$ Lac$^-$ Ara$^+$ Gal$^+$ Mtl$^-$ F$^-$ RecA$^+$ Uvr$^+$ Lon$^+$	Qiagen
S. carnosus TM300	Wild-type isolate, deficient of ΦSK1	[2]
S. carnosus m1	(Δ*nreABC::ermB*)	[3]
Plasmids		
pMW418	*E. coli / S. carnosus* shuttle-vector with *amp*^{R} *cam*^{R}, *nreABC* with native promotor of *S. carnosus*	[4]
pMW1040	pMW418 with *nreABC*, but *narG- lip* (*narG* promoter of *S. carnosus* fused to lipase of *S. hyicus*, *amp*^{R} *cam*^{R}	[5]
pMW1393	pMW1040 derivative with *nreA* deletion (*nreBC narG-lip*) *amp*^{R} *cam*^{R}	[5]
pMW1532	pMW1040 but *nreBC* deletion (*nreA narG-lip*)	This study
pMW1064	pMW1040 but NreA-W45A	This study
pMW1298	pMW1040 but NreA-Y95A	This study
pMW1514	pMW1040 but NreA-W45F	This study
pMW1517	pMW1040 but NreA-Y95L	This study
pQE31-nreA	pQE31 with *nreA* (*amp*^{r})	[6]
pQE31-nreA_W45F	pQE31-nreA but NreA-W45F	This study
pQE31-nreA_Y95A	pQE31-nreA but NreA-Y95A	This study
pQE31-nreA_Y95L	pQE31-nreA but NreA-Y95L	This study

1. Yanisch-Perron, C., Vieira, J. & Messing, J. (1985). Improved M13 phage cloning vectors and host strains: nucleotide sequences of the M13mp18 and pUC19 vectors. *Gene* **33**, 103-19.
2. Rosenstein, R., Nerz, C., Biswas, L., Resch, A., Raddatz, G., Schuster, S. C. & Gotz, F. (2009). Genome analysis of the meat starter culture bacterium Staphylococcus carnosus TM300. *Applied and environmental microbiology* **75**, 811-22.
3. Fedtke, I., Kamps, A., Krismer, B. & Götz, F. (2002). The nitrate reductase and nitrite reductase operons and the narT gene of Staphylococcus carnosus are positively controlled by the novel two-component system NreBC. *Journal of bacteriology* **184**, 6624-34.
4. Müllner, M., Hammel, O., Mienert, B., Schlag, S., Bill, E. & Unden, G. (2008). A PAS domain with an oxygen labile [4Fe-4S](2+) cluster in the oxygen sensor kinase NreB of Staphylococcus carnosus. *Biochemistry* **47**, 13921-32.
5. Nilkens, S., Koch-Singenstreu, M., Niemann, V., Gotz, F., Stehle, T. & Unden, G. (2013). Nitrate/oxygen co-sensing by an NreA/NreB sensor complex of Staphylococcus carnosus. *Mol Microbiol*.
6. Schlag, S. (2008). Dissimilatory nitrate and nitrite reduction in staphylococci: regulation and implication in biofilm formation. Ph.D. Thesis, University of Tuebingen.

Table S3. Primers used for mutagenesis in pMW1040 and pQE31.

primer	sequence (5'-3')
03_W45A-for	CGGTCATTAAAGCGAAATATGCTTCCGG
03_W45A-rev	CCGGAAGCATATTTCGCTTTAATGACCG
09_Y95A-for	GACAAATTAGGTGCTCCGATTGTTTTGAG
09_Y95A-rev	CTCAAAACAATCGGAGCACCTAATTTGTC
19_W45F-for	GCGGTCATTAAATTTAAATATGCTTCCGG
19_W45F-rev	CCGGAAGCATATTTAAATTTAATGACC
22_Y95L-for	GACAAATTAGGTTTGCCGATTGTTTTGAG
22_Y95L-rev	CTCAAAACAATCGGCAAACCTAATTTGTC